April 2010

Development of MRI as an Enabling Technology for Tissue Science and Engineering

Evan Arthur Demers-Peel
Worcester Polytechnic Institute

Jayanth Bisa
Worcester Polytechnic Institute

Matthew A. Gonsalves
Worcester Polytechnic Institute

Repository Citation

Demers-Peel, E. A., Bisa, J., & Gonsalves, M. A. (2010). *Development of MRI as an Enabling Technology for Tissue Science and Engineering*. Retrieved from https://digitalcommons.wpi.edu/mqp-all/1255

WORCESTER POLYTECHNIC INSTITUTE

Development of MRI as an Enabling Technology for Tissue Science and Engineering

Jayanth Bisa
Evan Demers-Peel
Matthew Gonsalves

Advisors:
Prof Christopher Sotak
Prof. George Pins

April 29, 2010

Table of Contents

Authorship

The three project team members, Jaynath Bisa, Evan Demers-Peel, and Matthew Gonsalves, contributed equally to the content found in this report. Extensive collaboration was demonstrated on each section while writing, revising, compiling, and finalizing the report

Acknowledgements

The project team would like to thank the following group of individuals and organizations for their assistance in completion of the project.

- Funding from Biomedical Engineering Department at WPI
- MRI from Radiology Department at UMass Medical School
- Salman Shazeeb for assistance with MRI testing
- Jon Grasman, Deepti Kalluri, & the Microthread MQP Team for collagen microthread production

Most especially the team would like to thank our MQP advisors Professor Christopher Sotak, Ph.D. and Professor George Pins, Ph.D. Their guidance and expertise over the past academic year has not only aided in the quality of our report, but also in the development of professional engineering design and written skills that will be utilized for years to come.

Abstract

Magnetic resonance imaging (MRI) was used for accurate and dynamic monitoring of tissue embedded microthreads; a novel biomaterial utilized to promote cardiac regeneration. An in vitro cardiac modeling system was developed that mimicked the MRI properties of native cardiac tissue by using gelatin of varying concentrations. Microthreads were treated with an iron-based superparamagnetic MRI contrast agent (ferumoxtran), embedded into the cardiac modeling system, and then imaged using MRI. Based on experimental measurements, the concentration of MRI contrast agent used to treat the microthread was chosen to optimize the MRI contrast between the microthread and the surrounding gelatin in the cardiac modeling system. T_1- and T_2-weighted MR images showed no statistical difference between actual thread location and diameter when compared with the same measurements obtained from optical images of the same cardiac modeling system. Microthread location and diameter measurements were affected by susceptibility artifacts caused by the ferromagnetic properties of the applied MRI contrast agent.

1.0 Introduction

Myocardial infarction (MI) – more commonly known as a heart attack – has become an increasingly prevalent topic of interest in the medical field today, particularly as a result of its increasing incidence. Affecting 8 million Americans in 2005 alone, and resulting in the death of roughly 1 in every 40 incidents, MI has been a leading contributor to cardiac related deaths. [17] A myocardial infarction (MI) occurs when blood flow from the pathways within the coronary arteries to the cardiomyocytes are significantly restricted. If the restriction is large enough or persists for an extended amount of time, a portion of the cardiac muscle becomes ischemic and eventually dies. [24] Unfortunately, lost cardiomyocytes, which can total up to 25 percent of the cells found in the heart, are unable to be regenerated via natural processes. The inability of the heart to restore a significant portion of cellular myocardium lost after infarction, if left untreated, can result in further cardiac-related health issues, including reductions in cardiac performance and increases in the risk of ventricular aneurysm and rupture. [41] Currently, treatments for myocardial infarction are limited to interventions that only limit the subsequent effects and include prescription medications, coronary-artery-bypass grafting (CABG), and ventricular remodeling via surgery.

The application of human mesenchymal stem cells (hMSCs), have been proposed for cardiac cell therapy post MI, primarily because they can be grown efficiently in culture and possess the potential to differentiate into cardiomyocytes. [42] Currently, in pre-clinical and clinical studies, there is an assortment of means to transplant hMSCs into the heart to promote myocardial regeneration. These means can be generally categorized into infusion, injection, and biomaterial techniques. Progression of infusion and injection techniques of stem cells have been limited, as cell retention, differentiation, and integration rates have been minimal. The development of specific biomaterials designed to direct cellular behavior; an attribute that the previous methods have lacked, however, is an emerging technique implemented to control local cellular microenvironments and increase proliferation rates. [20] In general, there are still limitations to these biomaterials, specifically in their inability to diffuse growth and differentiation factors into the infarcted area. A solution to this current problem could potentially be found utilizing recently developed tissue-embedded microthreads. These microthreads provide superior structural properties and the ability for site-specific and controlled scaffold placement. [6,7]

Currently, monitoring methods for microthread placement are limited to histological techniques. Histology allows for the effective examination of the anatomy and physiology of complex organs, as well as cell activity and function. A histological slide or “section” of tissue is prepared by first cutting a thin slice, typically anywhere from 3 to 10 microns thick, from the extracted tissue.[14,26] Staining (enhancement of cell components), mounting, and covering of the section then must occur prior to observation and analysis. The process as a whole is long and arduous, but unavoidable in order to effectively view static cell activity and function. [4,14] The compilation and examination of the anatomy and physiology of complex organs via histological analysis is laborious, intricate, and inefficient.

The goal of this project was to develop a method to efficiently and effectively monitor the placement and functionality of microthreads using Magnetic Resonance Imaging (MRI). MRI is a noninvasive imaging tool that is able to noninvasively deduce the nuclear magnetic resonance (NMR) properties of tissue and interstitial space within the body. The varying relaxation rates of water protons within a specific body, tissue, or specimen varies. These variations in relaxation rates correspond to varying spatial signal intensities and ultimately create contrast in the acquired image that allow for distinction of anatomy. [15, 21]

Following a detailed design process during which project objectives, constraints, functions, specifications were defined and alternative designs were created and tested. Ultimately the final design consisted of a simple and inexpensive gelatin-based cardiac modeling system, where gelatin of varying concentrations was used to mimic the MR relaxation properties of normal and diseased cardiac tissue. Collagen microthreads were soaked in Ferumoxtran, superparamagnetic iron oxide nanoparticles that serve as a “negative” MRI contrast agent. Ferumoxtran produces more contrast (I.e., MRI signal intensity difference) between the threads and surrounding tissue, effectively increasing the ability to locate the threads and differentiate their boundaries. To produce results consisted with project goals, gelatin and contrast agent concentrations were determined via initial MR relaxivity measurements as a function concentration. Utilizing the preliminary data and the knowledge of MR imaging, appropriate parameters for the final design could be determined. With the project team confident the modeling system would mimic in vivo results and embedded microthreads would be easily distinguishable, design variables – specifically contrast agent exposure time – were varied to further optimize results. Thread exposure time and hydration were both examined to determine if they had an effect on resulting thread signal contrast and thus differentiation.

Results and conclusion from the experiment verified the calculations made regarding properly designed cardiac phantom and MR parameters. The microthread location in the cardiac phantom was apparent and statistically similar in diameter regardless of the agent application process. Apparent microthread diameter estimated from the MR images was statistically comparable to that measured from optical images of the same microthreads, suggesting that the current design and procedure is highly accurate. Accurate *in vivo* thread location and measurements using MRI techniques requires significantly less time as compared to histological methods. This approach offers the client and all potential users a significantly improved method for not only thread visualization, but also as a means to evaluate stem cell delivery and potential myocardial regeneration.

2.0 Literature Review

2.1 Basic Functions of the Heart

The circulation of blood throughout the body is achieved by the constant, repeated contraction and relaxation of the heart. [31] The heart acts as a mechanical pump, taking in deoxygenated blood via the vena cava, cycling it through the lungs, and pumping out oxygenated blood to the body. The heart can be divided into two sections; the right and left side. To help summarize the process in which deoxygenated blood becomes oxygenated and circulated throughout the body, Figure 1 below illustrates the passage of blood flow into and out of the heart.

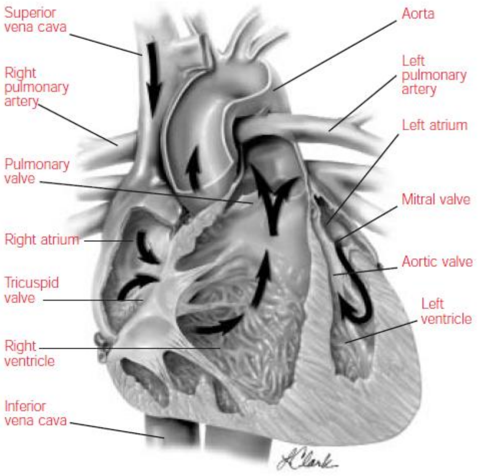

Figure 1: Cross Section and Blood Flow of Heart [18]

The right side of the heart functions to receive deoxygenated blood from the body and transfer it into the lungs. Deoxygenated blood is pumped into the heart at the right atrium, a thin-walled muscular chamber, via the superior vena cava, inferior vena cava, and the coronary sinus. During ventricular diastole a pressure gradient causes blood to flow through the tricuspid valve, into the right ventricle. The right ventricle then contracts, expelling the blood through the pulmonary arteries and into the lungs where oxygenation occurs between the alveolar sacs of the lungs and the surrounding capillary beds. [31]

The left side of the heart functions to receive oxygenated blood from the lungs and deliver and distribute it around the body as needed. The oxygenated blood from the lungs enters the left side of the heart at the left atrium, a thin-walled chamber similar to the right atrium, via the pulmonary veins. The pressure gradient from the atrium to the ventricle caused during diastole results in the flow of blood to flow through the bicuspid valve, into the left ventricle. The left ventricle then contracts, increasing the ventricular pressure, causing the aortic valve to open, and allowing circulation throughout the body. The increased pressure in the left ventricle, during the ventricular contraction is known as systole and forces the bicuspid valve close, preventing blood from re-entering the left atrium. As a result of the corresponding forces necessary to generate sufficient pressure to transport blood through the body it is important to note that the left ventricle is typically three times thicker than the right ventricle. [31]

2.2 Myocardial Infarction

Every segment of the heart plays a significant role in the circulation of blood. The cardiac muscle composing the walls of the heart, known as the myocardium, is responsible for the diastolic and systolic functions of the ventricles which ultimately transports blood. In order for the myocardium to perform these rhythmic contractions, it must receive oxygenated blood from the coronary arteries. If blood vessels within the coronary arteries are blocked, the surrounding myocardium is deprived of oxygen and nutrients, and metabolic and physiological changes occur within seconds. [24] Immediately after all of the available oxygen in the myocardium is consumed the tissue becomes oxygen deprived and the means by which energy is metabolized in the heart changes from aerobic to anaerobic glycolysis. As a result the myocardium expands with each subsequent cardiac cycle because it no longer has sufficient energy to contract. This lack of energy is caused by the cardiomyocytes, which demand more ATP (in an attempt to cause contraction) than anaerobic glycolysis can supply. Hydrogen ions accumulate in the myocardium as anaerobic glycolysis continues and the pH of cardiomyocytes decreases, ultimately causing edema in the myocardium. Over time, the formation of edema causes the heart to swell and the surrounding cardiomyocytes to permanently die. This physiological phenomenon is known as a myocardial infarction (MI). [13,18,24] The dead or infarcted tissue forms a scar within weeks to months of MI as fibroblasts accumulate fibrous collagen in the area of infarct. Further expansion of the infarcted tissue and myocardial collagen degradation occurs when neutrophils infiltrate the area of infarct and release matrix metalloproteinase (MMPs) as an inflammatory response. [39]

According to the American Heart Association, MI affected 8 million Americans in 2005 alone [17]. Those who have survived an MI are likely experience lifelong side-effects and increased cardiac-related health risks caused by their permanently weakened heart. [18] Unfortunately, 50-70% of heart attack survivors die within 5 years because of a lack of effective treatments. [42]

2.3 Clinical Treatments of Myocardial Infarction

The inability of the heart to restore the often significant portion of cellular myocardium lost via myocardial infarction, if left untreated, can result in further cardiac-related health issues. In particular, the region of dead, scarred tissue that replace necrotic tissue in subsequent weeks following an infarction often become increasingly thin and dyskinetic, resulting in the deformation of the left ventricular cavity. [14, 15] This deformation, in conjunction with the initial loss of functional myocardium, results in significant reductions of cardiac performance. The ejection fraction, defined as the fraction of blood ejected from the total volume contained within the ventricle, has been noted to decrease with increasing infarct size. The decrease in the ejection ratio results in an array of compensatory responses, initiated in attempts to maintain adequate stroke volumes and thus cardiac functionality. As depicted in Figure 2, larger ventricular volumes are generated to maintain proper ejection volumes but result in an undesirable increase in ventricular pressure, putting the chamber at risk of aneurysm and rupture, particularly in the area of thin infarct tissue. [41]

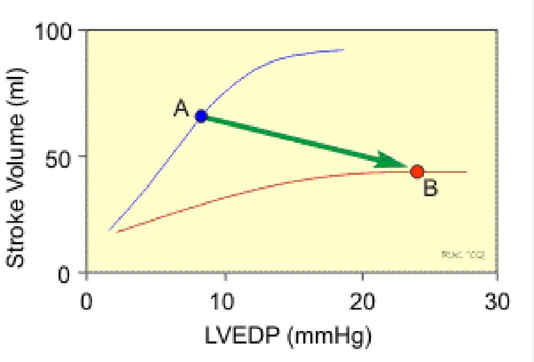

Figure 2: Increase in LV Pressure (B) in an attempt to Maintain Efficient Stroke Volume [23]

Currently, treatment methods of myocardial infarction are limited to interventions that only treat its effects. Prescription medications and coronary artery bypass grafting (CABG) are the most commonly utilized treatments although relatively new remodeling techniques have gained popularity over the past 5 years. [22] Therapeutic intervention via medication aim to improve cardiac heart function post MI through the usage of cardio-stimulatory and vasodilator drugs. Cardio-stimulatory drugs increase cardiac output by increasing heart rate and myocardial contractility. Pumping small volumes of blood more rapidly and efficiently, as opposed to pumping greater volumes less often, significantly reduces undesirable ventricular pressures and the associated risks. Vasodilator drugs aim to reduce the high blood pressure and stress on ventricular chambers caused by post MI responses via relaxation of smooth muscle and dilation of the corresponding blood vessels. Vasodilator drugs can achieve reduced blood pressure via dilatation of arterial or venous vessels, with most consisting of a mixture of the two. [22]

Although increasingly popular, the application of prescription medication to maximize cardiac output normalcy has obvious limitations. Medications do well in easing the stress on the ailing heart, but do nothing to restore it back to its original condition. The significant loss of cardiomyocytes, thinning of ventricular walls, and bodily compensatory responses post MI make heart failure imminent, as five-year survival rates drop below 50%. [42] Regardless of the survival forecasts, the lack of better treatment methods has resulted in continual market growth, as sales of post-MI therapeutics are projected to exceed $13 billion in 2012. [11]

Developed in 1954 by Charles Bailey, the evolution and use of ventricular remodeling methods over the past half decade has becoming increasing popular as clinical trials have begun to demonstrate its effectiveness. [1] Currently, the two surgical procedures of choice in remodeling are direct linear closure and endoventricular patch plasty. Although numerous studies and clinical trials of these surgical methods have been implemented, it is not yet clear which, if any, offer significantly better short and longer term results. [1,41] In direct linear closure, remodeling of the misshapen and malfunctioning tissue involves removal of the infarcted myocardium. The remaining heart tissue is then directly sutured back together in a way that maximizes restoration of the elliptical shape of the left ventricle. This procedure is extremely invasive, and also has many complications that could occur. If, however, there is not sufficient myocardial tissue available to achieve the proper ventricular dimensions, the use of a patch is employed. [25] In endoventricular patch plasty, patches typically 2.5 – 5 cm in diameter are sutured in place of the removed infarct to ensure sufficient ventricular volume and shape. [41] A balloon with a known volume of typically 60 mL/m^2 is inflated within the left ventricle as a guide, with sutures placed around the incision to tighten the ventricle to the shape of the balloon. Remodeling of the misshapen heart using this procedure can be seen below in Figure 3.

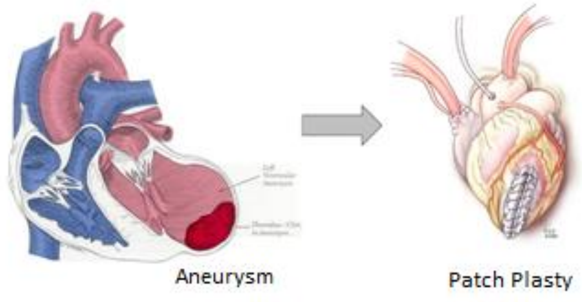

Figure 3: Endoventricular Patch Plasty or Dor Procedure

Photo Credit: Kathleen Wagner, Medical Illustrator

While this surgical technique restores normal ventricular dimensions and pressures, it does not accommodate for the loss of cardiomyocytes and ventricular contractile force. Furthermore, the materials utilized for the patch are often significantly stronger than native myocardium and produce surrounding areas of fibrosis, contributing further to variances in regards to normal cardiac functionality. The unwillingness of numerous surgeons to exclude necrotic normal appearing segments, often encountered after early reperfusion, has further attributed to the lack of method implementation. [2] Instead, coronary artery bypass grafting (CABG) is performed and the non-functioning muscle segment is left undisturbed. CABG is done to restore blood flow to tissue beyond coronary blockages; however, this procedure does nothing to treat the infarct.

In spite of its disadvantages, the overall decrease in cardiac output via patch plasty and linear closure appears to have limited impact on morality rates in comparison to therapeutic treatments. Cumulative survival rates for both methods at 5, 10, and 15 years were 91, 81, and 74%, respectively. [1] The procedure itself however, is particularly invasive and dangerous in comparison to proposed methods, as it requires opening of the chest cavity and fully arresting the heart. The thirty-day post-operation mortality rates among various studies were averaged and found to be, approximately 1 in 40. [1,25,41]

2.4 Human Mesenchymal Stem Cells

Human mesenchymal stem cells (hMSCs) are stem cells found in adult tissues, such as bone marrow, periosteum, trabecular bone, adipose tissue, synovium, skeletal muscle, and deciduous teeth. [42] Adult hMSCs are mostly found in bone marrow and like any other type of stem cell, hMSCs can divide indefinitely and differentiate into other types of cells, such as those found in cartilage, fat, bone, and muscle. [42,32] Although hMSCs only represent about 0.001% to 0.01% of the nucleated cells in bone marrow, these cells can easily be isolated and developed in culture. Because they can be grown so efficiently in culture and possess the potential to differentiate into cardiomyocytes, hMSCs have been proposed for use in cardiac cell therapy after MI. [42,45]

There have been several pre-clinical and clinical studies in which hMSCs have shown promise in cardiac cell therapy. In one study, five weeks after MI in a rat and four weeks after hMSC delivery into an infarcted rat heart, it was concluded that left ventricular function was significantly improved. [45] Another study done with the same time specifications as the previous one proved a significant decrease in infarct size and increase in left ventricular wall thickness. [40] Although such early studies have demonstrated the safety and effectiveness of hMSC in cardiac cell therapy, there are still several questions regarding the means by which the hMSCs differentiate into cardiomyocytes and ultimately improve cardiac function. [42]

2.5 Stem Cell Delivery Techniques

Currently there are a few different stem cell delivery techniques that are being employed in pre-clinical and clinical trials. The common means to deliver these cells are through infusion, injection, or with biomaterials. [42]

2.5.1 Infusion Techniques

The easiest way being researched to deliver stem cells into the heart today is by intravenous infusion. In this process, the stem cells are infused within a vein of the subject via a catheter (as shown in Figure 4). Although it is a simple procedure, the crucial drawback is its inefficiency. It has been proven that a significant number of cells fail to reach the infarcted myocardium after infusion and reside in other organs. In one study, which was done 48 hours after MI, less than 1% of the stem cells actually reached the infarcted myocardium four hours after infusion. [42]

Figure 4: Intravenous Infusion Method for Stem Cell Delivery [42]

The most commonly practiced stem cell delivery technique in clinical trials today is intracoronary infusion. With this method, cells are delivered into the distal end of the infarcted coronary artery using an over-the-wire balloon catheter (as shown in Figure 5). A balloon catheter is necessary in this case to prevent backflow of the stem cells. The advantages of this technique are that it is inexpensive, easy to conduct, and repeatable. Unfortunately, there are numerous disadvantages of this procedure as well. One potential risk to the subject is coronary artery re-stenosis, which is the re-narrowing of the coronary artery. This re-stenosis is usually a result of expanding the artery via inflation of a balloon catheter (coronary angioplasty). There have also been noted instances of decreased coronary blood flow in the subject, as well as micro-infarctions in the artery caused by the infused stem cells impeding the passage of blood in the vessels. Another drawback of this procedure is its inefficiency, as the majority of the cells do not remain in the heart and migrate to other organs. In one study, less than 10% of the infused stem cells remained in the myocardium. [42]

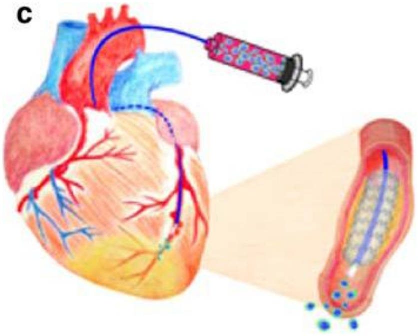

Figure 5: Intracoronary Infusion Method for Stem Cell Delivery [42]

2.5.2 Injection Techniques

Transepicardial injection is emerging as a common practice in cardiac cell therapy and is often used in pre-clinical trials. This is a repeatable method, which is carried out by directly injecting the stem cells into the infarcted myocardium (as shown in Figure 6). This is performed usually through a small incision in the chest through which a needle is inserted directly into the heart wall. Experimental data suggests that this type of cell delivery may overcome the problems associated with intravenous and intracoronary infusion. The more significant advantage of transepicardial injection is that it is extremely effective in delivering the cells to the region of interest. An MRI study suggested that a significant number of injected stem cells remained in the target area, three days following the injection [66]. Some cells however migrated to other organs, such as the spleen, lung, and liver. Although one study has suggested that cell delivery by this method is relatively more efficient, other studies involving injectable procedures into the heart have indicated that the injected cells have only a limited amount of time to adhere to the infarcted region. The cells that could not sufficiently adhere flowed back out of the heart from the point of entry. Thus, the efficiency of transepicardial injection is not yet clear [7,42].

Figure 6: Transepicardial Injection Method for Stem Cell Delivery [42]

An emerging, new modality of stem cell delivery is transendocardial injection. With this method, stem cells are injected intra-ventricularly via an injection catheter into the border of the infarcted myocardium (as shown in Figure 7). The injection catheter is guided by a cardiac mapping system, which identifies the infarcted region. The mapping system is extremely reliable and currently both skin contact and non-contact systems are being evaluated. The NOGA™ System is an FDA-approved minimally invasive platform developed by Biosense Webster (Diamond Bar, CA) for catheter-based intra-myocardial navigation and mapping. This system utilizes low intensity, active magnetic field energy and sensor-tipped catheters to locate the position of the catheter in three-dimensional space. The NOGA™ mapping system requires skin contact with the use of body surface electrodes, while other systems such as the ESI™ system developed by Endocardial Solutions (**St. Paul, MN),** does not. The advantage of this guided method is that it overcomes the problem of site-specific delivery associated with intravenous and intracoronary infusion. One disadvantage of such technologically-advanced electrophysiological cardiac-mapping systems is its relative cost in comparison to the previously discussed techniques. Another drawback is that this is an injectable procedure such as this allows only a limited time for the injected cells to adhere to the infarcted region of the heart, making its efficiency unclear [7,42].

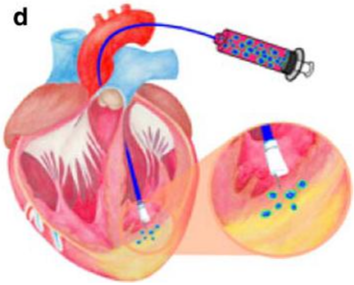

Figure 7: Transendocardial Injection with Cardiac Mapping System for Stem Cell Delivery [42]

2.5.3 Biomaterials for Cardiac Regeneration

Induced cellular growth and differentiation is an extremely particular process, often requiring highly specific conditions and growth factors orchestrated in the surrounding cell microenvironment. [20] In current studies, central to cellular regeneration, the microenvironments in which cells are successfully delivered are of particular interest. The development of specific biomaterials designed to direct cellular behavior – an attribute that previous delivery methods have lacked – is an emerging technique to control local cellular microenvironments and increase proliferation rates.[20] Scaffolding materials are chosen and designed based upon various parameters necessary for possible regeneration, with common focal points including material degradation, compliance, porosity, and cellular adhesion. [20]

The optimization of biomaterials to satisfy the conditions necessary for the functional repair of infarcted myocardium has proven to be a daunting task. Biomaterials currently studied at the pre-clinical level for cardiac applications are numerous and most notably include alginate, gelatin, collagen, Matrigel, self-assembling peptides, and fibrin. [7,22,27,33,34,38] Although these materials possess many of the qualities necessary for guided cell growth, chemical modifications prior to implantation are often made due to poor vascularization and cellular adhesion, inflammatory responses, instability, and toxic degradation. [7,46] Pre-clinical testing of various "optimized" biomaterials has shown great promise in both cellular delivery and cardiac regeneration via increased neovascularization, myofibroblasts, and cardiac function. [6,22,27,34,38] Currently, an outstanding issue of material delivery has been a limiting factor in the progression of the concept.

2.5.3.1 Patches and Gels

There are many proposed delivery techniques used to introduce these biomaterials including injectable gels, patches, and glues. [10,34,38,27,22] While the previously mentioned biomaterials show much promise in their ability to mimic the specific conditions needed for cellular growth and differentiation, integration of the biomaterial, particularly in the heart, has been met with little success. Delivery via injectable gels and glues typically results in limited amounts of cellular retention and transplant survival. [6] The bolus injected is given a limited amount of time to solidify or adhere to the area of infarct, and is often extruded away from the target area by the beating heart through the point of entry. The uneven cellular distribution found in injected gels is also a limitation in treating specific target areas in full. [6,20] The application of bioengineered patches on the region of infarction is similarly plagued with problems. Typically several millimeters in thickness, they are often unable to induce cellular diffusion towards the intended necrotic tissue, resulting in minute delivery percentages. The average thicknesses of the patches are also typically too large to support vascularization and nutrient diffusion throughout the scaffold thickness, limiting the feasibility of the construct while in vivo. [6,33]

Ultimately, the absence of a technique that addresses the needs of a biomaterial construct in full has led to limited progress towards the fulfillment of significant myocardial regeneration. In order to become a viable technique, site-specific and controlled scaffold delivery must be obtained while suitable to the highly specific conditions regarding cellular diffusion, growth, viability, and differentiation.

2.5.3.2 Tissue Embedded Microthreads

As opposed to the previously mentioned biomaterials, the application of microthreads as engineered scaffolds for cardiac regeneration has been a more promising development due to their combination of structural properties and compatibility. [8,9] Microthreads, which are often similar in structure and mechanical strength to natural tissue, are known to aid in cellular migration, and are biocompatible and bioreabsorbable. In particular, collagen and fibrin have been the material of choice for experimental thread-based delivery based upon numerous structural and cellular properties.

Collagen is the major insoluble fibrous protein in the extracellular matrix and in connective tissue. This matrix in the heart is a major determinant of myocardial stiffness as it is responsible for the support and alignment of myocytes and capillaries. [12] Found in the later stages of wound healing, collagen deposition increases the strength of the wound. Collagen is also a natural substrate for cellular attachment, growth and differentiation, and promotes cellular proliferation and differentiation. [35] Although there are numerous types of collagen in the body, approximately 85 percent consists of types I, II, and III. [35] To date, collagen biomaterial experimentations have been largely based upon type I collagen in the form of gels, glues, and most recently microthreads. [35] In many cases, collagen gels have encouraged cellular growth; however, these materials often lack sufficient mechanical strength necessary for the regeneration of load-bearing tissue. [8] Collagen is also a biodegradable molecule broken down by metabolic processes. The biodegradability of collagen can be reduced however, by the introduction of cross-linking. [5] Threads composed of collagen have been investigated *in vitro* and *in vivo* for regeneration of various tissues with promising results regarding cellular attachment and proliferation. [8]

Fibrin is a fibrous protein formed from the conversion of fibrinogen, a glycoprotein in the blood, into fibrin by the enzyme thrombin. In the body, fibrin plays a large role in the initial stages of tissue regeneration via a provisional matrix that fills the wounded area and promotes the infiltration and containment of cytokines. These matrices assembled from fibrin, fibronectin, and vitronectin regulate cell migration, proliferation, and gene expression through integrin signaling. [9,36] The role fibrin plays in the provisional matrix, biocompatibility, and high binding affinity for growth factors has led to research and development of fibrin biomaterials for applications central to cardiac regeneration. To date, fibrin biomaterials produced have been gel- or glue-based, with varying mechanical and structural properties dependent on fibrin concentrations. [6, 7] Similar to collagen gels, these materials often lack sufficient mechanical strength necessary for the regeneration of load-bearing tissue. [8]

Fibrin microthreads have recently been developed and tested as a scaffold for cardiac regeneration. Experiments have demonstrated that fibrin microthreads have similar structural homology to native tissues and significantly greater mechanical strength in comparison to fibrin gels. [6,9] In vitro studies have also proven the ability of fibrin threads to form microenvironments that mimic the highly specific physiologic conditions necessary for hMSC growth, migration, and differentiation. As depicted in Figure 8, microthreads range from 20-50 µm, are roughly circular, able to be cross-linked for increased strength and stiffness, and can be loaded with growth factors to influence cellular processes. [9] Additionally, studies have shown that the substrata of microthreads woven together aid in the natural alignment and orientation of cells. [9] The ability of microthreads to be specifically placed in infarct target areas, as depicted Figure 9, in conjunction with optimal cell orientations, offer additional advantages in comparison to fibrin gels, as thread and cell containment increases the efficiency of cellular delivery.

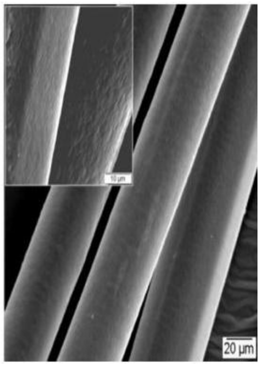

Figure 8: Microthread Size

Photo Credit: George Pins PhD

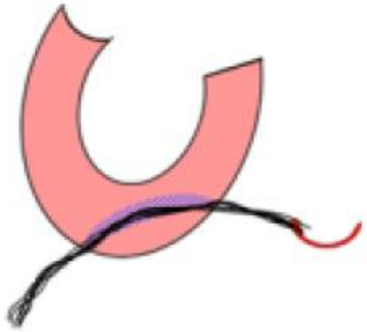

Figure 9: Site Specific Placement Tissue Embedded Microthread

Photo credit: Glenn Gaudette PhD

2.6 Histological Techniques – Evidence base for non-invasive techniques.

The methods of tissue preparation fall in two distinct groups, the observation of living cells and that of preserved or “fixed” dead cells. [26] The majority of tissue evaluations derive from fixed and prepared slides each of which is more or less permanent. A slide or “section” of tissue is prepared by first preserving the protoplasm, commonly in neutral buffered formalin, in a process called fixation. The tissue is then processed, using concentrated ethanol to dehydrate the sample and paraffin wax, turning the tissue into a hard paraffin block. The hard block is then cut into thin slices, typically anywhere from 3 to 10 microns thick, using a microtome. [14, 26] Tissue mounting, staining (enhancement of cell components), and covering of the section then must occur prior to observation and analysis. This process as a whole is a long and laborious method, in which a days’ work typically yields only a handful of photographs, but unavoidable in order to effectively view static cell activity and function. [4, 14]

The examination of the anatomy and physiology of complex organs via histological analysis is similarly a laborious and intricate process. In theory, histological techniques have been noted to produce superior spatial resolution and discrimination of cell types in comparison to magnetic resonance imaging (MRI), but are limited by their preparation and compilation processes. One must compile from the numerous two-dimensional sections, a three-dimensional picture in order to determine the significance of cellular activity. Histological images have to be registered, slice by slice, and transformed to create a 3D histological stack as depicted in Figure 10. [4] Compilation time aside, accurate tissue slice alignment is often lost during mounting and 2D imaging, resulting in the distortion of the 3D image. It must also be noted that static preservation techniques are not perfect and in instances can result in inaccurate representations prior to image compilation. Alterations in static conditions dubbed "artifacts" result in tissue shrinkage, folding, or wrinkling of sections, and can be attributed to various chemicals or imperfect sectioning during the preparation process. [26]

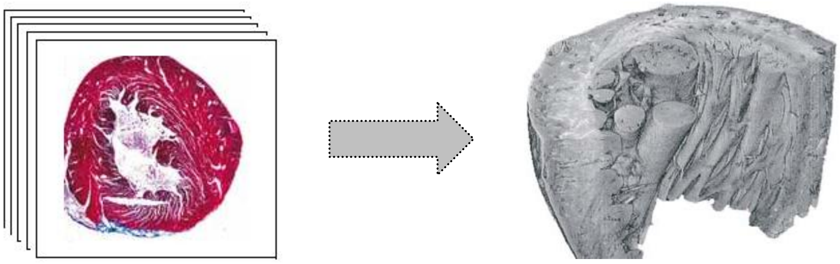

Figure 10: 3D Construct Via Histological Sectioning [26]

Studying the structure and function of living cells is less common, but holds numerous advantages in that these attributes can be observed simultaneously. The obvious limitation of observing living cells relates to the short time period in which they are usable. Preservation of living cells outside of the body has been achieved through the development of a technique known as tissue culture, in which the extracted tissue is placed in a physiological medium mimicking the natural environment.

2.7 MRI Overview

Magnetic Resonance Imaging (MRI) has proven to be an effective tool in the medical industry and has increasingly become the modality of choice for radiological examinations since its development and introduction in the 1970s. The imaging method, based principally on signals from water protons, allows for noninvasive evaluation of tissue and the surrounding medium in real time. Advancements in recent years have revealed its potential not only to visualize anatomy but also physiological processes, including cardiac regeneration. The physical principles regarding MR image acquisition are moderately complex, and thus great depth of the process will not be defined in this text. This section will cover a brief but concise description of fundamental nuclear magnetic resonance (NMR) principles, how this nuclear phenomenon is acquired to construct an accurate image, and an overview of different types of images and their image acquisition parameters. This section, adapted from Haacke[15], Hornak [21], McRobbie[29], Smith[37], and a dissertation by Stuart Howes[63], will help to provide an adequate understanding of the MRI principles necessary to follow the subsequent experimental design and analysis. If the reader wishes for a more in depth description of MRI and NMR they should refer to the texts cited for a more thorough description.

2.7.1 Nuclear Spin in a Magnetic Field

Biological tissue contains a high concentration of water and the attached hydrogen atoms each have a magnetic dipole moment, which arises from the nuclear spin associated the unpaired proton in the nucleus. The associated magnetic field can be considered comparable to microscopic bar magnet (Figure 11) and is commonly represented as a vector quantity with both direction and magnitude. [29]

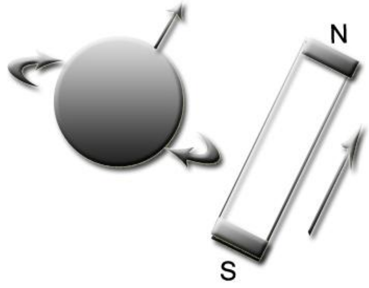

Figure 11: Magnetic Moment of a Nuclear Dipole

These nuclear magnetic moments are oriented randomly in normal tissue, however, in the presence of an external magnetic field B_o provided by the MRI system, the nuclear magnetic moments of the water protons will aligned themselves in one of two possible directions (parallel or anit-parallel) with respect to the B_o field direction as shown in Figure 12. The B_0 field is typically denoted in the Z-direction of a Cartesian coordinate system. The magnetic energy it takes for the nuclear magnetic moments to align parallel to B_o is slightly less than the energy required to align in the anti-parallel orientation, resulting in a slightly greater number of protons aligned in the parallel direction. [15] Since each nuclear dipole in the anti-parallel state cancels out one nuclear dipole in the parallel state, there is a slight excess of nuclei in the lower

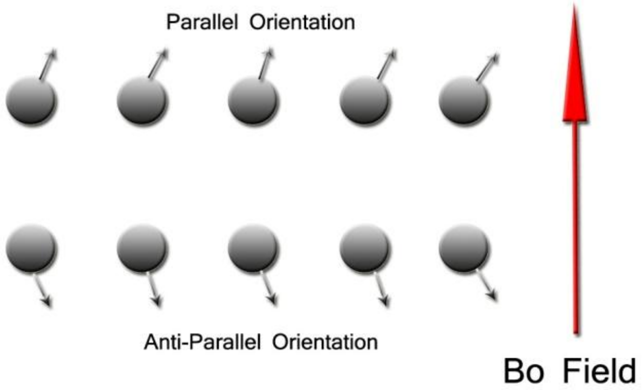

Figure 12: Parallel and Anti-Parallel Orientation

energy state at equilibrium, resulting in an overall net magnetization vector M_0, shown as the red arrow in Figure 13, which is aligned with the B_0 field.

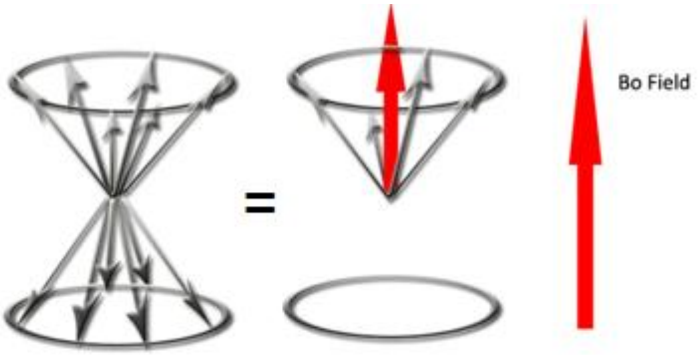

Figure 13: M_0 Vector

As depicted in Figure 14, the B_0 field also exerts a force (torque) on each of the individual nuclear magnetic moments which, because of quantum mechanical constraints, are inclined at an angle with respect to B_o. As a result, the nuclear magnetic moments precess about the direction of the B_0 field. [37] This precessional motion is characterized by an angular frequency which is denoted as ω_0. The angular frequency of protons, known as the Lamor frequency, is proportional to the applied external magnetic field given by:

$$\omega_0 = \gamma B_0$$

Equation 1: Larmor Equation [29]

where γ is the gyromagnetic ratio, a constant unique to each nuclei, and B_0 is the strength of the external magnetic field. For a hydrogen proton, γ is approximately 2.68×10^8 rad/s/Tesla. The range of the angular frequencies experienced by atoms in typical magnetic fields is approximately equivalent to the frequency range of radio waves (3 KHz to 300 GHz). [37]

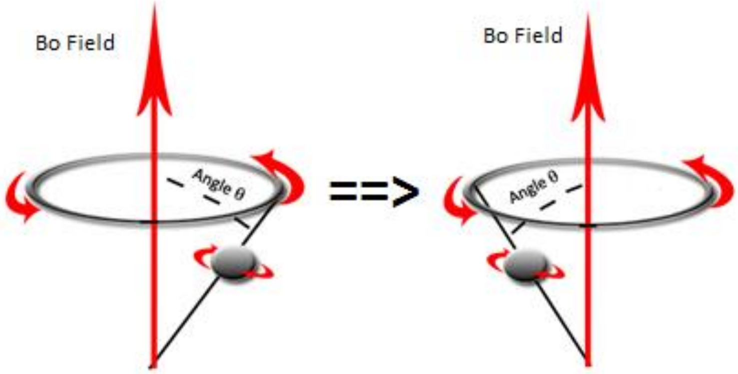

Figure 14: Nuclear Precession and Angle

2.8 MRI Parameters and Their Physical Origins

When at equilibrium, the protons in the system align with the applied B_0 magnetic field, producing an overall net magnetization (M_0) that is completely aligned in the z-direction and is often referred to as the longitudinal or M_z magnetization. At this point, M_Z is equal to M_0 and there is no magnetization within the plane perpendicular to the magnetic field; this is referred to as the transverse or X, Y plane (Figure 15). The transverse magnetization, M_{XY}, is equal to zero at equilibrium. [21]

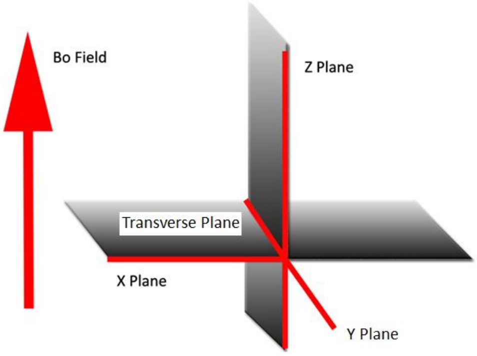

Figure 15: NMRI Coordinate System

A radiofrequency (RF) coil is used to excite the protons within the system and move them out of equilibrium by sending a current through the RF coil. This current is at a frequency equal to the precession frequency of the protons in the system. This creates a resonance condition and forces a transfer of energy to the nuclei. The applied current can be controlled in order to force the net magnetization vector, M_0, of the system to be rotated at a specific angle away from the direction of the B_0 magnetic field depending on the duration of the RF excitation. [15] In the process, transverse, M_{XY}, magnetization is created. The system then returns to equilibrium as a function of time. The RF coil that excites the nuclei can also be used as a current detector. This coil detects the current that is induced by the transverse, M_{XY}, magnetization as it returns to its equilibrium state. This detection forms a signal which looks like a dampened sine wave. This is known as the free induction decay (FID), which in normal MR imaging is never directly measured. Instead signal echoes are created and measured which are described in the following sections.[29]

2.8.1 Longitudinal Relaxation

The longitudinal relaxation is also referred to as the spin-lattice relaxation time. As depicted in Figure 16, an applied 90° RF pulse causes the net magnetization of the M_0 vector to rotate from the M_Z into the M_{XY} plane. Immediately after the 90° RF pulse M_Z equals zero and M_{XY} equals M_0. [21] The nuclei then relax back to their alignment along the M_Z direction until the equilibrium state is restored. The longitudinal relaxation time is a measurement of the amount of time it takes for the nuclei to return to their equilibrium state (in the Z-direction) after the system is excited by a 90° RF pulse.

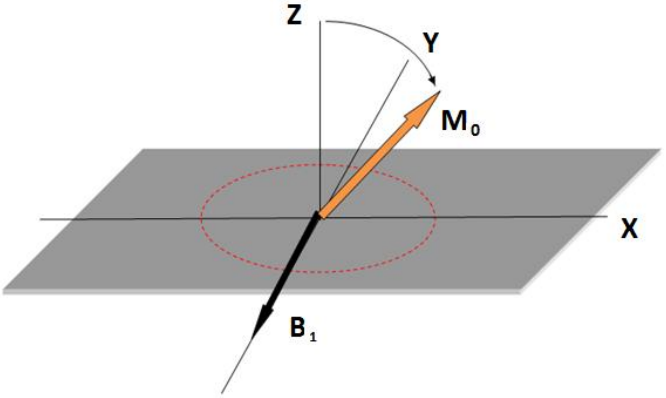

Figure 16: M_o Vector Rotation into the Transverse Plan following 90° Pulse

The nuclei dissipate the acquired energy with the surrounding environment, commonly known as the lattice, which is where the name spin-lattice relaxation originates. While the longitudinal M_Z magnetization returns to equilibrium, the transverse M_{XY} magnetization created following the 90° RF pulse returns to zero, its equilibrium value. The mathematical equation representing the behavior of the longitudinal magnetization as a function of time, i.e., $M_Z(t)$, is given in the following equation:

$$M_Z(t) = M_0\,(1 - e^{-t/T1})$$

Equation 2: The Change in Transverse Magnetization as a Funtion of Time [29]

where t represents time, and T_1 is the time constant associated with the rate of recovery of longitudinal magnetization, which is different for each different kind of tissue. The time scale is equal to zero immediately after the RF pulse is turned off. The T_1 parameter is typically defined as the amount of time that it takes for the magnetization to recover to 63% of its equilibrium value after the RF pulse is applied.[37] Figure 17 shows a plot of Equation 2 using the T_1 relaxation times of 898 ms and 382 ms for muscle and fat, respectively. At a RF pulse repetition time (TR) of approximately 650 ms, the curve shows the relative difference in signal intensity between the two different tissues is based on differences in their intrinsic T_1 relaxation time values. This is the fundamental basis of T_1-weighted MRI as a means of distinguishing between different tissue types.

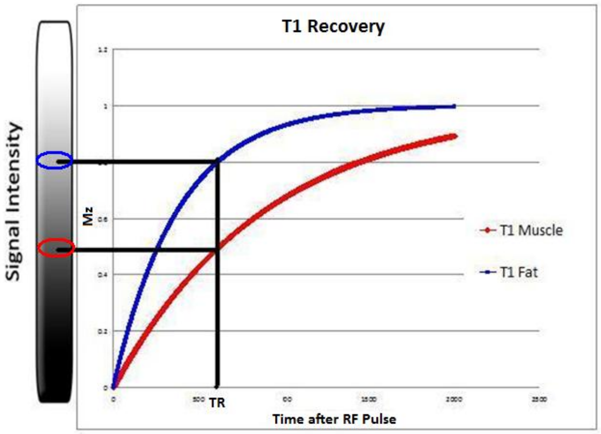

Figure 17: T_1 Recovery of Muscle vs. Fat

2.8.2 Transverse Relaxation

Transverse relaxation is another parameter that can be used to distinguish tissues. Transverse relaxation, unlike its counterpart, longitudinal relaxation, is a much faster process. Instead of this relaxation occurring in the longitudinal direction, it occurs within the transverse plane. This can also be commonly referred to as spin-spin relaxation, because the energy exchange that is measured between the various spins within the system itself. Immediately after the initial 90° RF pulse, all of the nuclear magnetic moments are aligned in the transverse plane. The spins then begin to separate, or un-align, because of the variations within the local magnetic field; which lead to variations in the precessional frequencies of the nuclei. These frequency variations, as shown in Figure 18, tend to cause the spins to "fan out".

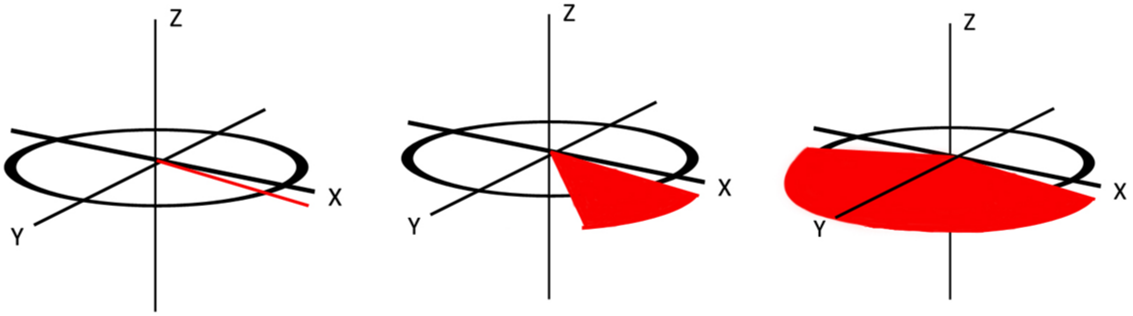

Figure 18: Un-alignment of Nuclear Spins Over Time

This reduces the overall net magnetization in the transverse (XY) plane. [15] This ultimately results in the overall sum of all transverse components converging to zero. The mathematical equation that shows the behavior of the transverse magnetization as a function of time, i.e., M_{XY} (t), is given by:

$$M_{xy}(t) = M_0 e^{-t/T2}$$

Equation 3: Change in Transverse Magnetization as a Function of Time [29]

where t represents time, and T_2 is the time constant associated with the rate of decay of transverse magnetization, which is different for each different kind of tissue. Just like the longitudinal magnetization, the time scale is equal to zero immediately after the 90° RF pulse is turned off. The T_2 variable is defined as the amount of time that it takes for the transverse magnetization to decay to 37% of its initial value. [37] In comparison to the longitudinal equation, the T_2 relaxation time is always less than or equal to the T_1 relaxation time. Figure 19 shows the plot of Equation 3 using the T_2 relaxation times of 29 ms and 68 ms of muscle and fat, respectively. At an echo time (TE) of approximately 45 ms, this curve shows the relative difference in signal intensity between the two different tissues. This is the fundamental basis of T_2-weighted MRI as a means of distinguishing between different tissue types.

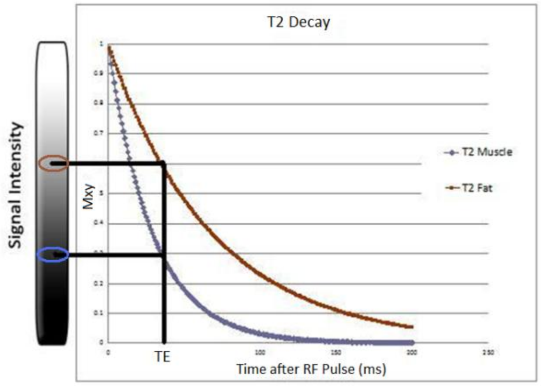

Figure 19: T2 Decay of Muscle and Fat

2.8.3 Image Acquisition

When attempting to acquire an MR image, there are electrical signals being detected from the protons at different locations within the specimen being imaged. These signals are then mapped back to their spatial locations when reconstructing the image. Each picture is made up of multiple pixels. An image is typically thought of as having x and y coordinates. This allows each pixel to have its own defined location using a specific set of x and y coordinates. The data recorded is primarily thought of as the amount of current induced within the RF coil from that location in space. This data has to be mapped from its location within the specimen, back to a specified location within the image itself. This is done with slice selection techniques, frequency-encoding magnetic field gradients, and phase-encoding magnetic field gradients. These techniques are able to encode the spatial position of the protons within the sample.

A magnetic field gradient varies the magnetic field strength with respect to position. For example, a one-dimensional linear magnetic field gradient along the x axis in a magnetic field increases the magnetic field linearly in the x direction. These gradients can be applied in the x, y, and z directions are denoted G_x, G_y, and G_z respectively. This creates a range of MR frequencies, with the acquired signal amplitude proportional to the number of nuclei at each location along the direction of the magnetic field gradient. This technique is called frequency encoding and causes the resonance frequency to be proportional to the spatial position of the nuclei giving rise to the signal. [21]

Slice selection in MRI is the selective excitation of nuclei in a particular plane via a one-dimensional, linear magnetic field gradient during the period that the RF pulse is applied. As depicted in Figure 20, a 90^o pulse applied in conjunction with a magnetic field gradient will rotate spins which are located in a slice or plane. Slice selection is the first process applied to encode the spatial signal location, followed by a phase encoding gradient and the previously mentioned frequency encoding gradient. Each pixel corresponds to a specific slice in the specimen, based upon the phase and frequency of the data collected. The signal is processed and separated into its different components through the application of the Fourier transform. [15]

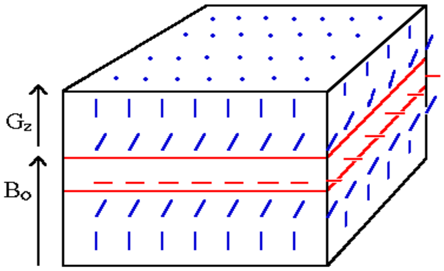

Figure 20: Slice Selection via Field Gradients and a 90^o RF Pulse [21]

The phase encoding gradient determines the spatial signal location along a second dimension by variations in the phase of the transverse magnetization. The phase encoding gradient assigns a specific phase angle to a transverse magnetization vector which is dependent on the location of the transverse magnetization vector along the direction of the phase encoding field magnetic gradient. A gradient in the magnetic field when applied along the X direction will result in vector precession about the direction of the applied magnetic field (Figure 21). While the phase encoding gradient is on, each transverse magnetization vector has its own unique Larmor frequency according to the vector location along the gradient. If the gradient in the X direction is turned off, the external magnetic field and thus the Lamor frequency of each spin vector will again be identical. As depicted in Figure 22, the phase angle of each vector however is not identical because of the previously applied phase encoding gradient. This difference uniquely defines the spatial location of the nuclei along the phase encoding gradient direction.

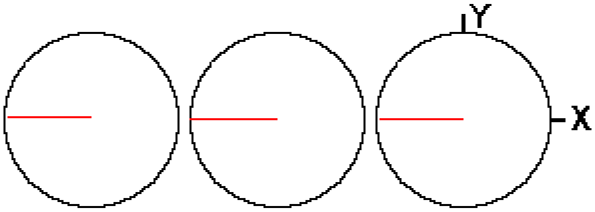

Figure 21: Vector Phase prior to Phase Encoding Gradient

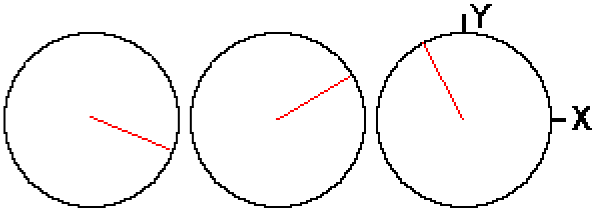

Figure 22: Vector Phases after Phase Encoding Gradient

2.8.4 Image Weighting

Each of the relaxation processes, longitudinal and transverse relaxation, occurs simultaneously. Therefore, the resulting signal contains contributions from both relaxation rates. Individual relaxation data can however be differentiated through a process known as image weighting. Image weighting can be achieved by varying the pulse sequences applied to the RF coil to select which relaxation process dominates the image. [29]

There are two basic timings regarding RF pulse sequence, which when altered correspond to a different type and strength of weighting; TE interval, or echo time, which is the time at which the signal is measured after the pulse happens, and TR interval, which is the time between excitation repetitions of the RF pulse.[21]

When creating a T_1-weighted image, short TR and TE intervals are used. This is used to enhance T_1 contrast and to minimize T_2 contrast. When creating a T_2-weighted image, long TR and TE intervals are used. These ultimately enhance T_2 contrast and minimize T_1 contrast. Another type of image-weighting is known as proton-density weighting. This is obtained by using long TR and short TE intervals. This reduces both T_1 and T_2 contrast, which can be extremely useful in determining the water content in a given specimen. [29]

2.9 Contrast Enhanced Imaging

Relaxation times of water protons can be manipulated by using MRI contrast agents. The principles of how these agents work is beyond the scope of this project. When introduced at minimal, non-toxic concentrations, these agents interact with the ^1H protons to reduce their T_1 and T_2 relaxation times. This then enhances the image contrast and allows for better analysis of targeted areas. Negative contrast agents are typically small, coated microcrystalline magnetite particles often called superparamagnetic iron oxide (SPIO). These agents produce local field inhomogeneities via spin-spin relaxation effects, resulting in shorter T_2 relaxation times. Positive contrast agents cause a reduction in the T_1 relaxation time. The active element is typically gadolinium, manganese, or iron; which have unpaired electron spins in their outer shells. The ability of contrast agents to cause an increase in proton spin energy or decrease in proton spin energy will result in the targeted medium to either brighten or darken, depending on whether T_1- or T_2-weighting is being used, respectively. [29, 63]

Gadolinium chelates have been commonly used as MRI contrast agents to essentially highlight certain tissues of interest. Superparamagnetic iron oxide (SPIO) particles were introduced after gadolinium-based agents and are often used to facilitate in differentiating between healthy and damaged tissues. [62] Due to their numerous advantages, they are now recognized as the preferred MRI contrast agent for certain applications. These particles provide the most change in signal intensity, especially in T_2 weighted images, and they mitigate the low contrast agent sensitivity of MRI since they are composed of thousands of iron atoms. Unlike gadolinium-based agents, SPIO particles are biocompatible since they are composed of biodegradable iron which could potentially be reused by cells for iron metabolism. Some other advantages of SPIO particles are: (1) that their surface is usually coated with dextran, which allows for straightforward chemical linkage of functional groups and ligands; (2) they can be easily distinguished by electron and light microscopy; (3) and they can be magnetically manipulated according to size. [63]

3.0 Project Strategy

Preliminary efforts to create a logical and effective approach to the project were concentrated on understanding and building upon the initial client statement. Through feedback and consistent communication with the clients and potential users, project objectives, functions, and constraints were defined, helping to provide clearly defined project goals and establish direction. A final revised client statement was written following this process and consistently referenced to gauge the compliance of each decision and procedure.

3.1 Initial Client Statement

To design and develop an *in vitro* model system using MRI technology to non-invasively evaluate the position of tissue-embedded microthreads that are used as cell-delivery systems to promote the regeneration of cardiac muscle.

3.2 Objectives Functions & Specifications

3.2.1 Objectives:

Based on meetings with clients and potential users of the final product(Appendix 1: Client Meeting Minutes), as well as a review of relevant literature, design objectives were produced for the experimental procedure and structures involved via an objective tree. These objectives were based upon the qualities and functions that stakeholder's 'want' the device to possess. Often apparently interchangeable, objectives were clarified and separated from goals, following the definition that objective statements claim what the design will be. Using a pairwise comparison chart, objectives were weighted in accordance to their importance to the stakeholders and considered in the design process. The implemented pairwise comparison chart and objective tree can be found in Appendix 2: Objectives. A summary of these objectives are organized and defined below:

Phantom Modeling System

1. Cardiac phantom representation should be accurate.

  1.1. Material strength in comparison to native and ischemic cardiac tissue.
  1.2. MR relaxation parameters in comparison to native and ischemic cardiac tissue.
  1.3. Anatomically accurate shape and volume in comparison to a normal heart.
  1.4. Anatomically accurate volume of infarct area.

    1.4.1. Shape of tissue.
    1.4.2. Positioning of tissue.

2. Cardiac modeling system should be stable and reproducible.

  2.1. Cardiac phantom composition should be consistent during subsequent tests.

    2.1.1. Normal tissue representation.
    2.1.2. Ischemic tissue representation.
    2.1.3. Embedded microthread.
    2.1.4. Applied contrast agent(s).

  2.2. Phantom component locations should be stable and reproducible during subsequent tests.

    2.2.1. Normal tissue representation.
    2.2.2. Ischemic tissue representation.
    2.2.3. Embedded microthread.
    2.2.4. Applied contrast agent(s) – minimal diffusion.

3. Tissue component representations and microthread should be easily differentiated.

  3.1. Native and ischemic relaxation rates should be altered via contrast agents to obtain desirable differentiation.
  3.2. Microthread relaxation rate should be altered via contrast agents to obtain desirable differentiation.

4. Modeling system should be easy to use.

  4.1. Construction should be simple and directions complete.

    - 4.2. Microthread placement and stabilization is easily achieved and maintained
    - 4.3. Cardiac phantom placement and stabilization in the MRI is easily achieved and maintained.
    - 4.4. System alterations can be easily calculated and implemented.

5. Modeling system should be cost effective.

Data Acquisition- Image Parameters

1. Image parameters should be similar to those used *in vivo.*

- 1.1. TE or echo time should be consistent with in vivo cardiac acquisition timing.
- 1.2. TR time should be consistent with in vivo cardiac acquisition timing.
- 1.3. Coil size in relation to the phantom should aim to achieve similar resolution.
- 1.4. Spatial resolution (Field of view/ # Digital points) should be considered to sufficiently view and accurately locate the embedded thread.

2. Safety considerations should be defined and applied to design and procedures.

- 2.1. Usage of ferromagnetic material.
- 2.2. Usage of protective hearing equipment.
- 2.3. Local RF power disposition.

3. Data acquisition should be easily obtainable and implementable.

- 3.1. MR parameters can be easily altered via provided calculations.
- 3.2. Acquisition of image is in a time efficient manner.

4. Utilization of MR machine should be done in a time and cost effective manner.

Data Analysis

1. Analysis procedure should be applicable to images acquired *in vivo.*
2. Software should allow for easy image analysis.
3. Imaging software should display areas of differentiation accurately.

- *3.1.* Microthread location, size, and shape.
- *3.2.* Infarct location, size, and shape.

4. Software analysis should be time and cost effective.

When establishing the objectives of this particular project, desired design functions and attributes were organized into distinct categories as illustrated above. In conjunction, each category serves to address the defined goals in the most comprehensive manner possible. The first category, the phantom modeling system, serves to address and define all objectives encompassed in the *in vitro* modeling system. This included not only the cardiac phantom but microthread and contrast agent design and integration within the phantom. Objectives within the category were weighted according to their importance via input from our clients and potential users. Accuracy, precision, and reproducibility were considered to be the most important primary objectives for the modeling system, as they are directly correlated with the production of plausible and applicable results. The relative ease of use and cost effectiveness, although objectives, were considered important only after plausible results were achieved. The pairwise comparison charts and final weights for each level of objectives can be found in Appendix 2: Objectives

The next category of objectives defined and weighted included those relevant to data acquisition of the designed *in vitro* modeling system. The determination and design of how valuable data will be acquired via MRI is equally important in the fulfillment of the project goals. The aim of *in vitro* experimentation was to model *in vivo* conditions to establish proof of concept and refine methodology and safety procedures prior to preclinical or clinical trials. Any experimental parameters that are not applicable *in vivo* should immediately be discarded. In light of this information, using MR parameters that will be applicable *in vivo* was determined to be the objective of utmost importance. Safety when using MR equipment is, in relation to the other two categories, a high priority. The usage of ferromagnetic material in and around MRI machinery can be particularly dangerous because of their attraction to the powerful magnets.

The analysis of the acquired data was the final category designed to more easily define project objectives in a complete and logical organization. Data analysis will utilize software and designed code to achieve desired analysis options and results. Accuracy and *in vivo* applicability were considered to be the most important primary objectives for data analysis, as they are again most directly correlated with the production of plausible and applicable results, and the achievement of defined goals.

3.2.2 Constraints:

Similar to design functions, identified constraints of our project must be met in all aspects of design considerations. It is important to note that each component and procedure of the design process must be fully integratable with each object. Failure or incompatibility of components or procedures in any instance must be considered a project constraint. Identified constraints will ultimately be used to develop and define project specifications. Listed below are the primary constraints defined for this project:

1. All materials and/or methods must be:
    a. Considered safe and non-detrimental to health of users and test subjects.
    b. Biocompatible within the experiment.
    c. Applicable to *in vivo* experimentation(s).
    d. Within the project budget.
2. Excluding the cardiac phantom, all materials must be biocompatible with regards to *in vivo* experiments.
3. Phantom size parameters must not exceed MRI machine parameters.
4. Spatial resolution must be the same order of magnitude as the microthread.

5. The phantom modeling system and internal components must remain in a static position in the MRI machine during testing.
6. The project must be completed within the allotted time frame.

Constraints via Limitations

1. Limitations of image noise reduction and contrast via image construction software and contrast agents respectively.
2. The ability of the tissue phantom and applied contrast agents to mimic the physiological conditions found in normal and infarcted myocardium.
3. The ability of the contrast agent(s) to remain in the area of intended delivery.

3.2.3 Functions:

Objectives by definition are desired attributes that describe what the object will *be*, while a function is a task the designed device should *do*. In principle there are five primary objects that must be considered when establishing design functions: the microthread, tissue phantom, contrast agents, data acquisition, and data analysis. All objects or processes that do not directly agree with any of the defined functions should immediately be disregarded or reengineered. Listed below is a brief summary of the primary functions derived from the complete list found in Appendix 3: Functions

1. Phantom modeling system should accurately and precisely mimic the corresponding *in vivo* system.
2. Application of contrast agent(s) should allow for differentiation of relaxation times of the embedded microthread and phantom modeling system.
3. Resulting image (via the phantom modeling system, data acquisition parameters, and analysis tools) should display the desired differences in signal intensity between the microthread and the surrounding tissue phantom.

4. Data acquisition and analysis tools should allow for 3D reconstruction of the cardiac phantom and embedded microthread.
5. Applied software should allow for microthread analysis.
6. Resulting image (via the phantom modeling system, data acquisition parameters, and analysis tools) should accurately and precisely display microthread location.

As stated above, the phantom modeling system should accurately and precisely mimic corresponding *in vivo* systems. The development of a model that represents an *in vivo* system is crucial to the eventual application of test parameters *in vivo* and relevance of collected experimental data. The application of contrast agent(s) will be the primary tool utilized to differentiate the embedded microthread. Doping (treating) the thread and targeted areas of the *in vitro* system should allow for sufficient differentiation via different relaxation times. The resulting image acquired given the experiment design and parameters should also display differences in signal intensity corresponding to differences in set relaxation times. It is important that the acquired images and designed analysis of them are accurate relative to *in vitro* experimental results.

3.3 Specifications

Following the definition of the project objectives, constraints, and functions; design specifications were defined. Specifications aim to denote the various standards that the design system must fulfill. There are certain specifications that must be met by individual components in order for the total design system to function properly. Similar to the defined objectives, project specifications were categorized into the phantom modeling system, the MR data acquisition, and the software image analysis tools. Categorization of specifications was utilized in hopes to address project specifications to the fullest extent possible as well as evaluate the efficacy of the device after experimental analysis. The evidence base for defined specifications and calculations can be found in Appendix 4: Calculations for Specifications

General

1. Project must stay within budget, \$156/person and \$468 in total.
2. Project must be completed by April 21, 2010.

Phantom Modeling System

1. Phantom must mimic the relaxation rates of both normal and ischemic heart tissue at 3T which are 31.9 ms and 44.1 ms, respectively (see Appendix 4: Calculations for Specifications).
2. Phantom size must be no larger than 38 mm in diameter in order to fit inside the RF coil.
3. Normal cardiac and ischemic cardiac representations must have MR contrast differences of at least 20% in order to accurately represent the differences expected in actual normal and ischemic heart tissue.

Data Acquisition

1. The field strength of the MRI machine is 3T. (Original field strength was to be 4.7T)
2. Rate of change of the magnetic field must not exceed 60 dB/dt.
3. Spatial resolution of the MR image must be the same order of magnitude as the micro thread for viewing purposes. Resolution should be approximately 30 μm to account for 2-3 pixels of the thread size.
4. Image acquisition must mirror the heart rate of the patient (approximately 80 bpm).

Data Analysis

1. Microthread and tissue phantom must differ in signal intensity by at least 20%.
2. Image size should be a 256 x 256 x 128 image.

3. Repetition times (TR) must be a minimum of 50 ms and a maximum of 800 ms and the echo time (TE) must be static, for T1 weighted image.
4. Repetition times (TR) must be static, and the echo time (TE) must be a minimum of 10 ms and a maximum of 200 ms For a T2-weighted image.

3.4 Revised Client Statement

The objective is to address the current constraints regarding the accurate and dynamic monitoring of cardiac regeneration using human mesenchymal stem cells (hMSCs). The design and development of an *in vitro* modeling system will consider safety, reproducibility, size and physiological specifications, and ease of use among other factors. Embedded microthreads utilized must be biocompatible and able to support hMSC growth, migration, and differentiation. Magnetic Resonance Imaging (MRI) will be used as the primary non-invasive modality to optimize the differentiation of normal and ischemic cardiac tissue and the embedded microthreads. Introduction of MR contrast agents to increase differentiation should be safe, biocompatible, and contained within the intended area of delivery. Software analysis will facilitate in the acquisition of quantitative data concerning the microthread and infarct region, specifically its location and dimensions within the phantom.

3.5 Project Approach

3.5.1 Project Assumptions

When developing a project approach several initial project assumptions in regards to the implementation of crucial design components were defined. These assumptions aim to rationalize the usage of materials and methodologies provided by the clients in their initial project statement.

- Implementation of MRI technology and contrast agents on an *in vitro* cardiac model representation is the best choice for non-invasive differentiation and analysis.

- Microthread technology is among the most promising forms of cellular therapy and will aid in the progression of myocardial regeneration and cardiac functionality.

- Completion of experimentation and analysis is achievable given project constraints, with the most notable being time, budget, and resource constraints.

3.5.2 Project Goals

Defined in the initial client statement, the primary goal of the project was to develop an *in vitro* cardiac modeling system and utilize MR technology in such a way as to evaluate and confirm the position of tissue-embedded microthreads. Primary users specializing in cellular therapy, specifically through implementation of biomaterials, have the need for an improved material evaluation method that is quick, easy, and accurate in comparison to current techniques. To fulfill the project goal a list of specific aims was defined:

1. Design experimental parameters to increase accuracy and ease of thread location.
    a. Determine optimal MR settings applicable for phantom tissue differentiation.
    b. Explore contrast agent possibilities and agent concentrations as a technique to enhance microthread and tissue differentiation.
        i. Determine the best agent application methodology on the microthread.
        ii. Determine the best agent application methodology on the tissue phantom.
    c. Enhance software parameters for image analysis and thread differentiation.
    d. Design an image mapping system to enhance location confirmation.
2. Design and develop an *in vitro* cardiac modeling system that mimics *in vivo* physiological parameters necessary for tissue differentiation via MR imaging.
3. Develop an accurate 3D modeling system.
    a. Explore software and compilation possibilities to optimize microthread/tissue differentiation and thread location accuracy.

b. Explore the possibility of designing and implementing various 3D image analysis tools.

3.6 Project Hypotheses

In addition to the revised client statement, project hypotheses and specific aims were formulated in accordance with the defined project goals. The provided literature review was utilized to rationalize the various hypotheses made regarding MR imaging, cardiac phantom accuracy, and contrast agent differentiation.

3.6.1 Hypothesis #1

In comparison to current techniques, magnetic resonance imaging will allow for accurate, non-invasive, and less time consuming detection and differentiation of infarct and normal tissue.

Rationale: Magnetic Resonance technology is a noninvasive imaging tool that is able to noninvasively deduce the nuclear magnetic resonance (NMR) properties of tissue and interstitial space within the body. When MR parameters are properly defined and applied, variations in water proton MR relaxation times give rise to varying spatial signal intensities that create contrast that depicts functional anatomy and physiological processes. Studies have shown that the mature scar tissue resulting from an infarction is comprised primarily of collagen and has significantly less water concentration in comparison to native cardiac tissue. [47] These differences produce significant contrast between representative scar and native tissue signal intensities on T1- and T2-weighted images, allowing for visual differentiation. With an accurate model of tissue locations and boundaries, the placement of the microthread can be determined pre-operation in such a way as to maximize effectiveness.

In theory, histological techniques have been noted to produce superior spatial resolution in comparison to magnetic resonance imaging, but are ultimately limited by artifacts accumulated during the preparation and compilation processes. MR technology also has advantages in regards to its non-invasiveness and constant monitoring capabilities.

Specific Aim: Develop optimal MR parameters that maximize tissue differentiation and image quality. (Noise, blurring, contrast factors must be analyzed and set for optimization)

3.6.2 Hypothesis #2

A cardiac tissue phantom designed within the constraints of the project can accurately mimic attributes crucial to tissue differentiation and thread location in vivo.

Rationale: In regards to the scope of this project, the parameter essential for tissue differentiation and accurate thread location via MR imaging is the variation in water proton MR relaxation times as a function of tissue water concentration. Average concentrations of H_2O in native cardiac and fibrous scar tissue have been calculated in numerous studies resulting in representative approximations to incorporate in tissue phantom design. Representative solid state and containable viscous models of native tissue have been developed commercially and independently for experimental purposes within the defined constraints of this project. [64] Incorporation of tissue representative of the scarred region of infarct is hypothesized to be achieved via contrast agents or through alterations in the water concentration of a defined and containable area.

Specific Aim: To design an accurate working model representative of native and ischemic tissue within the designated objectives, functions, and constraints.

3.6.3 Hypothesis #3

Contrast agents when properly chosen will aid in optimization of differentiation and thread location accuracy.

***Rationale**:* MR relaxation times have the ability to be manipulated through the application of contrast agents. When introduced these agents interact with targeted ^{1}H protons, affecting the relative spin energy and energy transfer rate, resulting in the decrease in MR relaxation times. Positive contrast agents alter signal intensity via reduction in T_1 and T_2 relaxation times while negative contrast agents result in altered signal intensity via a reduction in T2 relaxation times. Proper application of image contrast agents can greatly enhance tissue and thread contrast and the relative ease of differentiation.

Specific Aim: Experiment and determine optimal agent concentrations for differentiation and application for tissue and microthread containment.

4.0 Design Alternatives

Developing and analyzing design alternatives were utilized to select the best possible design given project objectives, functions, and limitations. In order to commence the design phase, the project team first had to understand the wants and needs of both the clients and potential users. Although we were able to accomplish much of this with the completion of the revised client statement, we needed to assure that our clients and users agreed with our methodology and progression. To do this, a series of pairwise comparison charts (PWCC) were implemented to prioritize the upper and lower level objectives as defined in the revised client statement.

4.0.1 Pairwise Comparison Charts

Table 1 (shown below) is an example of the pairwise comparison charts (PWCC) designed by our project team for first order of objectives. Using these tables, input from the client and users, and information from the conducted literature review, we were able to rank the objective in each row against the objective in each column. If it was decided that the objective in the corresponding row was more important than that of the corresponding column the objective was assigned a "1." The total score and objective importance was then calculated by adding up each objective row. The opinion of objective importance increased with the increase in the collective total. Complete ranking of the objectives in each section of the experimental design can be found in Appendix 2: Objectives.

Table 1: Objective Pairwise Comparison Chart Example

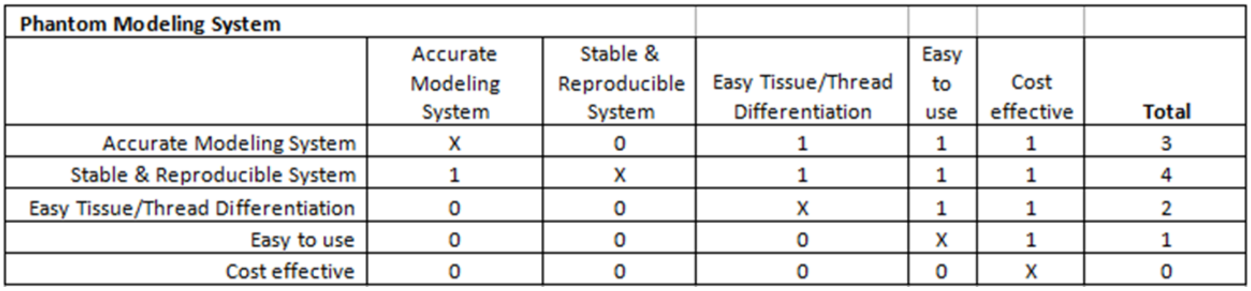

Phantom Modeling System						
	Accurate Modeling System	Stable & Reproducible System	Easy Tissue/Thread Differentiation	Easy to use	Cost effective	**Total**
Accurate Modeling System	X	0	1	1	1	3
Stable & Reproducible System	1	X	1	1	1	4
Easy Tissue/Thread Differentiation	0	0	X	1	1	2
Easy to use	0	0	0	X	1	1
Cost effective	0	0	0	0	X	0

Table 2 depicted below is an example of the weighted objectives for the first order of objectives as completed by our clients (Professor Pins and Sotak), the project team, as well as a potential user (Professor Gaudette, a cardiac tissue engineering and cardiovascular biomechanics specialist). Objectives were ranked from 0 – 4 by each noted person or group according to the objective's importance in the final design. The opinion of objective importance increased with the increase in the corresponding number assigned. It is important to also note that each number could only be used once by each person or group. Once the initial ratings were collected they were averaged and weighted, resulting in the final rating of objective importance. The objectives with the highest weighted totals were considered the most important during the experimental design process as they were crucial to accomplish project goals and objectives. Complete ranking of the objectives in each section of the experimental design can be found in Appendix 2: Objectives.

Table 2: Weighted Objectives from Project Stakeholders Example

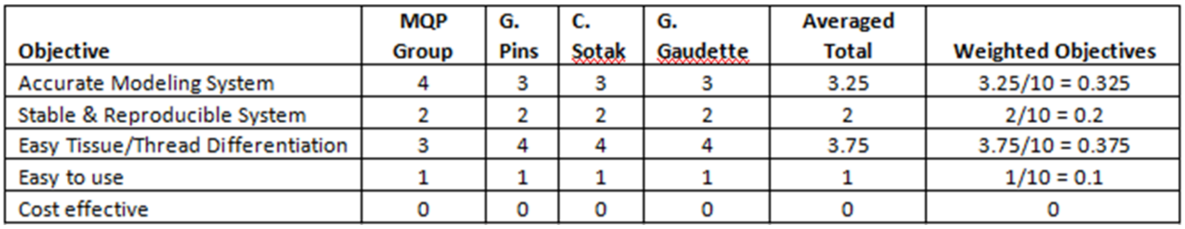

Objective	MQP Group	G. Pins	C. Sotak	G. Gaudette	Averaged Total	Weighted Objectives
Accurate Modeling System	4	3	3	3	3.25	3.25/10 = 0.325
Stable & Reproducible System	2	2	2	2	2	2/10 = 0.2
Easy Tissue/Thread Differentiation	3	4	4	4	3.75	3.75/10 = 0.375
Easy to use	1	1	1	1	1	1/10 = 0.1
Cost effective	0	0	0	0	0	0

4.0.2 Needs Analysis

Although prioritizing the project goals and objectives provides a good basis for the experimental design phase, it is equally important to determine and separate client/user wants and needs. While omitting design parameters and attributes that the user wants can often affect the relative performance and success of the design, omitting design needs can result in the immediate failure of the design. A needs analysis was completed in order to determine the functional needs of the final product (properties that the results must have), as well as the physical limitations. During this step of the design process, the defined project functions, specifications, constraints, and weighted objectives were all taken into account to conduct a proper need vs. wants analysis:

Client/User Needs

1. Cardiac Phantom must:

    a. Be smaller than 38 mm in diameter due to the RF coil size.
    b. Contain microthread in a static position.
    c. Contain a contrast agent adhered to the embedded microthread with minimal diffusion into the surrounding medium.
    d. Contain a microthread with evenly applied concentration of contrast agent.

2. Data Acquisition:

  a. Parameters must produce at least 20% grayscale contrast between the phantom and microthread.
  b. Signal-to-noise ratio must be much greater than 20.
  c. Spatial resolution must be the same order of magnitude as the micro thread for viewing purposes.

3. Data Analysis must allow for:

  a. Accurate healthy and infarcted tissue volume/shape/location measurements.
  b. Accurate microthread volume/shape/location measurements.

Client/User Wants

1. Cardiac Phantom

  a. Signal intensity of healthy and infarcted areas of the phantom should mimic calculated *in vivo* values.
  b. Shape, including location and relative size of infarction should be representative of typical *in vivo* measurements.
  c. Should possess the ability to contract/expand, similar to an *in vivo* system.
  d. Should produce minimal resistance when delivering the microthread.

2. Data Acquisition

  a. Acquire 3D images since they have larger SNR than and are superior in image analysis potential than 2D images.
  b. Contrast-to-noise ratio should be calculated to optimize contrast.
  c. Use advanced techniques to mimic *in vivo* parameters and enhance image quality and data analysis.

3. Data Analysis

  a. Software should be easy to use and inexpensive.
  b. Allow for further analysis via processing functions, including contrast enhancement, density profiling, smoothing, sharpening, edge detection, median filtering, and spatial convolution.

4.1 Conceptual Designs

The completion of the needs analysis and objective prioritization transitioned the design process into the conceptual design phase. This stage began by identifying various means to execute the previously defined project functions. These means were then considered to be conceptual designs and were critiqued via evaluation matrices based on their potential ability to fulfill the project objectives and constraints. The morphological chart, shown in Appendix 3: Functions lists the defined functions along with the possible means that were produced via brainstorming. To devise design alternatives, combinations of feasible and compatible means were paired. The compiled design alternatives were organized and evaluated via a numerical matrix. The following list briefly describes a number of the possible alternatives for each category of the design. A more thorough description of each alternative design, including means weighting and 3D CAD modeling can be found in Appendix 5: Design Alternatives.

4.1.1 Cardiac Phantom Modeling System

Cardiac Mold

Conceptual designs of the material representing and mimicking normal and ischemic cardiac tissue were limited, primarily because of the unique and numerous characteristics needed. In total tissue models comprised of gelatin, various vegetation, and synthetic water-based polymers were conceptualized, determined to be viable, and analyzed via evaluation matrices. The following list briefly describes each conceptual design:

- An *In vitro* WP phantom model comprising of one type of vegetation will be doped with a varying degree of a contrast agent to model approximate normal/infarct myocardial tissue relaxation rates and rate differences. A non-metallic divider will be placed in between the differing representative tissue to restrict the diffusion of contrast agents

- An *In vitro* VF phantom model comprising of two different types of vegetation doped with a varying degree of a contrast agent to model approximate normal/infarct myocardial tissue relaxation rates and rate differences. Each component will be sectioned off via a non-metallic divider to restrict the diffusion of contrast agents.
- An *In vitro* Gelatin Model. The inside of a compartmental mold would contain gelatin of varying concentration used to mimic the differing relaxation rates of normal/infarct myocardial tissue.
- Numerous cardiac phantoms designed specifically for imaging purposes were discovered on the web, most notably an MRI specific phantom composed of a synthetic water-based polymer called zerdine. The signal intensity created from the material was stated to be consistent with that of normal cardiac tissue.

Contrast Agent Application

In addition to the design of viable cardiac material the application of a contrast agent is a vital component to the final phantom modeling system. A contrast agent will be applied to the embedded microthread and possibly the cardiac material itself to ultimately increase image contrast and phantom component differentiation. As stated in the literature review, contrast agents can be either negative or positive, affecting the spin-spin relaxation and spin-lattice relaxation, respectively. The numerous positive and negative contrast agents researched can be found in Appendix 5: Design Alternatives.

- A calculated concentration of Superparamagnetic Iron oxide (SPIO) particles, a negative contrast agent, will dope the microthread and/or cardiac phantom to produce a variation in relaxation and thus signal intensity.
- A calculated concentration of a positive contrast agent will dope the microthread and/or cardiac phantom to produce a variation in relaxation and thus signal intensity.

4.1.2 Data Acquisition

Conceptual designs for data acquisition parameters revolved around review of relevant material, specifically the MR portion of the literature review and utilized scholarly articles. Given the countless number of imaging techniques and parameter combinations proposed designs were kept relatively simplified, with limited cardiac specific applications.

- Delayed enhancement MRI (DE-MRI) utilizing ECG-gating, inversion recovery (IR), and rewound (fast) gradient echo sequencing (FGE). IR time will be chosen to null the normal myocardium making areas of infarction appear hyper-enhanced.

- Fast Spin Echo MRI (FSE-MRI) utilizing ECG-gating and blood suppression preparation (BSP). The FSE technique can acquire multiple lines of data per repetition limiting the effect of image artifacts due to movement of thoracic cavity during pulse sequences.

- Spin Echo MRI (SE-MRI). The SE technique is similar to the FSE described in the previous design however this technique will be simplified. All techniques and preparations regarding cardiac imaging will be ignored limiting this technique to stationary objects.

4.1.3 Data Analysis

Similar to data acquisition, numerous programs were found to be applicable to fulfill the goals of the project. The analysis techniques below were chosen on their ability to analyze the compiled data in a efficient and effective manner.

- ImageJ [70] software with 3D analysis plug-in. ImageJ is a public domain, Java-based image processing program developed to display, edit, analyze, and process a variety of image formats. ImageJ can calculate area and pixel value statistics, measure distances and angles, and supports standard image processing functions.

- Matlab program is a high-level language and interactive environment that enables computationally intensive tasks to be performed, such as 3D image reconstruction, or even image analysis, faster than with traditional programming languages such as C, C++, and Fortran.

- Segment is a free image analysis tool for Windows developed specifically for cardiovascular MR image analysis. This program has the ability to acquire and analyze 2D, as well as 3D MRI and CT images. Some analyses that can be done in the program are length, volume, and area measurements in the regions of interest.

4.1.4 Design Evaluation

As the excerpt of the matrix in Table 3 below shows, each alternative was weighted according to how well they fulfilled relevant objectives and constraints. The top column lists design alternatives, while the left column and its corresponding rows list the design objectives and constraints. The second column denotes the objective weights that were established earlier via the weighted objective trees. Each objective was categorized in regards to how promising they were to fulfill defined objectives, with 0 being the least promising and 2 being the most promising. To gauge the objective promise, discussions within the group were conducted, noting the pros, cons, and limitations of each design to fulfill the objective. The designs were then rated by multiplying the design promise (from 0 - 2), by its corresponding objective weight. The final weighted score for each design was obtained by adding the weighted metric score for each objective, as shown in Table 4. Constraints were given a score of Y or N based on the designs ability to fulfill the constraint. A complete list of evaluated designs and comparison scores can be found in Appendix 5: Design Alternatives.

Table 3: Example Evaluation Table

Example		**Design** →			
Objectives & Constraints	**Weight**	**D1**	**D2**	**D3**	**D4**
O: Objective 1	**0.325**				
C: Constraint 1	**Y/N**				

Table 4: Design Alternatives

Phantom Design Alternatives	**Total Score**
WP phantom w/ corresponding relaxation and tissue differentiation	***2***
VF phantom w/ corresponding tissue differentiation	***1.675***
Gelatin phantom w/ corresponding relaxation and tissue differentiation	***1.8***
DAQ Design Alternatives	**Total Score**
Delayed enhancement MRI (DE-MRI) utilizing ECG-gating,IR, and FGE	***1.624 (-)***
Fast Spin Echo MRI (FSE-MRI) utilizing ECG-gating and BSP	***1.624 (+)***
Simple Spin Echo MRI with limited cardiac monitoring techniques	***1.082***
Image Analysis Design Alternatives	**Total Score**
ImageJ software with 3D analysis plug-in (NIH)	***1.833***
Matlab data visualization and analysis (Mathworks)	***1.833***
Segment software for Windows (Cardiac MR group & Medviso AB)	***2***

After the fundamental methodology was determined it was necessary to further devise and weight detailed alternative design components within the cardiac modeling system. Methodology including microthread placement, contrast administration, and contrast type among others were all crucial in the achievement of a phantom compliant with defined functions and specifications. Designs were evaluated against the design objectives using another numerical matrix utilizing the same process described above. Depicted below is first an example of the matrix structure, Table 5, followed by the resulting scores associated with each design candidate, Table 6. Complete calculations and tables can be found in Appendix 5: Design Alternatives.

Table 5: Example Sub-objective Table

Static placement of Phantom		**Method** →		
Objectives	**Weight**	**M1**	**M2**	**M3**
O: Objective 1	**0.375**			
O: Objective 2	**0.325**			

Table 6: Design Alternatives Sub-objectives

Candidate Methods to:	**Subcategories**	**Total**
Statically place phantom in RF coil		
	Secured containment	***1.9***
	Phantom pinning	***1.325***
	Flat bottom phantom	***0.725***
	Clamp	***1.525***
	Velcro	***1.675***
	Double sided tape	***1.675***
Deliver phantom contrast agent		
	Injection	***1.625***
	Static Saturation	***1.625***
	Dynamic Saturation	***2***
Deliver microthread contrast agent		
	Adhesion	***1.9***
	Static Saturation	***1.425***
	Dynamic Saturation	***1.6***
Aid in relaxation differentiation		
	Gadolinium based	***1.1***
	Iron Oxide based	***2***

4.2 Feasibility Study for Alternative Designs

4.2.1 Feasibility for Cardiac Phantom

We performed feasibility tests for each of our four initial cardiac phantom designs in order to determine which could suffice for future MRI testing. For each model feasibility testing consisted of attempting to insert a thread, which mimicked a microthread, into the representative tissue, using a surgical needle (3/8 circle cutting edge). Observations and notes were then taken regarding the ease of delivery and the ability of the material to statically contain the thread. We were not able to test the contrast agent application or undergo any MRI testing for these models, due to material availability at the time, but research was done to determine if the proposed methods were plausible.

Design 1 – Single Vegetation Model

In order to test the single vegetation phantom model, we used a regular store bought white potato in an attempt to replicate cardiac tissue. This model was cost effective and could easily be reproduced since there is an ample supply of vegetation. We then tried to place a thread into the potato using a surgical needle (3/8 circle cutting edge). Unfortunately, we were not able to effectively pierce the potato using the surgical needle. The stiffness of the potato limited insertion of the needle and the amount of microthread encased in the material.

Design 2 – Dual Vegetation Model

We performed feasibility studies on the dual vegetation model (design 2), which comprised of a white potato and carrot. The white potato represented healthy myocardium, while the carrot characterized infarcted myocardium. Once again, although it was slightly more expensive than the previous model due to the fact that it requires two different types of vegetation, it was still extremely cost effective and reproducible. After properly placing these two components, we administered a thread using a surgical needle (3/8 circle cutting edge). As depicted in Figure 23, with significant effort the needle was successfully able to pierce into the carrot and remained in place.

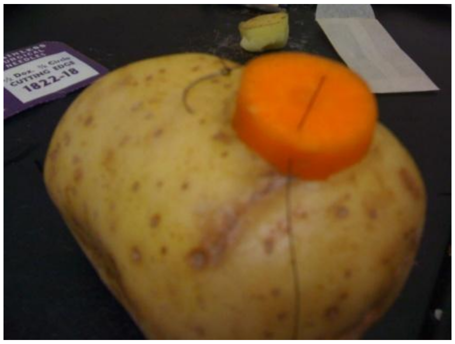

Figure 23: WPC Model

Design 3 - Gelatin Model

To test the gelatin phantom, Jell-O® gelatin was created in a plastic Easter egg container. Before we placed the Jello-O® mixture into the egg, we drilled two holes, one at each end of the bottom portion of the egg to eventually use for microthread placement. This design was not as cost effective as the other two models, but it was still fairly cheap and easily reproducible. The bottom portion of the egg would potentially represent the infarcted myocardium while the top would represent the healthy myocardium. The gelatin mixture was placed in the two portions of the Easter egg as shown in Figure 24, in order to prevent the mixture from leaking out of the drilled holes. The gelatin mixture was refrigerated overnight for it to gel.

Figure 24: Gelatin Formation in Phantom

After the gelatin was formed we took a surgical needle (3/8 circle cutting edge) and a thread and placed it inside the gelatin phantom through the drilled holes. This is shown in Figure 25 The needle was easily able to pierce into the gelatin phantom, and the thread was able to follow the needle tract and remained in position inside it.

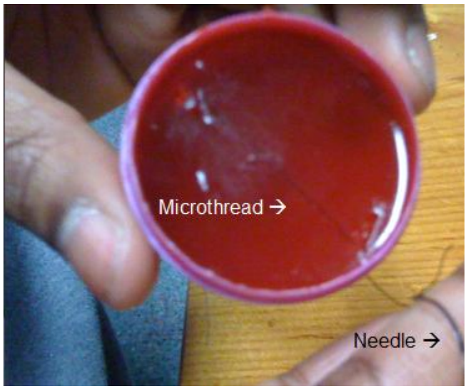

Figure 25: Initial Gelatin Cardiac Phantom

Design 4 – Commercial CIRS Model

No feasibility studies were conducted on the commercial CIRS cardiac phantom [64], as shown in Figure 26 due to an inability to obtain a sample of the synthetic zerdine based material. To determine if this model was feasible the product information, particularly the specifications, were analyzed. Ultimately the design was deemed unfit as a model for this project for several other reasons. This product is not cost effective or within the project budget as it costs $2000.

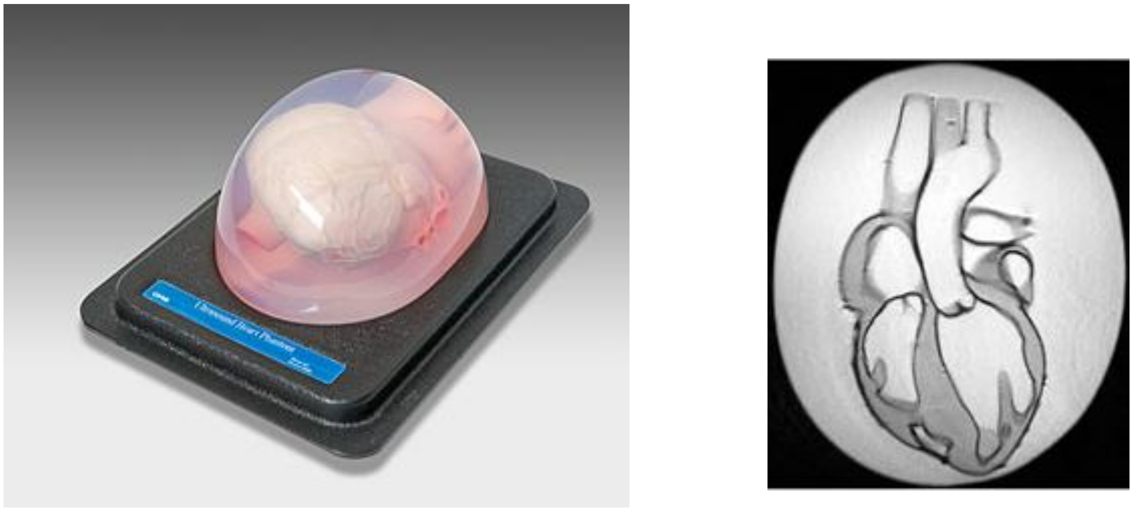

Figure 26: CIRS Synthetic Phantom Model

These cardiac phantom feasibility tests led us to believe that the gelatin model (design 3) was the best cardiac phantom. Although it was not as time efficient as the other models, in regards to the project budget it was cost effective and could further sustain and deliver the thread the easiest.

4.2.2 Feasibility for Data Acquisition

With the limited time and budget available for imaging, the project team was unable to test the feasibility of the conceptual MR parameter designs. Based upon the research compiled regarding basic and cardiac imaging techniques and consultation with of our project advisor Professor Christopher Sotak, an expert in the field, it was determined that the proposed methods were all reasonable. When deciding what particular data acquisition design to utilize, previous design evaluations and advisor recommendations were taken into account.

4.2.3 Feasibility for Data Analysis

Feasibility analysis for the chosen possible image analysis tools consisted of testing the capabilities applicable to our analysis project goals. Using a synthetic data set and multiple 2-D cranial MRI images, Segment, ImageJ, and MatLab were tested, analyzing the effectiveness and efficiency at which the data could be analyzed. Among the most important tests performed was the ability to calculate the volume and signal intensity of a chosen area. In Figure 27 and Figure 28 below, image analysis was performed of the signal intensity and the area of the highlighted portion, respectively.

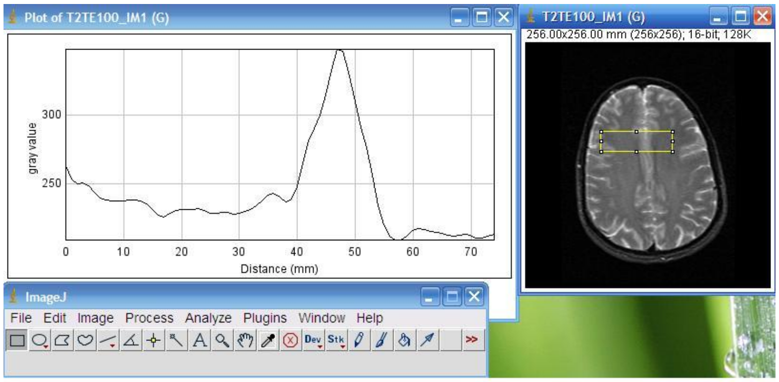

Figure 27: Signal Intensity Measurements using ImageJ

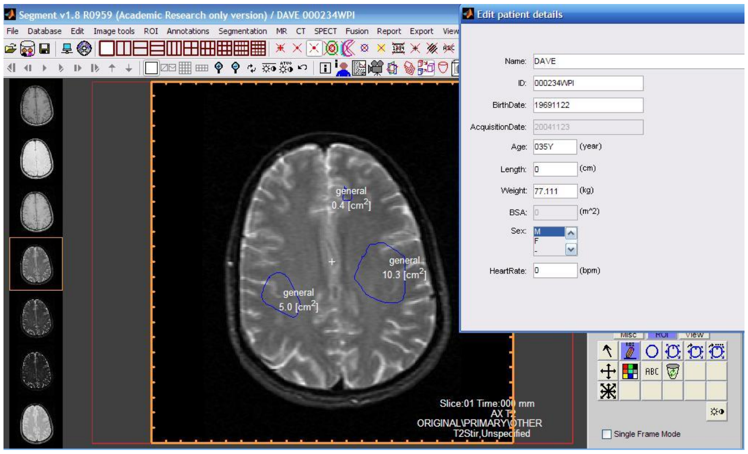

Name: DAVE
ID: 000234WPI
BirthDate: 19691122
AcquisitionDate: 20041123
Age: 035Y (year)
Length: 0 (cm)
Weight: 77.111 (kg)
BSA: 0 (m^2)
Sex: M
HeartRate: 0 (bpm)

Figure 28: Area Measurements using Segment

4.3 Preliminary Experiments

4.3.1 Phosphate Buffered Saline Preparation

The purpose of utilizing a phosphate buffered saline (PBS) was to ensure pH neutrality for the gelatin and ferumoxtran samples. The PBS was prepared using de-ionized (DI) water, 1.06 mM of potassium phosphate monobasic (KH_2PO_4), 155.17 mM sodium chloride (NaCl), and 2.97 mM of sodium phosphate dibasic ($Na_2HPO_4 - 7H_2O$). One liter of the PBS solution was prepared using 0.144 g of KH_2PO_4, 9.000 g of NaCl, and 0.794 g of $Na_2HPO_4 - 7H_2O$ in 1000 mL of DI water. The DI water was heated until warm in order to dissolve the other three ingredients in the water. The other three ingredients were then added and the mixture was stirred until there were no visible particles. The cooled solution was stored in two 500 mL sterile glass bottles to be used to buffer the gelatin.

4.3.2 Gelatin Formation Analysis

The gelatin used in our experiments was unflavored, unsweetened Knox® Gelatin, packaged in individual 8-ounce packages. Preliminary experiments aimed to determine the minimal concentration at which the gelatin/PBS mixture would become gelatinous. The gelatin concentrations (grams/mL) which were originally chosen were ¼%, ½%, 1%, 2%, 4%, and 10%. Each concentration was prepared by first measuring the appropriate volume and weight of PBS and gelatin powder, respectively. The components were then added into a 200 mL beaker and dynamically mixed at 200 °F until dissolved. Table 7 below notes the exact measurements used to prepare each concentration.

Table 7: Actual Gelatin and PBS Measurements

Volume PBS	Weight Gelatin	Percent Gelatin
99.75mL	0.252g	0.25%
99.5mL	0.506g	0.50%
99mL	1.002g	1%
98mL	2.009g	2%
96mL	4.001g	4%
90mL	10.002g	10%

After the gelatin was fully dissolved, 15 mL of each sample was then measured out using a motorize pipette and transferred into a 12-well plastic plate, as shown in Figure 29. Each sample was duplicated to ensure efficiency, so there were 2 samples of each gelatin sample in the 12 well plate container. The plate was then covered, and placed in a refrigerator at 37°C overnight to solidify.

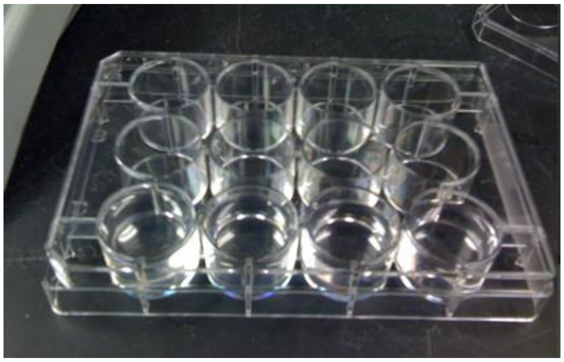

Figure 29: 12-Well Plate

The prepared gelatin was removed from the refrigerator after 24 hours and observed. The minimal gelatin concentration needed to form a gelatinous solid structure was approximately 1%. Each concentration greater than 0.5% solidified to a varying degree and was noted to increase in stiffness with increasing concentration.

4.3.3 Gelatin Reconstruction

From the previous observations, the minimum concentration which could be used in gelatin testing was 1%. In order to achieve a good concentration curve after imaging, a series of 4 concentrations were then chosen, 1%, 3%, 6%, and 10%. These percentages were prepared in a similar fashion to the previously prepared gelatin, however, instead of a 12-well plate, 4 separate 35-mm culture dishes were used. Table 8 below notes the exact measurements used to prepare each concentration.

Table 8: Actual Gelatin Concentration for Preliminary Imaging

Volume PBS	Weight Gelatin	Percent Gelatin
49.5 mL	0.5004 g	1%
48.5 mL	1.5007 g	3%
47 mL	3.003 g	6%
45 mL	5.004 g	10%

4.3.4 Ferumoxtran (AMI 227) Preparation

Ferumoxtran is an iron oxide based contrast agent, which was determined through analysis and its availability to be the best contrast agent to administer. The original sample that was received contained 17.8 mg of Ferumotrax iron oxide nanoparticles per mL of PBS. In order to conduct meaningful relaxation experiments as a function of agent concentration, solutions were choosen in increasing concentration increments. Concentrations of 5 µg/mL, 10 µg/mL, 20 µg/mL, 30 µg/mL, and 50 µg/mL were made by first diluting 10 µL of the original sample to of Fe to make the solution concentration more manageable to work with. After completion of the process the samples were ready to be imaged and analyzed. The calculations below list the concentration determination process.

10 µL + 35.56mL of PBS = **5 µg/mL**

10 µL + 17.9mL of PBS = **10 µg/mL**

10 µL + 8.89mL of PBS = **20 µg/mL**

10 µL + 5.92mL of PBS = **30 µg/mL**

10 µL + 3.55mL of PBS = **50 µg/mL**

4.3.5 Imaging Process and Parameters

The gelatin phantom and contrast agent imaging process was performed on the Philips Achieva 3.0T X-Series MRI, using a homemade 38 mm x 127 mm copper, birdcage RF-coil seated within a plexiglas tube. The software used, which was provided, was the Philips MRI SmartExam software. All of the testing was performed at the UMASS medical school, with the assistance of Mohammed Shazeeb, a PhD student at Worcester Polytechnic Institute. The Larmor Frequency for the samples was determined by multiplying the magnetic field (3.0T) by the gyromagnetic ratio of 42.56 MHz/T to give 127.5 MHz. Proper safety precautions were followed when performing all of the tests.

During this preliminary imaging session there were three gelatin samples that were measured, 3%, 6%, and 10% gelatin by concentration along with 5 samples of Ferumoxtran (AMI 227) 5 µg/mL, 10 µg/mL, 20 µg/mL, 30 µg/mL, and 50 µg/mL by concentration. The gelatin samples had been previously prepared in individual sterile polystyrene 35mm x 10mm cell culture dish (Corning Inc., Corning, N.Y.). The ferumoxtran samples were previous prepared and housed in 20 mL teardrop containers. Prior to imaging, each gelatin sample was individually seated inside the RF coil, aligned within the magnet itself, and the Larmor frequency set. The fermuxotran samples followed the same process, individually seated on top of plastic block and secured using electrical tape.

The first image of each sample taken was a survey image to verify proper placement and MR functionality. The sample was then run through various adjustable tests, with the purpose of figuring out roughly what TR and TE values to use for T1 data and T2 data, respectively. Finally, a magnetic resonance spectrum of each sample was taken in order to examine the frequency spectrum of the sample inside the RF coil. The following Table 9 shows the TR and TE values use for the different gelatin samples, as well as Table 10 shows the TR and TE values for the different AMI 227 sample scans.

Table 9: TR and TE Scan Values for Gelatin Samples

Gelatin Concentration (%)	Start TR (ms)	TR Interval (ms)	End TR (ms)	Start TE (ms)	TE Interval (ms)	End TE (ms)
3%	25 (ms)	400 ms	5625 ms	50 ms	100 ms	2350 ms
6%	25 (ms)	400 ms	5625 ms	50 ms	100 ms	2350 ms
10%	25 (ms)	800 ms	11225 ms	50 ms	100 ms	2350 ms

Table 10: TR and TE Scan Values for AMI 227 Concentration

Ferumoxtran Concentration (µg/mL)	Start TR (ms)	TR Interval (ms)	End TR (ms)	Start TE (ms)	TE Interval (ms)	End TE (ms)
5 µg/mL	25 ms	300 ms	4225 ms	25 ms	50 ms	1175 ms
10 µg/mL	25 ms	200 ms	2825 ms	25 ms	25 ms	600 ms

20 µg/mL	25 ms	200 ms	2825 ms	15 ms	15 ms	195 ms
30 µg/mL	25 ms	100 ms	1425 ms	11 ms	10 ms	191 ms
50 µg/mL	25 ms	50 ms	725 ms	11 ms	20 ms	371 ms

Each of the previous scans were performed consecutively starting with the 10% gelatin concentration and ending with the 3%, then again starting with the 5 µg/mL and ending with the 50 µg/mL. The first scans that were performed were the T_1-weighted scans, followed by the T_2-weighted scans.

4.3.6 Curve Fitting and Data Analysis

The program which was used to analyze our preliminary data was Matlab. Matlab provides a curve fitting tool that was used to plot and determine the T_1 and T_2 relaxivities of each set of samples. The data collected from the MRI was stored in a .xls extension documents and consisted of two data columns for each sample; one was the time and the other the signal intensity value. Two arrays were created from the two data columns and then plotted using the cftool(Time, Signal_Intensity) function in Matlab (a careful note is that the x-axis always comes first, where as the y-axis comes second).

After each graph was created for each sample, the curve fitting tool provided by Matlab was used. This tool fit a curve for the T_1 and T_2 relaxation curves for each data set and provided T_1 and T_2 values. The curve that we used to fit to the T_1 data was, y = (1 - 2 * exp ((-x) / t), where y is the signal intensity and the x is the time. The t is then determined through this curve fitting tool and is the T_1 relaxivity time for that data set. The curve in which we attempted to fit to the T2 data was, y = (2 * exp ((-x) / t), where y is the signal intensity and the x is the time. The t is then determined through this curve fitting tool and is the T_2 relaxivity time for that data set. The following two figures, Figure 30 and Figure 31, are two examples of the concentration curves that were received. The remainder of the concentration Curves can be found in Appendix 6: Preliminary Data

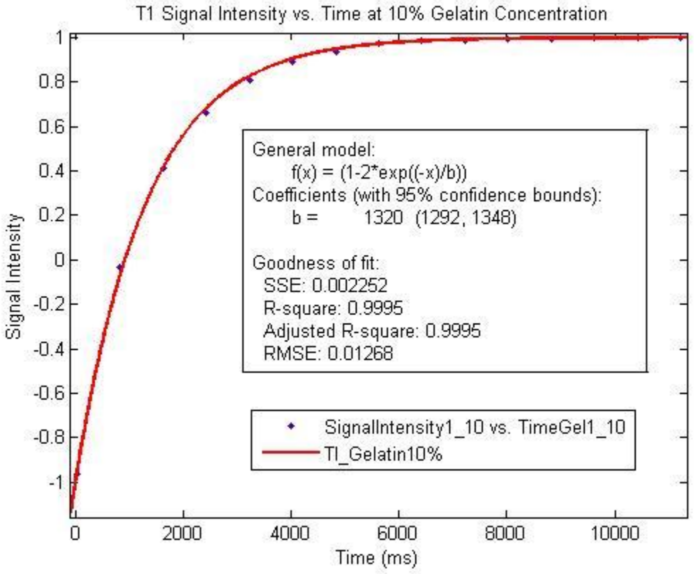

Figure 30: T1 Signal Intensity vs. Time at 10% Gelatin Concentration

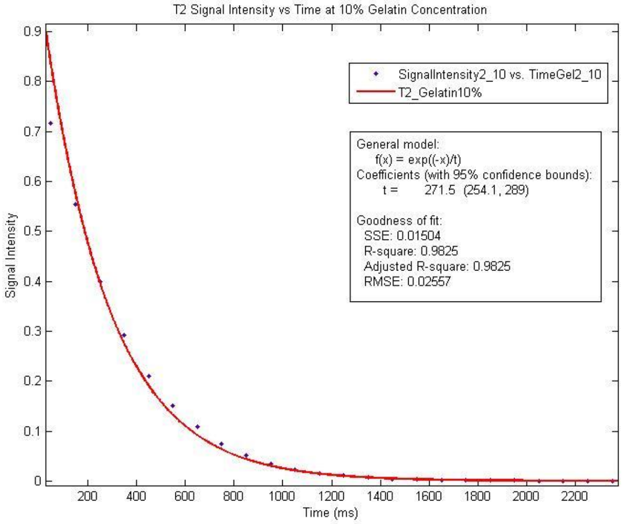

Figure 31: T2 Signal Intensity vs. Time at 10% Gelatin Concentration

4.3.7 Preliminary Data Results and Conclusions

4.3.7.1 Gelatin Initial Results

The following set of graphs, Figure 32 and Figure 33, provide results of the entire data set for each gelatin concentration, both for T_1 and T_2 weighting. The following Table 11 has each T_1 and T_2 value for each initial gelatin.

Table 11: Gelatin Concentration Initial Results

Concentration (%)	*T_1 (ms)*	*T_2 (ms)*	*R_1 (1/s)*	*R_2 (1/s)*
0.10	1320	271	0.76	3.68
0.06	1520	363	0.66	2.75
0.03	1800	294	0.56	3.39

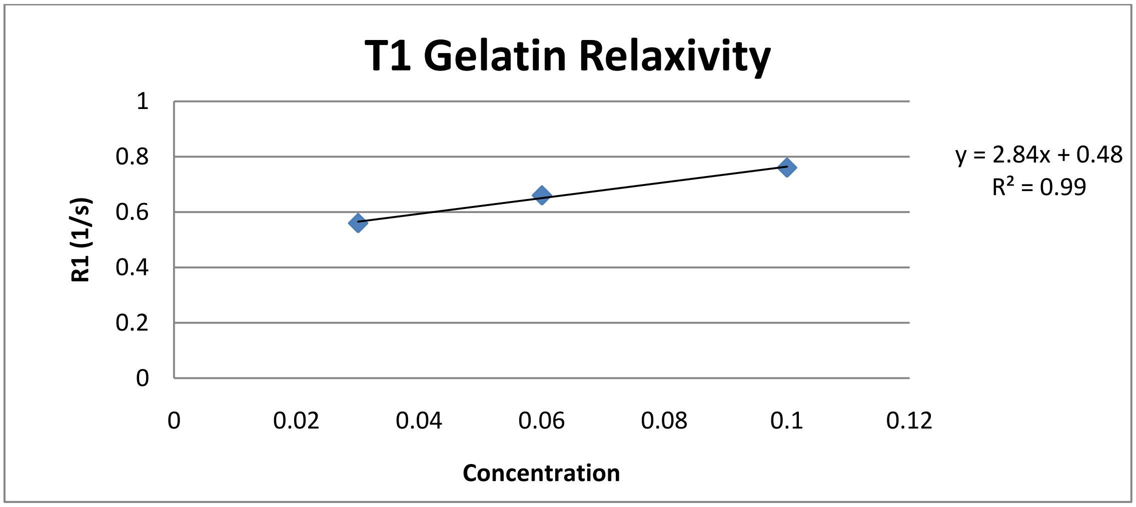

Figure 32: 1/T1 vs. Gelatin Concentration

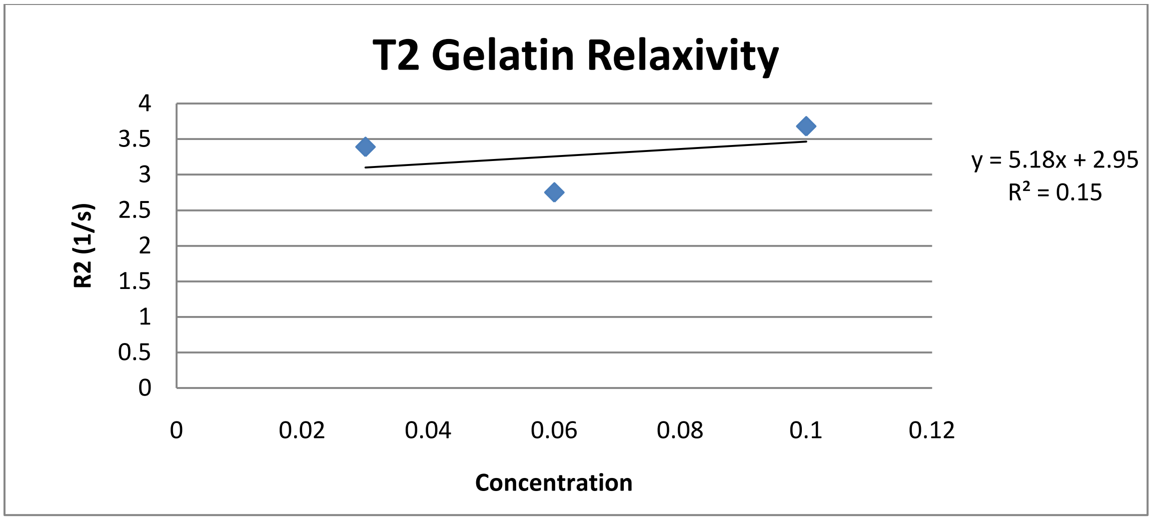

Figure 33: 1/T2 vs. Gelatin Concentration

4.3.7.2 Ferumoxtran Initial Results

The following set of graphs, Figure 34 and Figure 35, provide results of the entire data set for each Ferumoxtran concentration, both for T_1 and T_2 weighting. The following Table 12 has each T_1 and T_2 value for each initial Ferumoxtran sample.

Table 12: Ferumoxtran Concentration Initial Results

Concentration (ug/mL)	*T_1 (ms)*	*T_2 (ms)*	*R_1 (1/s)*	*R_2 (1/s)*
5	1033	143	0.968	0.699
10	640	70.5	0.156	1.41
20	401	29.7	0.249	3.36
30	244	20.8	0.409	4.79
50	157	12.9	0.634	7.73

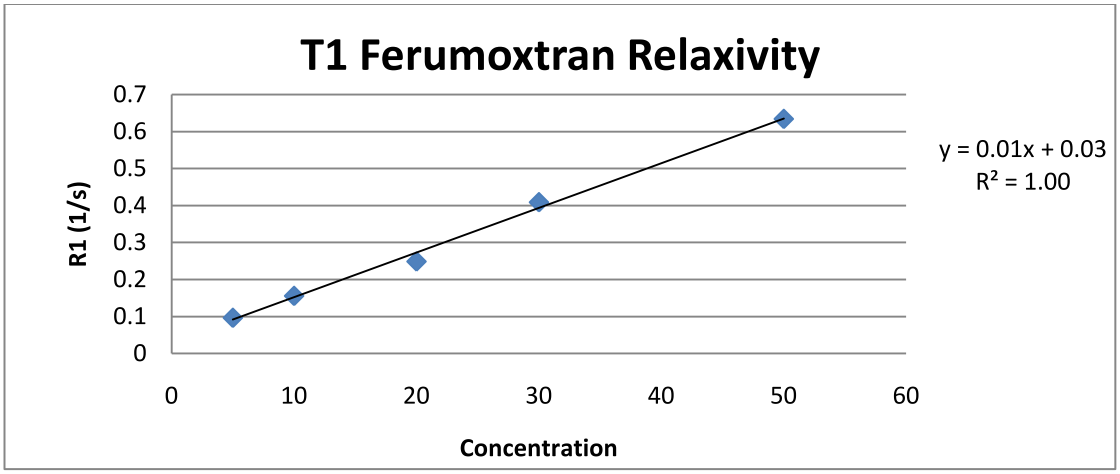

Figure 34: 1/T1 vs. Ferumoxtran Concentration

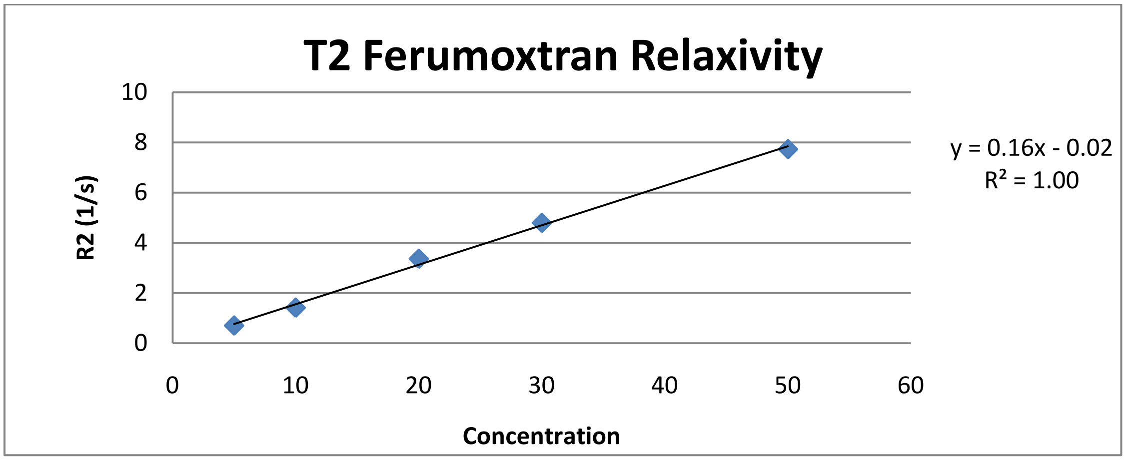

Figure 35: 1/T2 vs. Ferumoxtran Concentration

4.3.7.3 Preliminary Conclusions

Utilizing the data from preliminary results, the components of the phantom modeling system were calculated. The T_1 Gelatin curve, Figure 32, worked extremely well given the known value for T_1 relaxation of normal myocardium, approximately 1450 ms. To determine the percent concentration of gelatin needed to replicate native myocardial tissue 1450 ms was plugged into the concentration curve equation, $y = 2.84x + 0.48$, yielding a value of 7.1%. This value fits inside the range of data that was collected from the analysis of relaxivity (R_1) as a function of gelatin concentration and help to confirm the feasibility of our results. The concentration of gelatin needed to replicate *in vivo* infarct tissue was determined in a similar fashion, plugging in the known T_1 relaxation time, 1700 ms, into the concentration curve equation, $y = 2.84x + 0.48$. The resulting value was determined to be 3.1% gelatin by concentration.

Unfortunately, at the gelatin concentration needed to reproduce the cardiac T1 value (7.1%) the estimated *in vivo* T2 relaxation time of approximately 40 ms could not be accurately mimicked. Following the T2 concentration curve, at 7.1% gelatin concentration, the T2 relaxation time would be approximately 320 ms, a factor of 8 longer than the *in vivo* value. In light of this information it was decided to focus on producing accurate T_1 values, as altering the concentration of gelatin to mimic *in vivo* T_2 relaxation times would subsequently affect the T_1 value. Although T_2 relaxation times could not be mimicked, it was determined that the phantom could reproduce T_2-weighted contrast difference between the microthread and tissue itself. An analysis was performed to determine what value of TE would produce a 20% difference in cardiac signal intensity. At that TE value the concentration of Ferumoxtran that would produce a 60% reduction in signal intensity was determined, ultimately resulting in a 3:1 signal intensity ratio between the infarct tissue representation and thread doped with Ferumoxtran. Similarly this TE analysis can be done to produce the exact same signal intensity ratio imaging in vivo, the only difference being the TE value and Ferumoxtran concentration. It was concluded through the analysis that a TR of 1600ms, TE's ranging from 25 ms to 100 ms, and concentration of 10 ug/mL of Ferumoxtran would most closely produce the resulting signal intensity ratios described above. The preliminary parameter results are found in Figure 36.

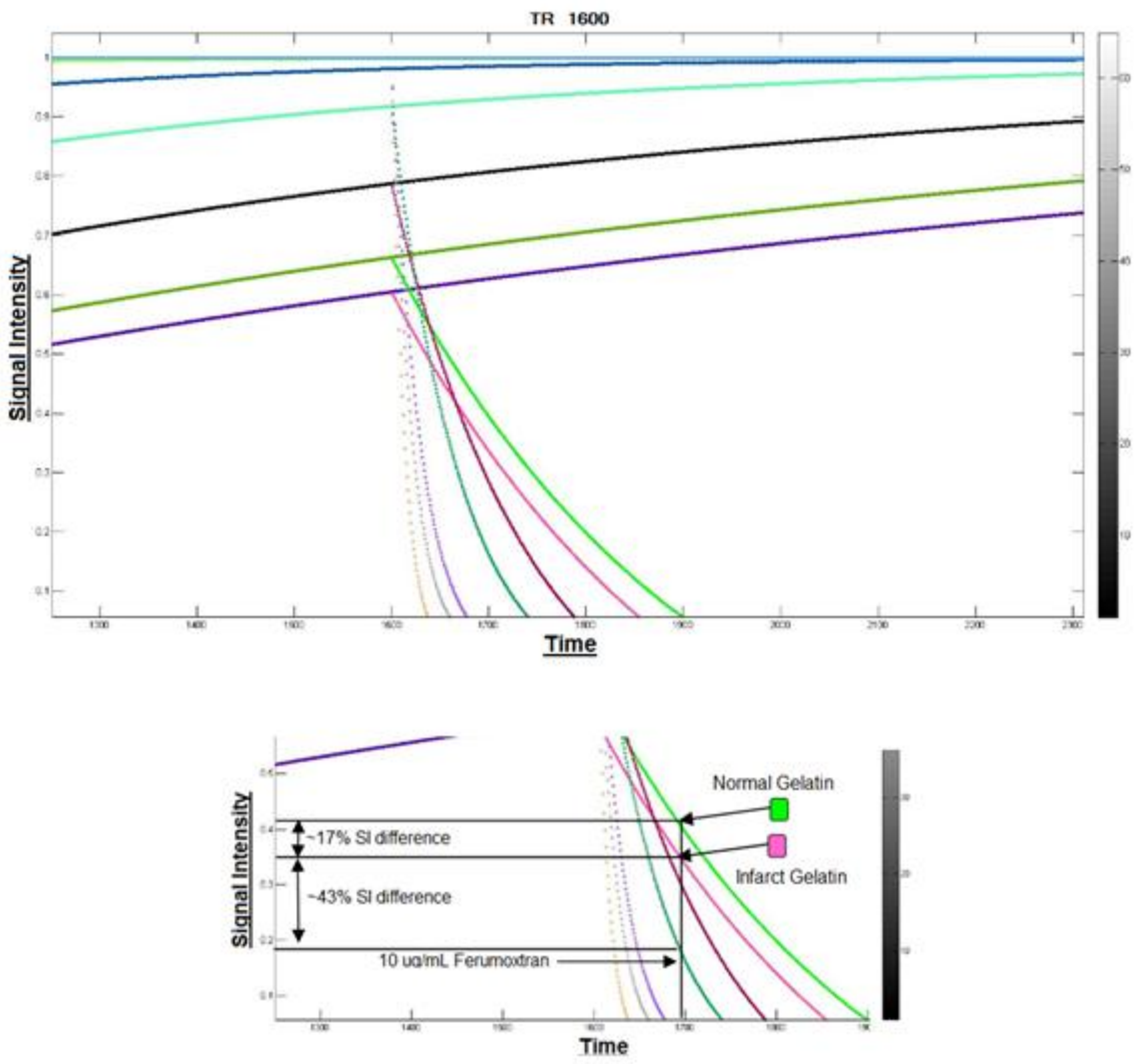

Figure 36: T2 Contrast Agent Study - Final Parameter Results

5.0 Design Verification

The final design and verification section of this report encompasses the techniques used to produce and conduct the selected methods to, via MRI, analyze MR-contrast-agent-doped tissue-embedded microthreads in a cardiac phantom. The construction of the cardiac phantom and microthreads, doping of the microthread, construction of the final phantom system, imaging of the system, and usage of the imaging analysis tool is discussed in detail.

5.1 Collagen Microthread Production

The proceeding section describing the production of self-assembling collagen microthreads is comprised of numerous detailed and sequential procedures adapted from Cornwell and Pins [67]. For simplicity, the production of collagen microthreads is organized into two distinct processes, the extraction and preparation of acid-soluble collagen and collagen thread extrusion. In total 8 – 2.0 cm bundles of 12 collagen microthreads were formed and utilized in the final design modeling system.

5.1.1 Preparation of acid-soluble collagen

Using hemostatic clamps, acid-soluble type I collagen was extracted from tendon fibers in Sprague-Dawley rat tails. Following the dissection, the tendon fibers were rinsed twice in phosphate buffered saline (PBS) and dissolved in 1600 mL of a 3% acetic acid solution overnight. The solution was then refrigerated and centrifuged for 2 hours at 4˚C and 8000g, after which the resulting components, supernatant and precipitate, were retained. To isolate the collagen within the solution, 320 mL of 30% NaCl was slowly added, forming a collagen precipitate. The precipitate and solution was once again centrifuged for 30 minutes at 4˚C, discarding the resulting supernatant. The collagen precipitate was re-suspended in 400 mL of a 0.6% acetic acid solution and stirred at 4˚C until completely dissolved (typically overnight). The solution was dialyzed five times, each for at least four hours, against 4 L of 1 mM HCl and then lyophilized and stored at 4˚C.

5.1.2 Collagen thread Extrusion

Before the threads were extruded, the lyophilized collagen was dissolved at 4˚C overnight in a rotating vessel with 5 mM HCl, with a final concentration of 10 mg/mL. Air bubbles that were in the collagen solution were also removed by centrifugation.

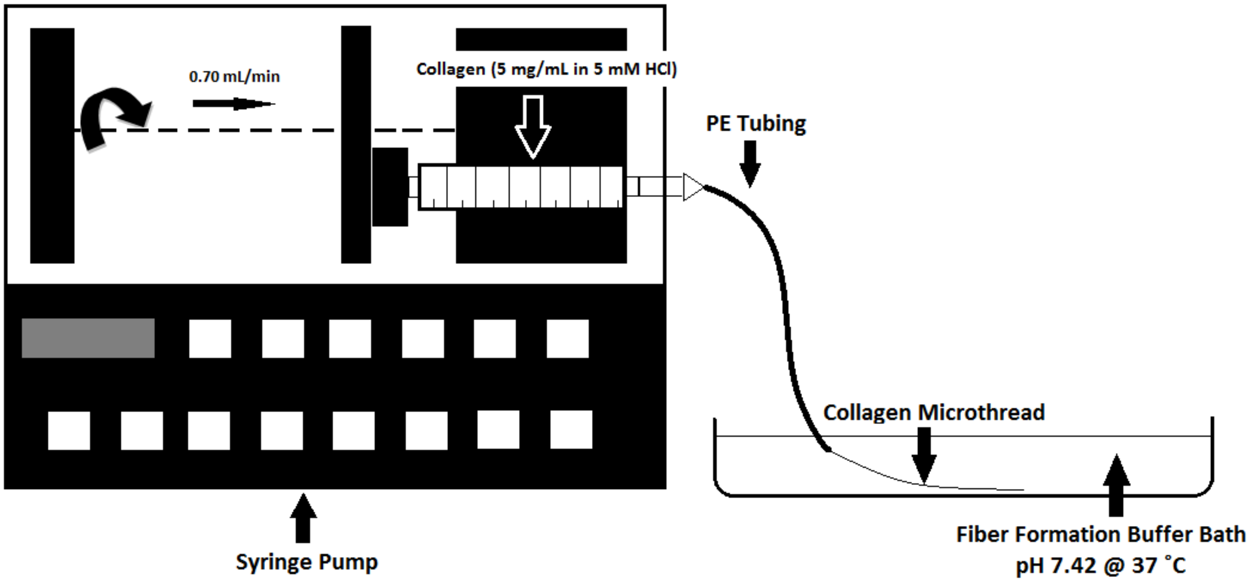

Figure 37: Collagen Microthread Extrusion Process

As depicted above in Figure 37, thread extrusion was driven by a syringe pump connected to 0.86-mm-diameter polyethylene tubing. The threads were extruded at a flow rate of 0.7 mL/min into a fiber formation buffer bath (pH of 7.42 at 37˚C) consisting of 135 mM NaCl, 30 mM TrizmaBase, and 5 mM $NaPO_4$. After 24 hours, the buffer was replaced with distilled water, and the microthreads were incubated for another 24 hours at 37˚C. The threads were then taken out of the distilled water bath, air dried, and stored at room temperature in a desiccator.

5.2 Gelatin Production

5.2.1 Phosphate Buffered Saline (PBS) Production

The construction of the final gelatin phantom design involved dynamically mixing gelatin powder with a phosphate buffered saline (PBS). In regards to the scope of this project using PBS as a buffer has numerous advantages over distilled (DI) water. The osmolarity and ion concentrations of PBS are similar to those found in the body, keeping the gelatin isotonic and limiting its effects on the seeded stem cells. The utilized PBS formula consisted of DI water, 1.06mM KH_2PO_4, 155.17 mM NaCl, and 2.97 mM $Na_2HPO_4 – 7H_2O$) (Invitrogen Corp., San Diego, CA). The solution components were dynamically mixed for approximately 5 minutes at 200 F° using a ceramic hot plate stirrer (VWR, West Chester, PA) and stored in sterile glass media bottles for future usage. Upon cooling, the pH of the solution was recorded with Baker-pHIX (J.T Baker, Phillipsburg, USA) and visually approximated to be consistent with the expected pH of 7.4 ± 0.1 (Figure 38).

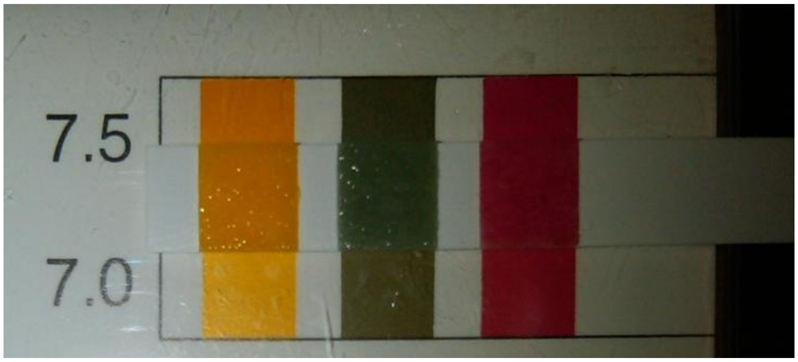

Figure 38: pH approximation of the PBS solution

5.2.2 Gelatin Concentration & PBS Integration

Gelatin is a protein produced by partial hydrolysis of collagen and, with water, forms a semi-solid colloid gel. The percent concentration of Knox Original Unflavored Gelatin (Knox, Johnstown, N.Y.) required in the phosphate buffered saline to mimic the T_1 relaxation rates of both normal and ischemic myocardial tissue were determined via initial magnetic resonance testing and referenced literature and found to be 7.1% and 3.7%, respectively. Calculated concentrations of gelatin were constructed based on these findings via percent weight of gelatin powder (grams) per volume of PBS (milliliter) and are 7.1 g gelatin and 93.9 mL PBS for normal tissue and 8.3 g gelatin and 91.7 mL PBS for infracted tissue. The gelatin powder was weighed using a Mettler Toledo Classic Plus, AB-S/Fact analytical balance (Mettler-Toledo International Inc., Columbus, OH) and transferred using Fisherbrand 3” x 3” weighing paper (Fisher Scientific, Hampton, N.H) into a 200 mL beaker containing the calculated volume of PBS. Once introduced into the PBS solution, the gelatin was dynamically mixed at 400 rotations/min for approximately 5 minutes at 200 °F with a ceramic hot plate stirrer (VWR, West Chester, PA). As depicted in Figure 39 and Figure 40, approximately 30 mL of the liquefied gelatin was then immediately transferred from the mixing beaker into a sterile polystyrene 35 mm x 10 mm cell culture dish (Corning Inc., Corning, N.Y.) using a motorized Fisherbrand pipette dispenser (Fisher Scientific, Hampton, N.H) and 10 mL serological pipette (Becton-Dickinson Labware, Franklin Lakes, NJ). The cell culture dish was then sealed, taped closed, marked to indicate the concentration, and placed inside a 37 °C refrigeration unit for three hours.

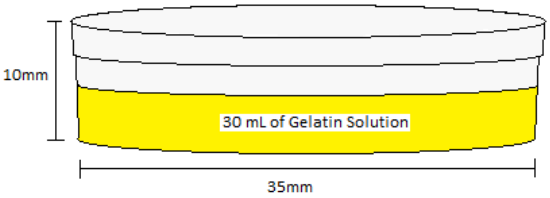

Figure 39: Sterile 35mm Petri Dish w/ Gelatin

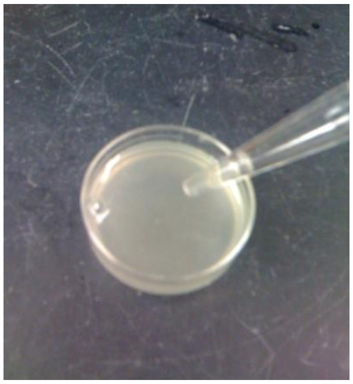

Figure 40: Gelatin Delivery into 35mm Petri Dish

5.3 Microthread Contrast Agent Application

As previously stated, a total of 8, 2.0 cm bundles of 12 collagen microthreads were formed for delivery into the gelatinous cardiac phantom. To determine optimal agent application, a variety of thread preparation techniques were conducted. The microthread bundles were divided into two groups of four, with thread preparation prior to implantation varying for and within each group. To determine if microthread MR differentiation varied as a function of agent exposure time, each thread bundle within each group was placed in 10 ug/mL of Ferumoxtran, the chosen contrast agent, for differing time increments. Table 13 below illustrates the time of agent exposure for each thread in their respective group. Figure 41 depicts the location and agent exposure time of each thread in the cardiac modeling system.

Table 13: Contrast Agent Application

	Group 1 - "Air-dried Threads"	Group 2 - "Hydrated Threads"
Thread #		
1	60 min. Exposure in Ferumoxtran	60 min. Exposure in Ferumoxtran
2	30 min. Exposure in Ferumoxtran	30 min. Exposure in Ferumoxtran
3	5 min. Exposure in Ferumoxtran	5 min. Exposure in Ferumoxtran
4	60 min. Exposure in PBS	60 min. Exposure in PBS

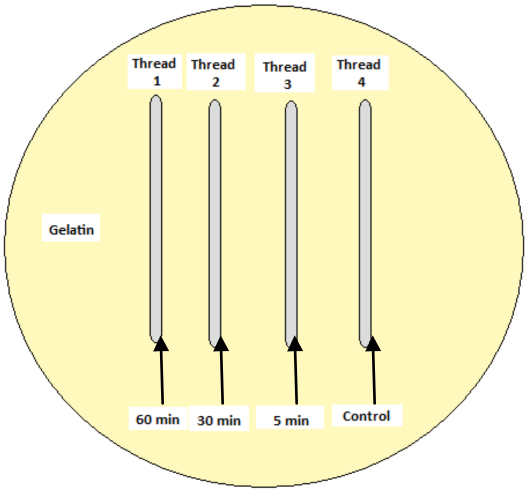

Figure 41: Thread Location and Agent Exposure Time

The second variation in microthread preparation consisted of differences between each group, and would examine the effects of thread hydration on MR differentiation. The microthreads in group 1, called the “Air-dried Group”, were exposed in the varying time increments described above, rinsed 3 times in distilled water, and then air dried prior to implantation in the cardiac phantom. Group 2, called the “Hydrated Group”, was similarly exposed in the time variant manner to Ferumoxtran and PBS solutions, but then directly inserted into the phantom.

5.4 Cardiac Phantom Construction

Construction of the final cardiac modeling phantom comprised of integrating the phantom gelatin components and the doped collagen microthread. As previously stated the percent concentration of Knox Original Unflavored Gelatin (Knox, Johnstown, N.Y.) required in the phosphate buffered saline to mimic the relaxation rates of both normal and ischemic myocardial tissue were determined to be 7.1% and 3.7%, respectively. Using the same techniques and materials as previously described, 30 mL mixtures consisting of 7.1% and 3.7% gelatin will prepared, placed into separate sterile 35 mm culture dish, and allowed to solidify overnight. In total 2 phantom modeling systems were constructed and tested, one containing the 4 microthreads in Group 1- “Air-Dried Threads” and the other containing the remain 4 microthreads in Group 2 – “Hydrated Threads”. Each microthread within the 2 phantom modeling systems was placed approximately 5mm apart on top of the solidified gelatin representative of normal tissue. The gelatin mold representing the infarct tissue was then extracted from the culture dish, making sure to keep the gelatin in one piece, and then placed on top of the threads and “infarct gelatin”, effectively “sandwiching” the threads between the 2 gelatin concentrations. Figure 42 and Figure 43 below depict gelatin placement housed within the 35-mm culture dish and the microthread bundles sandwiched in between these layers.

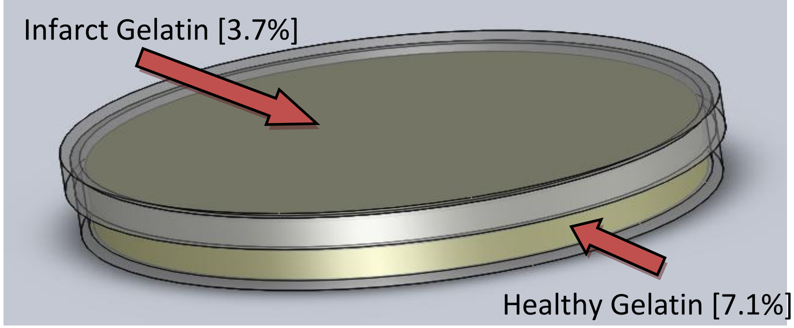

Figure 42: Gelatin Concentration and Placement

Figure 43: Microthread Placement in between Gelatin Layers of Varying Concentration

5.5 Imaging Process and Parameters

The gelatin phantom and contrast agent imaging process was performed on the Philips Achieva 3.0T X-Series MRI, using a homemade 38mm x 127mm copper, birdcage RF-coil seated within a plexiglas tube. The software used, which was provided, was the Philips MRI SmartExam software. All of the testing was performed at the UMASS medical school, with the assistance of Mohammed Shazeeb, a PhD student at Worcester Polytechnic Institute. Proper safety precautions were followed when performing all of the tests.

After the cardiac phantom process with the microthreads introduced, the image testing could occur. The phantom was placed within the birdcage coil aligned parallel to the xy-plane, as accurately as possible. This allowed the cross sectioning of the phantom slices during imaging to be as ideally perpendicular to the phantom bottom. The birdcage was then hooked up to the MRI machine, then properly aligned and placed within the bore of the magnet. This then allowed the setup for the imaging parameters in order to perform our image testing.

The entire sets of imaging parameters are shown in Table 14. In all of the experiments the number of slices which were acquired were 15 slices per experiment. The T_1-weighted imaging experiments were acquired using a multi-slice, single-echo technique. The T_2-weighted imaging experiments were performed using a multi-echo, multi-slice technique, in order to allow the acquisition of separate echo times in a shorter amount of time. Each echo time produces a separate set of images. The TR was determined by finding the maximum difference in signal intensity between the healthy and normal gelatin, and determined using our concentration analysis curves. The sets of images that were acquired were saved as a DICOM format, and were also converted to .tiff format for use in image analysees.

Table 14: TR and TE Times for Imaging Experiment

Phantom	**Experiment**	**Repetition Time (TR)**	**Echo Time (TE)**	**Image Matrix Size**
Air- Dried	T1 Weighted Image	700 ms	8.7 ms	256 x 256 pixels
Air- Dried	T2 Weighted Image	1600 ms	25,50,75,100 ms	384 x 384 pixels
Hydrated	T1 Weighted Image	700 ms	8.7 ms	256 x 256 pixels
Hydrated	T2 Weighted Image	1600 ms	25,50,75,100 ms	384 x 384 pixels
Phantom	**Field of View**	**Slice Thickness**	**Slice Gap**	**Voxel Size**
Air- Dried	10 x 35 x 25 mm	1.5mm	.15mm	.09 x.09 x 1.5mm
Air- Dried	10 x 35 x 25 mm	1.5mm	.15mm	.14 x .14 x 1.5mm
Hydrated	10 x 35 x 25 mm	1.5mm	.15mm	.09 x.09 x 1.5mm
Hydrated	10 x 35 x 25 mm	1.5mm	.15mm	.14 x .14 x 1.5mm

5.5.1 Air-Dried Phantom Imaging

The first experiment was performed on the air-dried thread phantom. There were two image acquisitions that were performed, the first was a T_1-weighted image and the second was a T_2-weighted image. The T_1-weighted image was performed with the imaging parameters of a TR of 700 ms and a TE of 8.7 ms, with a field of view of 10 x 35 x 25 mm, a slice thickness of 1.5 mm and a slice gap of .15 mm, which produced a voxel size of .09 x .09 x 1.5 mm per pixel. The images that were acquired were 256 x 256 pixel size images. The T_2-weighted images were performed using a TR of 1600 ms the TE acquisition times were 25, 50, 75, 100 ms, the field of view of 10 x 35 x 25 mm, a slice thickness of 1.5 mm and a slice gap of .15 mm, which produced a voxel size of .14 x .14 x 1.5 mm per pixel.

5.5.2 Hydrated Phantom Imaging

The second experiment was performed on our hydrated thread phantom. There were two image acquisitions that were performed, the first was a T_1-weighted image and the second was a T_2-weighted image. The T_1-weighted image was acquired with a TR of 700 ms and a TE of 8.7 ms, with a field of view of 10 x 35 x 25 mm, a slice thickness of 1.5 mm, and a slice gap of .15 mm, which produced a voxel size of .09 x .09 x 1.5 mm per pixel. The images that were acquired were 256 x 256 pixel-size images. The T_2-weighted images were acquired using a TR of 1600 ms, the TE acquisition times were 25, 50, 75, 100 ms, the field of view of 10 x 35 x 25 mm, a slice thickness of 1.5 mm and a slice gap of .15 mm, which produced a voxel size of .14 x .14 x 1.5 mm per pixel.

5.5.3 T_1-Weighted Image Acquisition

One slice of a T_1-weighted image that we acquired through the cardiac phantom containing the hydrated microthreads are shown in Figure 44 and Figure 45 shows a T_1-weighted slice of the phantom containing the air-dried microthreads. Both of these images represent one out of the 15 slices that were obtained from each phantom. The entire set of 15 T_1-weighted images for both phantoms can be seen in an attached document under the directory D*:\MQP Final Submittal\Imaging Experiment\Original data* or D*:\MQP Final Submittal\Imaging Experiment\T1 Data*. The microthreads were poorly depicted in the T_1-weighted scan as shown by the small holes in the middle of each image. From left to right in both Figure 44 and Figure 45, the microthreads align as 60 minutes, 30 minutes, and 5 minutes contrast agent exposure and finally one without any contrast agent but just a PBS exposure. The fact that the microthreads are oriented in the middle of the images shows that they remained stable after being sandwiched in between the "infarcted" and "healthy" gelatin. The top half of the images correspond to the infarcted gelatin comprised of 3.7% gelatin and the bottom half correspond to the healthy, which is 7.1% gelatin. It is important to note that some of the T_1-weighted images in the separate document contain more than four holes. Any extra holes in the images can be explained by air bubbles that may have occurred while sandwiching the microthreads in between the infarcted and healthy gelatin.

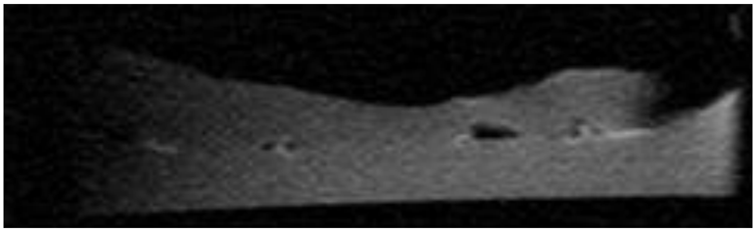

Figure 44: T_1-Weighted Image of Cardiac Phantom with Hydrated Microthreads

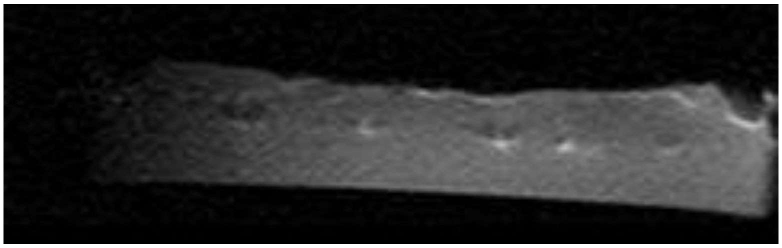

Figure 45: T_1-Weighted Image of Cardiac Phantom with Air-Dried Microthreads

5.5.3 T_2-Weighted Images Acquisition

One T_2-weighted slice of the phantom containing the hydrated microthreads at a TE of 100 ms is shown in Figure 46. Another T_2-weighted slice at 100 ms TE, displaying the phantom containing the air-dried microthreads is shown in Figure 47. The entire set of T_2-weighted images of both phantoms at all four echo times (TE = 25, 50, 75, and 100ms) can be seen in an attached document under the directory D*:\MQP Final Submittal\Imaging Experiment\Original data* or D*:\MQP Final Submittal\Imaging Experiment\T2 Data*. Just as with the T_1-weighted images, the black holes were oriented in the middle of each T_2-weighted image. Some images contained more than four holes which once again can be explained by air bubbles created while inserting the microthreads inside the phantoms. The top half of the image corresponds to the infarcted gelatin comprised of 3.7% gelatin and the bottom half corresponds to the healthy which is 7.1% gelatin.

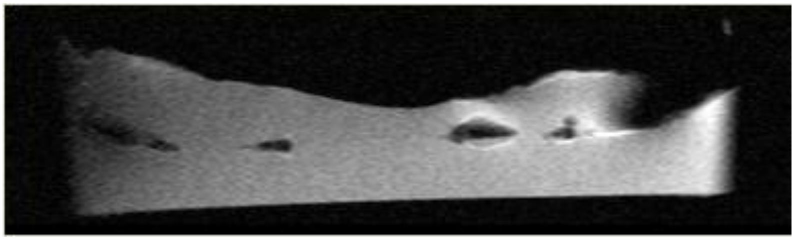

Figure 46: T_2-Weighted Image of Cardiac Phantom with Hydrated Microthreads at 100ms TE

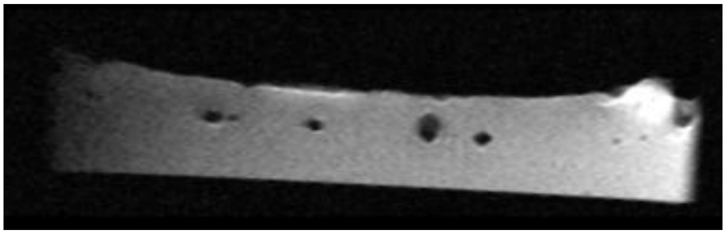

Figure 47: T_2-Weighted Image of Cardiac Phantom with Air-Dried Microthreads at 100ms TE

5.6 Data Analysis Procedure

The program that was chosen was ImageJ in order to perform our thread diameter and location analysis along with our signal intensity and contrast measurements. A set of programming macros were developed in order to reproduce the results across all of the images, these are shown in a separate set of documents, which are labeled and stored on the final DVD in directory *D:\MQP Final Submittal\Image Analysis\Imaging Macros*.

These analysis macros performed a diameter analysis of what were determined as the microthreads in the images. Each line of the macro required a ";" at the end of it for syntax purposes. These macros took and opened the given image file, using the *open("file_name")* command. This file was then ran in 8 bit by using the *run("8-bit")* command. The correct tool was then selected using the *//setTool(4).* A line was then made across the middle point of what was determined to be each thread. This line was then plotted on a graph using the *run("Plot Profile").* Then there was a full width half maximum height (FWHMH) measurement taken , which is explained in the a later paragraph, taken on it. This was done using the *run("Measure")* command.

There were 4 threads per single slice, 15 slices per image, however we only used 10 slices to perform measurements on, and there were 8 images analyzed. So there were 320 measurements made in total. Each echo time had a set of 10 images for each sample that were analyzed. So after each macro run, this produced 40 measurements for each image set. These measurements were to scale because previously the image pixel size was set to our scale of .14 x .14 1.5mm per pixel for hydrated threads and .09 x .09 x 1.5 mm for the air-dried threads. These measurements were then exported to an excel document and separated, with every fourth measurement separated into a different column making it so that measurements for each thread (60, 30, 5, and control threads) were separated into their own column. This gave the entire data set, once each of the 8 macros were performed. The results are found in Appendix 7: Results.

The analysis which we performed was a full width half maximum height analysis. This is an analysis where the maximum full width of the depression is evaluated, then the maximum height is evaluated, and the diameter is taken at half of this height. (As shown in Figure 48)

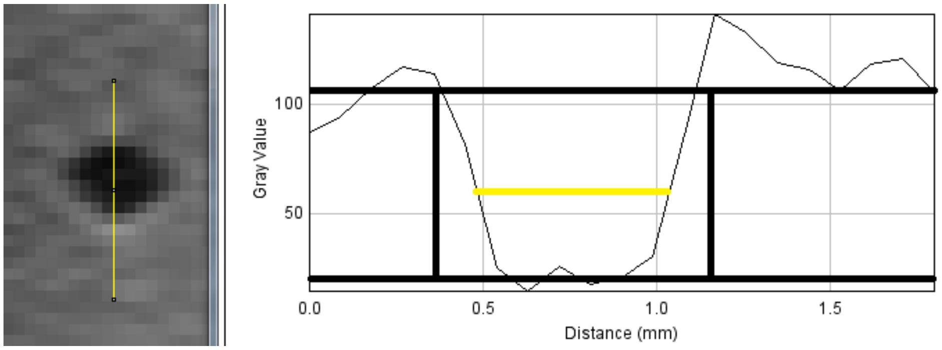

Figure 48: Image Analysis, Full-Width Half-Maximum-Height

A separate analysis of our actual phantom was performed as well. An optical picture of our phantom was taken next to a ruler in order for to provide a scale tool to analyze the optical thread width. The scale for the image was set by taking the line tool making it read 10 mm on the ruler, and using a *Set Scale* command to our known scale of 10 mm. This allowed the scale to be applied to every measurement that was taken. Then 10 sections were analyzed in line with the slices from the MR images. These results are shown in Appendix 7: Results.

5.6.1 Hydrated Microthread Diameter Measurements

Figure 49 displays the average hydrated microthread diameters from the T2-weighted images at each separate contrast agent application time. It also displays the average hydrated microthread diameters of the optical image of the cardiac phantom. In order to determine each microthread diameter for the MRI slices, we utilized the full width at half maximum height (FWHMH) method which is discussed in 5.6 Data Analysis Procedure. A detailed methodology for optical image microthread measurements are also discussed in 5.6 Data Analysis Procedure. The fact that the standard deviations overlap suggests that there is no statistical difference between the microthread size and the contrast agent exposure time. It also suggests that there is no statistical difference between the microthread diameter in the T_2-weighted MR images and the optical image containing hydrated microthreads. This same analysis was done at each echo times, and yielded similar results. There was no significant difference between contrast agent exposure time as well as imaging type and microthread diameter. Each measurement was done at every echo time and the graphs that correspond to these data are shown in Appendix 7: Results.

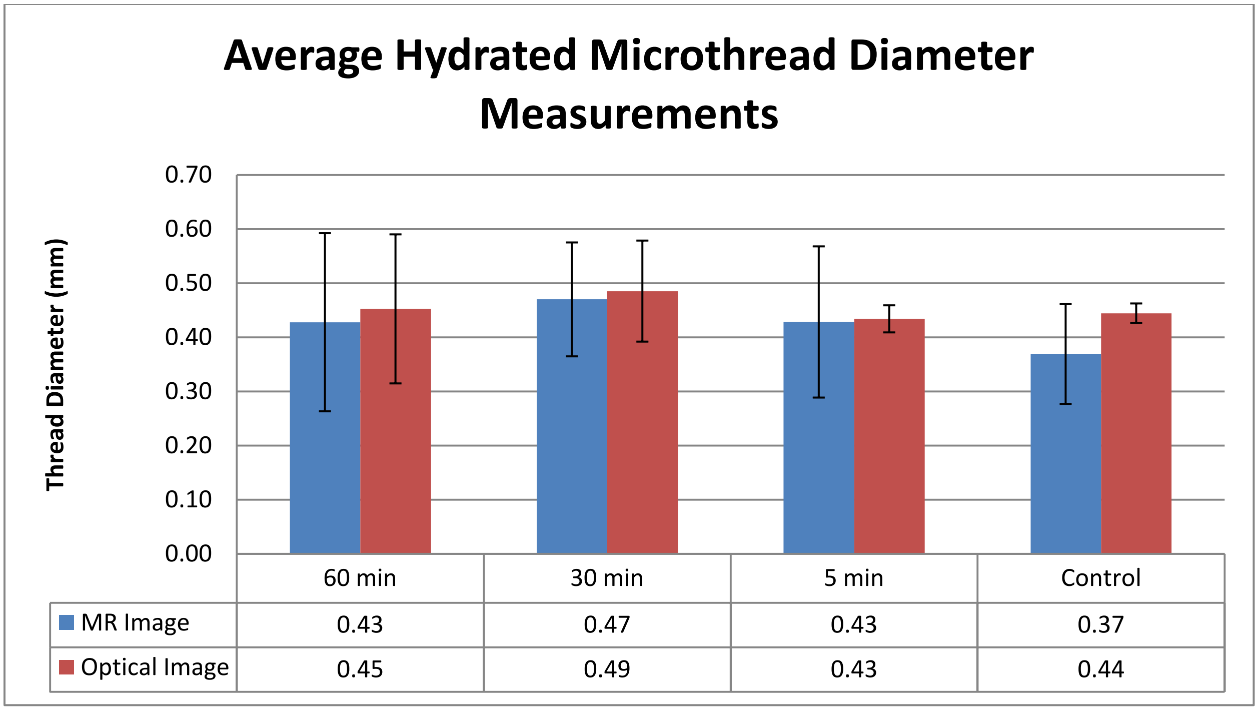

Figure 49: Average Hydrated Microthread Diameter Measurements

5.6.2 Air-Dried Microthread Diameter Measurements

Figure 50 shows the average air-dried microthread diameters for the T_2-weighted images at each different contrast agent exposure time. This bar graph also displays the air-dried microthread diameters from the optical image. The overlap in standard deviations shows that once again there is no statistical difference between the microthread diameter and contrast agent exposure time. It also suggests that there is so significant difference in the measurements between the MR images and the optical image containing the air-dried microthreads. All of the measurements taken at different echo times and their corresponding graphs can be seen in Appendix 7: Results. Just as with the hydrated microthreads, all of the air-dried analyses showed that there was no significant difference in diameter at different contrast agent exposure times, echo times, or with different imaging types.

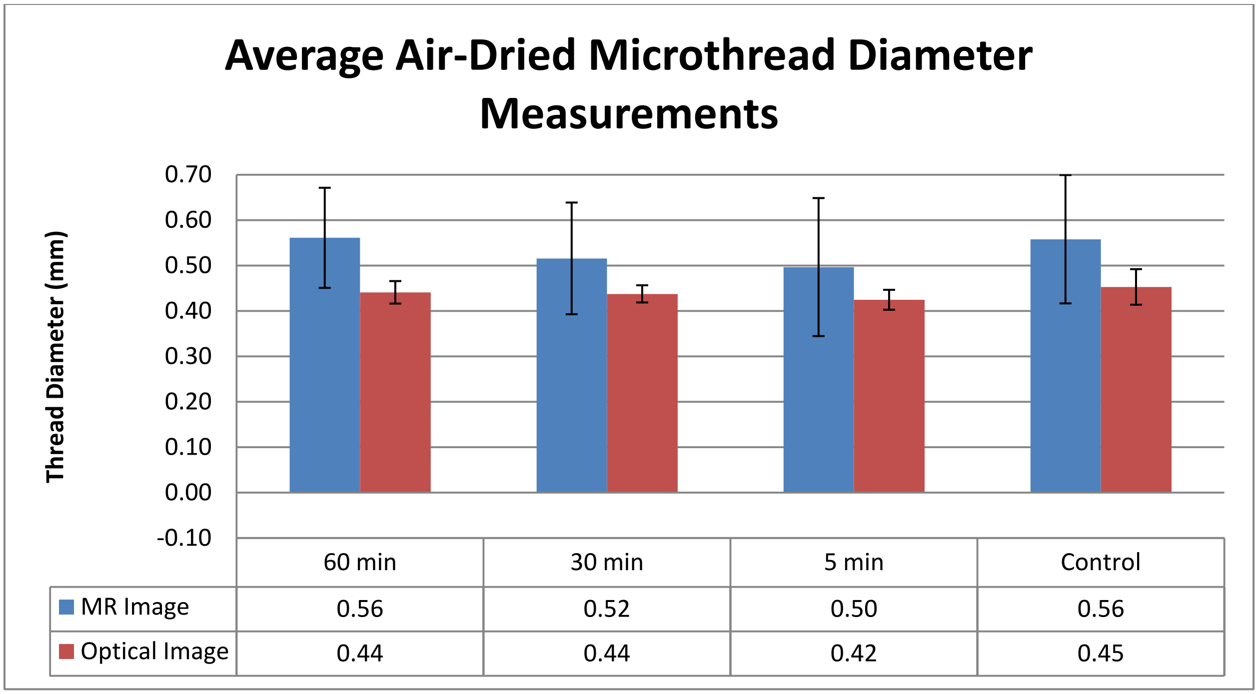

	60 min	30 min	5 min	Control
🟦 MR Image	0.56	0.52	0.50	0.56
🟥 Optical Image	0.44	0.44	0.42	0.45

Figure 50: Average Air-Dried Microthread Diameter Measurements

5.6.3 Contrast as a Function of TE

Figure 51 depicts close up images of the highlighted region for the 4 applied MR echo times of 25, 50, 75, and 100 ms, respectively. Upon visual analysis the magnitude of contrast between the microthread and surrounding gelatinous medium appeared to increase as a function of increasing TE. To verify this observation a signal intensity analysis was performed on the hydrated and air dried MR images via ImageJ software. Starting with an image slice with TE = 25 ms, a straight line segment was drawn across the apparent center of a selected microthread, making sure to encompass the diameter of the thread in its entirety. With the line segment remaining stationary signal intensity profiles of the same imaged location with TE = 50, 75, and 100 ms were collected. All signal intensity profiles were then imported into an Excel spreadsheet and analyzed. A total of 10 separate signal intensity profiles were conducted across varying threads and image slices, with 5 being air dried thread images and the remaining 5 hydrated thread images.

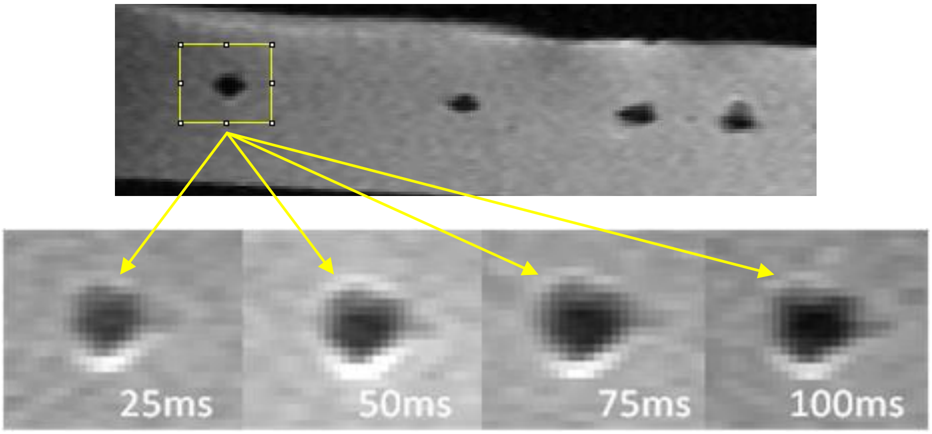

Figure 51: Image Contrast as a Function of Increasing TE

Figure 52 depicts an example of the resulting signal intensity across a line segment as a function of data points taken. The maximum signal intensity difference of each SI profile for the range of echo times were collected, averaged, and finally compared. Table 15 displays the average maximum signal intensity difference for each applied echo time, which increases as a function of increasing TE as expected by previous microthread MR image visualization.

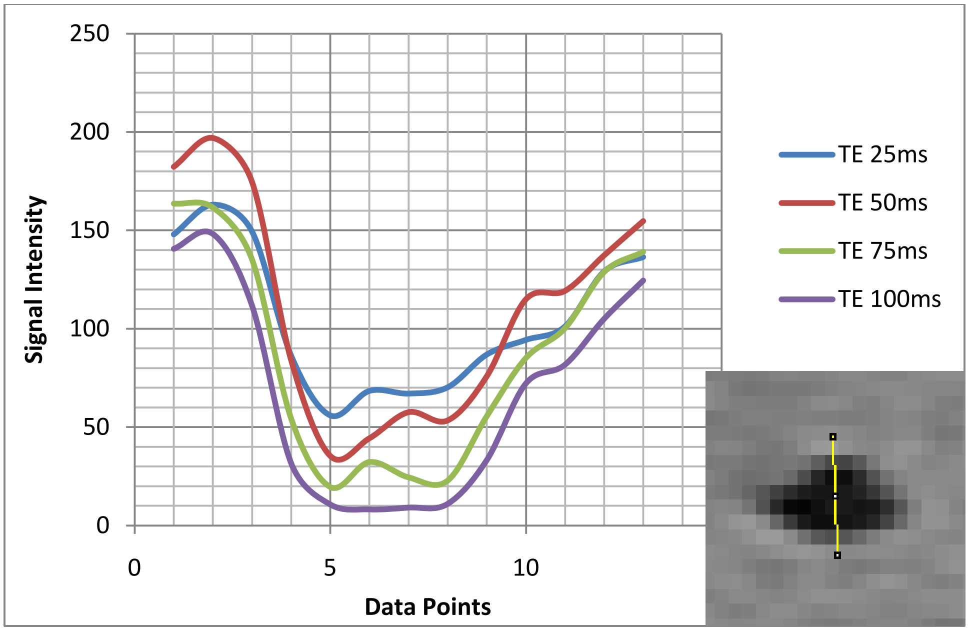

Figure 52: Signal Intensity as a Function of Echo Time

Table 15: Average Maximum SI Difference as a Function of TE

	TE 25ms	TE 50ms	TE 75ms	TE 100ms
Hydrated				
Thread 1	56	67	70	78
Thread 2	65	80	81	89
Thread 3	73	89	90	92
Thread 4	70	82	85	90
Thread 5	81	90	93	90
Air Dried	**TE 25ms**	**TE 50ms**	**TE 75ms**	**TE 100ms**
Thread 1	54	66	70	81
Thread 2	61	70	75	79
Thread 3	58	62	76	78
Thread 4	58	69	69	85
Thread 5	68	73	82	88
Average:	64.4	74.8	79.1	85

5.6.4 Image Artifacts

As expected, image artifacts were scattered throughout the acquired T_1 and T_2 image slices. Two recurring artifacts observed were areas of increased signal intensity or "hyperintensity" around the perimeter of the microthread and arrowhead shape distortion of the thread itself. Figure 53 below depicts two areas of signal hyperintensity highlighted in red. Similar to previous methods numerous signal intensity profiles across the thread diameter and into the gelatinous medium were taken and compared. On average the signal intensity of these locations highlighted were 1.6 times that of the gelatin.

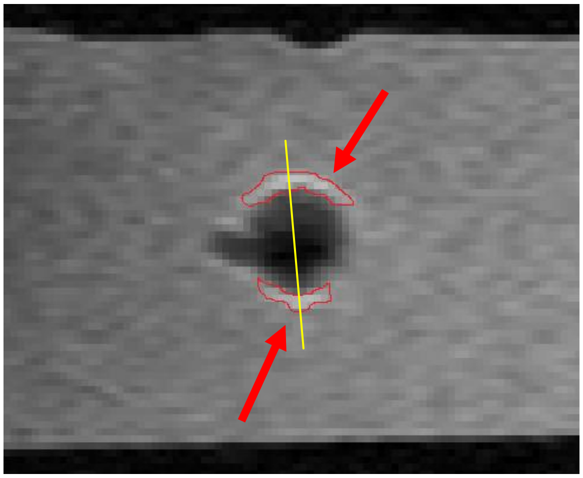

Figure 53: Hyperintensity Artifact

As depicted in Figure 54 the circular area of decreased signal intensity representing the microthreads were occasionally misshapen. Through a visual analysis, the majority of these distortions were "arrowhead" shaped, as shown by the region highlighted in red. The direction in which the distortion occurred was also noted to be strictly vertical.

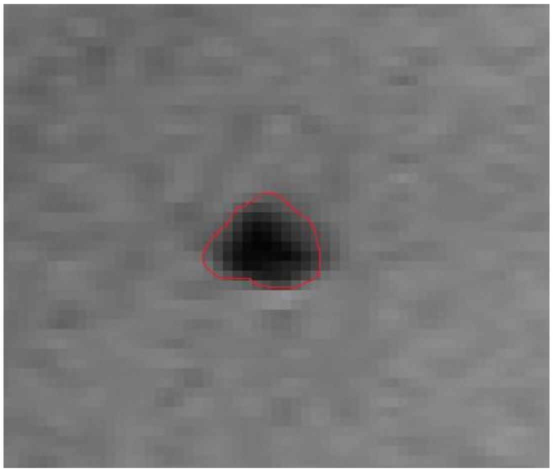

Figure 54: Microthread Shape Distortion

5.7 3D- Reconstruction Design

The idea of three dimensional reconstruction is to be able to see the MR images in another dimension and visually analyze the phantom. This reconstruction was again done using ImageJ. A plugin for ImageJ was required in order to perform this reconstruction called “ImageJ 3D Viewer”. This tool allowed each slice to be imported as a separate entity. The scale was then set for the image size of .14 x .14 x 1.5mm per pixel for hydrated threads and .09 x .09 x 1.5 mm for the air-dried threads. Each of the 15 images has the same size, and each of these images for each separate echo time was oriented in the same place on the xyz plane. The bottom left pixel of each image was oriented in the +x,+y,+z quadrant. This location provided a reference point for the image assembly. The image stack then aligned along from this reference point and the grey scale images were then assembled as a three dimensional figure. This programming plugin then provided an ability to shade the signal intensities of the individual slices of each image together. Doing this performed a three dimensional reconstruction of our cardiac phantom model.

5.7.1 3-D Reconstruction Results

The idea of the 3-D reconstruction was to be able to visualize the microthreads and the phantom using a computer generated image set. However, measurements were not able to be made in three dimensions on these images. Figure 55 and Figure 56 show a three dimensional reconstruction of our phantoms using the ImageJ 3D viewer. These were compiled and the smoothing surfaces were removed in order to view the slices individually.

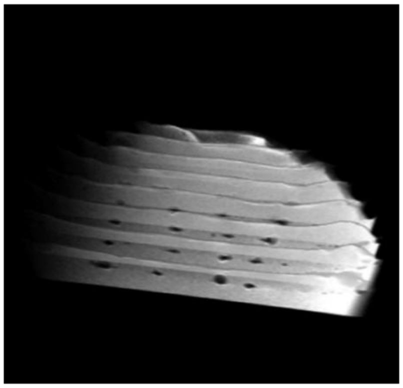

Figure 55: 3-D Air-Dried Phantom Reconstruction

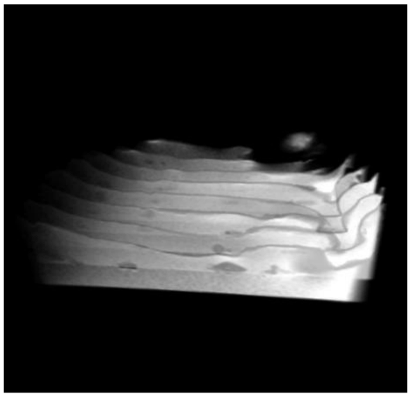

Figure 56: 3-D Hydrated Phantom Reconstruction

Figure 57 shows a box cut-out of our microthreads. This was done in order to show the thread tracks by themselves without the phantom surrounding it. This image was achieved by reversing the contrast of the images then using a box cut-out and then compiling the images in three dimensions. Figure 58 gives a very effective visualization of the thread track through the phantom itself. Figure 59 provides a cross section in order to compre to the optical images. The methodology on how the 3-D reconstruction was conducted is depicted in 5.7 3D-Reconstruction Design.

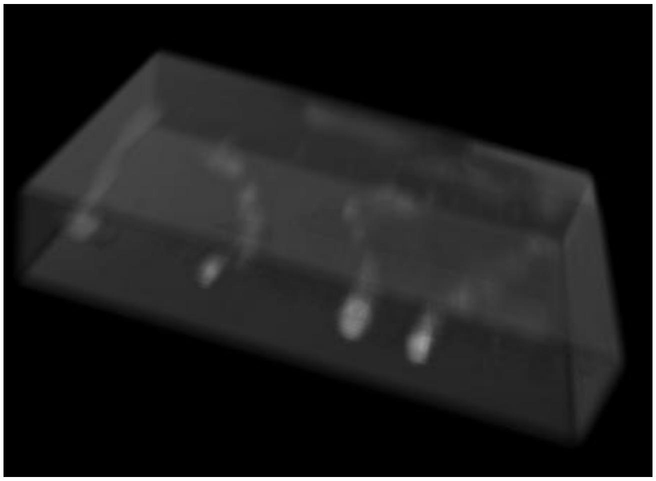

Figure 57: 3-D Reconstruction of Microthreads

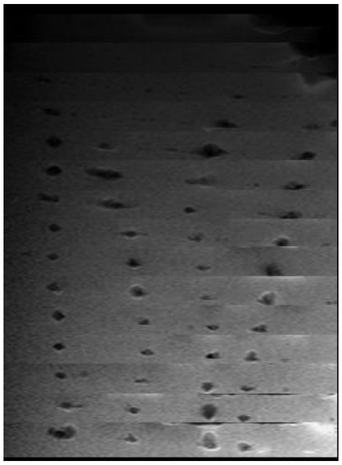

Figure 58: 3-D Montage of Individual Slices

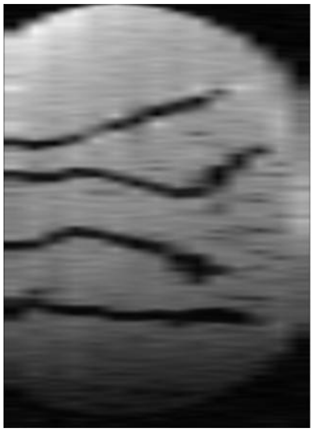

Figure 59: Orthagonal Phantom View

6.0 Discussion

6.1 T_1-Weighted Images

The T_1-weighted images showed some slight contrast between the infarcted and healthy regions of the cardiac phantom. The top portion of the images is somewhat darker than the bottom half, which is what we expected since the infarcted region was constructed to have a longer T_1-relaxation than the healthy region. However, we expected a much greater contrast in between these two locations. These images also seemed to have differences in signal intensities moving from left to right, which was not expected. In all of the T_1-weighted images, the signal intensities get lighter as you view them from left to right. This phenomenon may be explained by the phantom placement and alignment within the RF-coil. The main problem with the T_1 acquisition which we performed was that the images do not effectively show the microthreads. Thus, the microthread diameter or contrast measurements were not able to be performed using these images.

6.2 T_2-Weighted Images

As expected, the T_2-weighted images did not show contrast between the region of infarct and the healthy portion of the phantom. The reason why this was expected is explained in detail in 4.3.7.3 Preliminary Conclusions. The signal intensity of each phantom became brighter moving from left to right just as in the T_1-weighted images. Once again, this can be explained by positioning and alignment of the cardiac phantom in the RF-coil. In comparison to T_1-weighted images, the microthreads and their boundaries were more prominent in T_2-

weighted images allowing for accurate microthread diameter and contrast measurements, a primary objective of the experiment.

6.3 Image Artifacts

As expected, image artifacts were scattered throughout the acquired T_1 and T_2 image slices. Although there were no significant differences regarding thread diameter between the optical and MR images, these artifacts ultimately aided in the deviation of apparent thread diameter. The occurrence of susceptibility artifacts were expected due to the response of ferromagnetic-iron-based contrast agents and resulting susceptibility gradient. Magnetic susceptibility is a measure of a material's tendency to interact and distort an applied magnetic field. The large susceptibility of the iron particles map signals from spins near the object to the same image location as distant spins, resulting in areas of double exposure, thus producing hyperintensity. The spherical shape of the microthreads could have also aided in the production of hyperintense areas. The magnetic field around the perimeter of a sphere, if transverse to the applied field, is intensified, producing increased signal intensity. The magnitude of this magnetic field intensity is a function of the radius, applied magnetic field, and susceptibility gradient.

The shape distortion of imaged microthreads is typical. Spins just outside of an ellipsoid's surface do not map in a continuous fashion with those just inside. As shown in Figure 60, the image produced is an elongated v-shaped sphere. It is important to note that the severity of distortion is a function of the radius of the imaged sphere, with the degree of distortion increasing with decreasing sphere radius. [68]

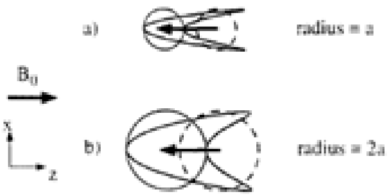

Figure 60: Arrowhead Distortion as a Function of Radius

6.4 Effectiveness of Contrast Agent

The microthreads were exposed to the contrast agent in order to increase the contrast in signal intensities between the microthread, infarcted gelatin, and healthy gelatin of the cardiac phantom. The microthreads were exposed to the contrast agent in a time variant manner in order to demonstrate whether exposure time had any significant effect on the contrast in the acquired images. Qualitatively, the T_2-weighted images show that the contrast agent exposure time had no significant effect on contrast between these areas of interest, meaning that contrast neither increased nor decreased significantly as exposure time was increased. Another interesting finding was that the control microthread had just as much contrast as those which were exposed to contrast agent, which questions the necessity of contrast agents in visualizing these microthreads via MRI.

6.5 Effect of Microthread Preparation Type

The microthreads were prepared in two different ways to determine whether preparation type played a significant role in contrast between areas of interest within the cardiac phantom. One set of four microthreads were simply exposed to the contrast agent in the time variant manner previously discussed and placed inside one cardiac phantom. Another set of four microthreads were exposed to the contrast agent in a time variant manner, air-dried, and then placed inside a separate cardiac phantom. During the experiment it was apparent that the microthreads which were not air-dried were clearly thicker in diameter. However, Figures 40 and 41 show that the microthread preparation had no significant effect on the microthread diameter. Qualitatively it was apparent that the microthread preparation type did not have an effect on contrast in the T_2-weighted images.

6.6 Contrast as a Function of TE

Based upon knowledge of magnetic resonance imaging the results suggesting an increase in image contrast as a function of TE can be rationalized. The echo time is the time at which the image signal is acquired after the RF pulse. Increasing TE allows for increasing time for nucleic relaxation, thus reducing the intensity of the signal acquired by the RF coil in the transverse plane.The resulting intensity of the microthread is reduced to near zero, making the thread more apparent. The increase in maximum difference in signal intensity as TE increases is most likely due the variation in relaxation rates between the microthread and the gelatin. Allowing for longer periods of relaxation also allows for a greater difference between the relaxation curves, thus producing more contrast.

6.7 Project Applications

6.7.1 Economics

The system design would influence the economy and everyday living by creating job opportunities for chemists, MRI technicians, and biomedical as well as electrical engineers. The contrast agent (ferumoxtran iron-oxide nanoparticles) production requires chemists while the tissue-embedded microthread production and contrast agent application requires biomedical engineers. MRI technicians and electrical engineers can benefit from the fact that MRI machines will be needed to function properly to provide accurate analysis of cardiac regeneration. Government funding may also be needed for clinical and pre-clinical trials in MRI cardiac regeneration monitoring. If cardiac regeneration is then deemed effective and brought into the market, such expensive treatments would be available for MI survivors.

6.7.2 Environmental Impact

There may be a decrease in the amount of waste products when monitoring cardiac regeneration via MRI than with a histological approach because there will be no need to manually create hundreds to thousands of slices to view under a microscope. The MRI machine is capable to creating the slices of an *in vivo* heart itself, which can be stored on a computer, which negates the need for creating slices in a lab and then throwing them away after the analyses are performed.

6.7.3 Societal Influence

As previously mentioned, the design could generate job opportunities for many individuals in society, as well as help save lives of those who have suffered from MI. Since current treatments only suppress the increase in stress on the ailing heart post MI, determining the effectiveness of delivering stem cells with microthreads via MRI can one day stimulate cardiac regeneration. Cardiac regeneration can potentially restore the heart back to full health and functionality, providing the survivors of a myocardial infarction with longer, healthier, and more productive lives.

6.7.4 Political Ramifications

The system design involves the use of stem cells for cardiac regeneration, which is an extremely controversial topic. The support of the federal government is needed for such research to continue. If MRI is able to demonstrate that cardiac regeneration is effective, such treatments may introduce new clauses in health insurance packages. Private health insurance companies or the federal government (with the passage of Barack Obama's global health insurance plan) may have to offer different types of health insurance packages to cover the expensive costs of these treatments to MI survivors. Such success may also influence other countries to adopt stem cell therapy which may not have been accepted in the past. This would in turn affect the global economy since more job opportunities would stem in foreign countries as well as the influence of foreign governments on their countries.

6.7.5 Ethics

The ethical implications concerning this particular project are limited. Potential false concerns are expected to most likely revolve around the usage of human mesenchymal stem cells (hMSCs). HMSCs, unlike embryonic stem cells, are found in adult tissues, including bone marrow, periosteum, trabecular bone, adipose tissue, synovium, skeletal muscle, and deciduous teeth. Although embryonic stem cells have numerous advantages, harvesting them has been known to destroy the embryo, an effect that has been met with great opposition. Adult hMSCs however can be harvested from tissue with minimal moral or ethical ramifications, and have demonstrated the ability to divide indefinitely and differentiate into other types of cells.

6.7.6 Health and Safety

The administration of iron based contrast agents into the body – specifically the circulatory system – were considered prior to their implementation, as further studies would potential aim to utilize the design parameters *in vivo*. Iron is found normally in the body and is an essential component of hemoglobin, the oxygen carrying pigment in the body. Numerous clinical tested have determined that iron based agents are well tolerated. No acute or toxic effects were detected by studies in rats or beagle dogs who received 150 times the dose proposed for MR imaging of the liver. [69] The ability to process and expel excess iron has also been demonstrated, as iron based agents' intravenously injection have been noted to cleared from the body within 7 days. [69]

The magnitude of the magnet utilized by the MR machine itself posses' further health and safety related issues. Prior to imaging there are noted safety related protocols that must be addressed. The greatest safety issue when imaging includes the magnets' attraction to ferromagnetic material. Introduction of ferromagnetic materials around the machine can result in them becoming harmful projectiles. For similar reasons, patients with magnetic implants such as a cardiac pacemaker are also put under increased risk.

6.7.7 Manufacturability

The manufacturability or reproducibility of the final design was considered extensively in the design process. The compliance of our final design with our objectives, functions, and constraints aided in the viability of the design being manufactured. All design goals were met, producing a low cost, easy to use, bio- and MRI-compatible, and reproducible experiment to locate tissue embedded microthreads in cardiac muscle. The necessary design components to be manufactured including the development of collagen or fibrin microthreads, gelatinous phantom, and contrast agent concentration and application, are simple enough to be accurately replicated when following the provided design parameters.

6.7.8 Sustainability

The sustainability of the *in vitro* modeling system is subject to questions that have yet to have been examined. The most important question to be looked into would most likely be the viability of collagen and fibrin microthreads as a function of time. When delivered *in vivo* the threads have been noted to degrade overtime, limiting the ability to locate them. It would be interesting to see if the microthreads experience the same effects in the gelatinous phantom, therefore limiting the potential time that MRI could be used to locate the microthreads. Another potential issue could be the ability of the gelatin to sustain the designed water concentration over time. Water diffusion or evaporation over time could severely affect the spatial water concentration and produce unrepresentative image contrast.

Although instances of potential sustainability are apparent, sustainability in general is not particularly relevant to the ultimate goals of the project. The ability to locate embedded microthread shortly after implantation is crucial to maximizing the effectiveness of stem cell and myocardial regeneration, however, once the placement is confirmed there more concern on the positioning of the cell overtime then the microthreads, thus eliminating the need for sustainability.

7.0 Final Design and Validation

In order to produce a successful end product, it is important to conduct extensive background research encompassing the full spectrum of project components. Proper background research allows for a clear understanding of what exactly the problem is and how to potentially solve it. It also provides information on the history behind the problem at hand and how solutions to the problem have previously been attempted. A clear and thorough definition of the problem then permits for plausible goals and objectives to produce a successful outcome.

Before the objectives and goals can be defined however, it is essential to create an interim project schedule with tasks designated to specific group members in order to efficiently begin the engineering design process. This can be accomplished using a Gantt chart, which helps in assigning specific duties of the project to group members, aids in the visualization of project progression, and establishes deadlines for important milestones in the project. If tasks are not divided up in the group, then the project may not comply with its time constraints. It is vital to realize that a Gantt chart is never concrete and that it is subject to change throughout the timeline of the project as obstacles and constraints are often encountered during the design process.

Once the objectives and constraints are defined, the focus of the project can once again be more thoroughly redefined with more specific needs, wants, functions, specifications, and constraints. Based upon the thorough need analysis it was determined that the location of embedded microthreads is crucial to the success of myocardial regeneration and restoration of cardiac functionality. Currently there lacks an effective and efficient method to determine the location and performance of these embedded threads, a problem that potentially can be addressed via magnetic resonance imaging.

Once the objectives, functions, and constraints were clarified the client statement was revisited and redefined using the new information at hand. This statement was more concise in addressing the overall goals of the project and the means by which they would be met. Creating a revised project statement also aids in establishing the direction of the design and credibility with the client. Utilizing the final project goals and direction alternative designs were created via brainstorming. To simplify the process the design was divided into three distinct components, the cardiac modeling system, data acquisition, and data analysis. Making sure that each chosen component was compatible with one another, the “best” design of each component was chosen via feasibility testing and weighted comparisons.

Ultimately the cardiac modeling system consisted of a simple and inexpensive gelatin-based medium, with gelatin concentrations and MR parameters designed to mimic the contrast of actual cardiac tissue. Collagen microthreads were soaked in Ferumoxtran, a superparamagnetic iron oxide and negative contrast agent, to produce more contrast between the threads and surrounding tissue, effectively increasing the ability to locate the threads and differentiate their boundaries. To produce results consisted with project goals, gelatin and contrast agent concentrations were determined via initial MR relaxivity measurements as a function concentration. Utilizing the preliminary data and the knowledge of MR imaging, appropriate parameters for the final design could be determined. With the project team confident the modeling system would mimic in vivo results and embedded microthreads would be easily distinguishable design variables were altered, specifically contrast agent application, to further optimize results. Thread exposure time and hydration were both examined to determine if they had an effect on resulting thread signal intensity and thus differentiation.

Results and conclusion from the experiment verified the calculations made regarding properly design cardiac phantom and MR parameters. The microthread location in the cardiac phantom was apparent and statistically similar in diameter regardless of the agent application process. Apparent microthread diameter of the MR image in comparison to the actual diameter measured via an optical image was statistically similar, suggesting that the current design and procedure is highly accurate. Accurate *in vivo* thread location and measurements utilizing imaging compilation techniques that takes fractions of the time when compared to previous methods offer the client and all potential users a significantly improved method for not only thread visualization, but also stem cell delivery and myocardial regeneration.

8.0 Conclusions and Future Recommendations

The development of MRI as an enabling technology for tissue science and engineering has proven to be highly effective. Through background research the problem was able to be identified, objectified, and put through the design process. A preliminary design was able to be drawn up, then a series of preliminary gelatin and contrast agent concentration experiments were made to provide proper contrast for the images, then a careful image analysis procedure was performed. A thread diameter data analysis protocol was designed, this is key due to the fact that without it there would be no way to actually determine the thread diameter. The three dimensional reconstruction and cross sectioning provided the means to match up the actual phantom to the re-rendered phantom proving it to be ideally one and the same. There were some image artifacts that occurred, but through the design of the experiment, were able to be almost eliminated using the data analysis tools.

There are a series of conclusions that are able to be drawn from our project. The first, of which is the ability to visualize bundles of microthreads that are impregnated with Ferumoxtran iron-oxide nanoparticles.This visualization was done using our preliminary concentration analysis of our concentration curves in order to provide proper contrast for our images, along with our designed image analaysis protocol. The second, is the ability to determine the microthread size and location in both our MR images and our optical images. This size and location was determined using our thread diameter analyzis protocol along with the three dimensional reconstruction and cross sectioning. The last conclusion, and the overall complete goal of the project, is the ability to take the microthreads introduce them into the gelatin phantom, design a set of imaging parameters in order to aquire images with proper contrast, then the ability to take these images and assemble them, then to take this data and analyze it and come up with demonstrated results.

Of course there are possible changes that can be made to this overall project. The first of which is the ability to design and develop a means to be able to accurately be able to take measurements once the 3-D reconstruction is compiled. This allows better visualization along with the same measurement accuracy which was received with the normal data analysis. The second goal is to be able to determine the necessity and viability of the use of contrast agents, in order to actually visualize the microthreads inside an MRI machine. The third future goal is the validation of the actual iron-oxide nanoparticle uptake of the microthreads. The idea of this is to ensure that the microthreads that were exposed to constrast agent actually soaked up the constrast agent. Of course the ultimate and final goal is to be able to take microthreads, treated with human mesenchymal stem cells, and be able to visualize them inside a living heart using magnetic resonance imaging.

Table of Figures

Table of Tables

Works Cited

1. Antunes, P. (2005). Left Ventricular aneurysms: early and long-term results of two types of repair. *European Journal of Cardiothoracic Surgery* , 27(2):210-215.
2. Athanasuleas, C. L., Buckberg, G. D., Stanley, A., Siler, W., Dor, V., Di Donato, M., et al. (2004). Surgical ventricular restoration in the treatment of congestive heart failure due to post-infarction ventricular dilation. *Journal of the American College of Cariology* , 47(7):1439-1445.
3. Barry, F. P., & Murphy, M. J. (2004). Mesenchymal stem cells: clinical applications and biological characterization. *The International Journal of Biochemistry & Cell Biology* , 36(4):568-84.
4. Burton, R. (2006). Three-Dimensional Models of Individual Cardiac Histo-Anatomy: Tools and Challenges. *Annals of the New York Academy of Sciences* , 1080:301-19.
5. Chevallay, B., & Herbage, D. (2000). Collagen-based biomaterials as 3D scaffold for cell cultures:applications for tissue engineering. *Institut de Biologie et Chimie des Proteins.* 38(2):211-8.
6. Christman, K. L., Vardanian, A. J., Fang, Q., Sievers, R. E., Fok, H. H., & Lee, R. J. (2004). Injectable Fibrin Scaffold Improves Cell Transplant Survival, Reduces Infarct expansion, and Induces Neovasculature Formation in Ischemic Myocardium. *Journal of the American College of Cardiology* , 44(3):654-60.
7. Christman, K., & Lee, R. (2006). Biomaterials for the Treatment of Mycardial Infarction. *Journal of American College* , 48:907-913.
8. Cornwall, K. (n.d.). Collagen and Fibrin Biopolymer Microthreads for Bioengineered ligament Generation: a Dissertation. *University of Massachusetts Medical School* .
9. Cornwall, K., & Pins, G. (2007). Discrete crosslinked fibrin microthread scaffolds for tissue regeneration. *J Biomed Mater Res A* , 82A(1):104-112.
10. Davis, M., Hsieh, P., Grodzinsky, A., & Lee, R. (2005). Custom Design of the Cardiac Microenvironment with Biomaterials. *Circulation* , 97:8-15.
11. Decision Resources, I. (2003). Total Market Value for Post Myocardial Infarction Therapeutics Will Exceed $13 Billion in 2012. *PR Newswire* .
12. Eghbali, M., & Weber, K. (1990). Collagen and the myocardium: fibrillat structure, biosynthesis and degredation in relation to hypertrophy and its regression. *Molecular and Cellular Biochemistry* , 96(1):1-14.
13. Ferrero, J. M. (2006). Wiley Encyclopedia of Biomedical Engineering. *John Wiley & Sons* .
14. Gabe, M. (1976). *Histological Techniques.* New York: Springer-Verlag.
15. Haacke, E. M. (New York). Magnetic Resonance Imaging : Physical Principles and Sequence Design. *J Wiley & Sons*: 1999.
16. Health, C. (2003). *Datasheet, Diagnostic Imaging PDF.* Retrieved from Multipurpose Tissue/Cyst Ultrasound Phantom.
17. Heart Disease andStroke Statistics. (2009). *American Heart Association* .
18. Heart and Stroke Facts. (2003). *American Heart Association* .
19. Heber-Katz, E., Leferovich, J., Bedelbaeva, K., Gourevitch, D., & Clark, L. (2004). The scarless heart and the MRL mouse. *Trans R Soc* , 359(1445): 785–793.

20. Ho, W. (2006). The Behavior of Human Mesenchymal Stem Cells in 3D fibrin Clots: Dependence on Fibrin Clots: Dependence on Fibrinogen Concentration and Clot Structure. *Tissue Engineering* , 12(6):1587-95.
21. Hornak, J. P. (2008). *The Basics of MRI.* Retrieved October 10, 2009, from The Basics of MRI: http://www.cis.rit.edu/htbooks/mri/
22. Huang, N., Yu, J., Sievers, R., Li, S., & Lee, R. J. (2005). Injectable Biopolymers Enhance Angiogenesis after Myocardial Infarction. *Tissue Engineering* , 11(11-12):1860-6.
23. Klabunde, R. (2004). *Cardiovascular Pharmacology Concepts.* Lippincott, Williams & Wilkins.
24. Kloner, R. A., & Jennings, R. B. (2001). Consequences of Brief Ischemia: Stunning, Preconditioning,and TheirClinical Implications. *Circulation* , **104:2981-89.**
25. Kocupura, P., Azeloglu, E., Kelly, D., Doronin, S., & Badylak, S. (2005). Tissue Engineered Myocardial Patch Derived from Extracellular Matrix Regional Mechanical Function. *Circulation* , 112:I-144 – I-149.
26. Leeson, T., & Leeson, R. (1970). *Histology.* Philadephia: Saunder.
27. Leor, J., Aboulafia-Etzion, S., Dar, A., Shapiro, L., Barbash, I. M., & Battler, A. (2000). Bioengineering Cardiac Grafts: A New Approach to Repair the Infarcted Myocardium. *Circulation* , 102:III-56-III-61.
28. McRobbie, D. W., Moore, E. A., Graves, M. J., & Prince, M. R. (2006). *MRI : Prom Picture to Proton.* UK, Cambridge: Cambridge University Press. Pg 155.
29. McRobbie, D. W., Moore, E. A., Graves, M. J., & Prince, M. R. (2006). *MRI : Prom Picture to Proton.* UK, Cambridge: Cambridge University Press.
30. O'Connor, M., & Caiati, T. (1995). Effects of Scatter Correction on the Measurement of Infarct Size from the SPECT Cardiac Phantom Studies. *The Journal of Nuclear Medicine* , 36 (11) 2080-2086.
31. Opie, L. H. (2004). *Heart Physiology: From Cell to Circulation.* Philidephia: Lippincott Williams & Wilkins.
32. Pittenger, M. F. (2004). Mesenchymal stem cells and their potential as cardiac therapeutics. *Circulation Research* , **95:9-20.**
33. Ponticiello, M. (2000). Gelatin based resorbable spounge as a carrier matrix for human mesenchymal stem cells in cartilage regeneration therapy. *Journal of Biomedical Materials Research* , 52(2):246-55.
34. Rowley, J. A., Madlambayan, G., & Mooney, D. J. (199). Alginate hydrogels as synthetic extracellular matrix materials. *Biomaterials* , 20(1):45-53.
35. Ruszczak, Z. Effect of collagen matrices on dermal wound healing. *Advanced Drug Delivery Reviews* , 55(12):1595-611.
36. Sherwood, L. (2007). *Human Physiology, from Cells to Systems 6th Edition.* Thomson Brooks/Cole.
37. Smith, R. C. (1997). *Understanding Magnetic Resonance Imaging.* Boca Raton: CRC Press LLC.
38. Stevens, M. (2004). A rapid-curing alginate gel system:utility in periosteum-derivedcartilage tissue engineering. *Biomaterials* , 25 (5):887-894.
39. Sutton, M., & Sharpe, N. (2000). Left Ventricular Remodeling After Myocardial Infarction: Pathophysiology and Therapy. *Circulation* , 101:2981-88.

40. Tang, J., & e. a. (2006). Mesenchymal stem cells participate in angiogenesis and improve heart function in rat model of mycardial ischemia with reperfusion. *Eupropean Journal of Cario-Thoracic Surgery* . 30(2):353-61.
41. Tonnessen, T., & Knudsen, C. W. (2005). Surgical Left Ventricular Remodeling in Heart Failure. *The European Journal of Heart Failure* , 7 (5):704-707.
42. Wei, H. (2009). Cell Delivery and tracking in post-myocardial infarction cardiac stem cell therapy: an introduction for clinical researchers. *Circulation* . (DOI: 10.1007/s10741-009-9134-1)
43. Wesbey, G., Higgins, C., Lanzer, P., & Botcinick, E. (1984). Imaging and characterization of acute mycardial infarction in vivo by gated nuclear magnetic resonance. *Circulation* , 69:125-130.
44. Williams, M., Knaut, M., & Be'rube, D. (2002). Application of Microwave Energy in Cardiac Tissue Ablation: From In Vitro Analyses to Clinical Use. *Annal of Thoracic Surgery* , 74:1500-1505.
45. Wollert, K. C., & Drexler, H. M. (2005). Mesechymal Stem Cells for Myocardial Infarction: Promises and Pitfalls. *Circulation* , 112:151-3.
46. Zimmermann, W. H., Melnychenko, I., & Exchenhagen, T. (2004). Engineered heart tissue for regeneration of diseased hearts. *Biomaterials* , 25 (9):1639-1647.
47. Lee K.T., Joseph MD & Glazer S. Harvey MD. (1990). Controversy in the MR Imaging Appearance of Fibrosis. *Radiology*. 177(1):21-2
48. Wenzhen, Z. et al. (2007) Superparamagnetic Iron Oxide Labeling of Neural Stem Cells and 4.7T MRI Tracking in vivo and in vitro*. Journal of Huazhong University of Science and Technology*. 27 (1): 107-110.
49. J. Krejčí , et al. (2008). *In vitro* labeling of mouse embryonic stem cells with SPIO nanoparticles. Physiol. *Biophys.* 27, 160–169.
50. Cobb J, et al. (2009) Improved In Vivo Measurement of Myocardial Transverse Relaxation with 3 Tesla Magnetic Resonance Imaging. *Journal of Magnetic Resonance Imaging*. 30: 684–689.
51. Boxt M, Lawrence, et al. (1993) Estimation of myocardial water content using transverse relaxation time from dual spin-echo magnetic resonance imaging. *Magnetic Resonance Imaging*. 11(3): 375-383.
52. Hosch W, et al. MR-relaxometry of myocardial tissue: significant elevation of T1 and T2 relaxation times in cardiac amyloidosis. *Invest Radiol.* 2007 Sep; 42(9):636-42.
53. Allmann KH, Horch R, Uhl M, Gufler H, Altehoefer C, Stark GB, Langer M. (1997) MR imaging of the carpal tunnel. *Eur J Radiology*. 25:141–145.
54. Imbriaco M, et al. (2007) MRI Characterization of Myocardial Tissue in Patients with Fabry's Disease. *AJR* . 188:850–853
55. Maris T, Mavrogeni S. (1998) Myocardial iron deposition in Beta-Thalassemia studied by magnetic resonance imaging. *International Journal of Cardiac Imaging.* 14: 117–122.
56. Marie P, Carteaux J, et al. (1998) Detection and prediction of acute heart transplant rejection: preliminary results on the clinical use of a "black blood" magnetic resonance imaging sequence. *Transplantation Proceedings.* 30, 1933–1935

57. Wedeking P, Sotak CH, Telser J, Kumar K, Chang CA, Tweedle MF. (1992) Quantitative Dependence of MR Signal Intensity on Tissue Concentration of Gd(HP-DO3A) in the Nephrectomized Rat. *Magnetic Resonance Imaging.* 10:97-108
58. Gold G, Han E. (2004) Musculoskeletal MRI at 3.0 T: Relaxation Times and Image Contrast. *AJR.* 183:343–351
59. Duewell S, et al. (1995) Musculoskeletal MR Imaging at 4T and 1.5T: Comparison of Relaxation Times and Image Contrast. *Radiology*. 196: 551-555.
60. Sharma P, et al. Post-Contrast T1 Measurements of Blood, Infarct and Normal Myocardium at 1.5T and 3T. Proceedings of the 13th Annual Meeting of ISMRM, Miami Beach, FL, USA, 2005.
61. Babes, L , et al. (1999). Synthesis of Iron Oxide Nanoparticles Used as MRI Contrast Agents A Parametric Study. *Journal of Colloid and Interface Science.* 212: 474-482.
62. Bulte, J and Kraitchman, D . (2004). Iron oxide MR contrast agents for molecular and cellular imaging. *NMR Biomed.* 17, 484-499.
63. Howes, S . Design of a Noninvasive System for the Evaluation of Collagen Scaffolds Using MRI. *Worcester Polytechnic Institute* . May 2007.
64. CIRS. (2009). *Ultrasound Phantoms.* Retrieved December 16, 2009. http://www.cirsinc.com/067_ultra.html
65. Gribouski E, Jaimes R. (2009) The Use of Iron-oxide Nanoparticles for Hyperthermia Cancer Treatment and Simultaneous MRI Monitoring. *Worcester Polytechnic Institute*.
66. **Zhang H, et al. (2007)** Injection of bone marrow mesenchymal stem cells in the borderline area of infracted myocardium: Heart status and cell distribution. *J Thorac Cardiovasc Surg* 2007;134
67. Cornwell, K. (2006) Crosslinking of discrete self-assembled collagen threads: Effects on mechanical strength and cell–matrix interactions. *Journal of Biomedical Materials Research* Part A DOI 10.1002/jbm.a.
68. Schenck,JF. The role of magnetic susceptibility in magnetic resonance imaging: MRI magnetic compatibility of the first and second kinds. *American Association of Physicists in Medicine.* 23:6, 839. June 2006 http://mrel.usc.edu/class/591/library/Schenck-Suscept.pdf
69. Weissleder R, Stark DD, Engelstad BL, Bacon BR, Compton CC, White DL, Jacobs P, Lewis J. Superparamagnetic iron oxide: Pharmacokinetics and toxicity. AJR. *American Journal of Roentgenology* 1989 Jan-1;152(1):167-73.
70. Image Processing and Analysis in Java. *NIH.* http://rsbweb.nih.gov/ij/ Version 1.43u 24 April 2010.

Glossary

Artifacts – distortion of pixels in an image created by susceptibility effects such as water diffusion or contrast agents

Contrast agent – chemical which allows extra contrast to occur when performing an image aquisition

Echo time (TE) – the time in which the actual imaging of the subject is performed after excitation of the RF pulse

Ferumoxtran – AMI-227, superparamagnetic iron-oxide nanoparticle. SPIO contrast agent

Full width half maximum height – analysis of depth of a hole, take the full width of the depression, then take the maximum height, and then perform the measurement at half that height

Human mesenchymal stem cells – (hMSCs) stem cells that are derived from humans, non-embryonic, provide the ability to differentiate into surrounding cell types

ImageJ – designed by the NIH, program to import, examine, manipulate, analyze, and export images.

in vitro – outside of the living body

in vivo – inside of the living body

Infarcted – damaged area of the heart, dead cells

Longitudinal relaxation – relaxation of nucleic energy within surrounding nuclei, spin-spin relaxation

Macro – programming language type inside the ImageJ program

Matlab – designed by Mathworks, very complex utility program, has its own script and programming involved.

Microthread – made up of collagen or fibrin, multiple are put together to form bundles, these threads are a housing and administering unit for human mesenchymal stem cells

Myocardial Infarction – usually occurs after a heart attack, blood clot or plaque build up is usuallythe cause.

Pairwise Comparison Chart – objective analysis chart, in order to provide a ranking of objectives, functions, specifications

Phantom – in vitro model that mimics relaxation properties of the tissue you are mimicing

Phosphate buffed saline (PBS) – sterile solution, purpose is to provide neutrality in mixtures

Relaxation rate – inate time period unique to each type of tissue or subject that has relaxivity properties

Relaxivity – time at which it takes for a tissue or subject to relax back to its equilibrium state

Repetition Time (TR) – time at which the rf pulse is applied

Signal Intensity – grey scale intensity used in order to provide contrast in an MRI image

T1-Weighted – designed in order to provide/show more anatomical differences

T2-Weighted – designed in order to provide/show more pathological differences

Transverse relaxation – relaxation of nucleic energy into the transverse plane, spin-laticce relaxation

RF Pulse – magnetic field that is applied to a subject in order to agitate or excite the nuclei, to generate signal intensity

Appendix 1: Client Meeting Minutes

Meeting: Professor Glenn Gaudette - Ph.D. Biomedical Engineering.
September 22nd, 2009 – 11:00am Goddard Hall

Background: Professor Gaudette's research is focused on cardiac tissue engineering and cardiovascular biomechanics. In particular, he has developed a novel method to regenerate heart muscle (embedded microthreads).

Notes: During our meeting with Professor Gaudette the project group listened in on a brief overview of a presentation he had given at the University of Akron entitled, “Biological Microthreads for the Delivery of Stem Cells”. Included in this presentation was an overview of current delivery techniques, the new base for new and improved methods, and an in depth description on the development and promise of biological microthreads. This information played a crucial role in the compilation of an accurate and fulfilling literature review.

Also obtained from the meeting was an understanding of the “wants” of Professor Gaudette in relation to our project. Insertion of microthreads into the intended area of delivery is a somewhat uncertain process, as there are no means of correct placement verification. Improper placement of microthreads can potentially affect the thread’s efficacy and result in numerous unnecessary reapplications. Thread location confirmation in the area of infarction is the first step in maximizing thread effectiveness. Utilizing MR technology and contrast agents can aid in the thread visualization process and potentially be used for further thread analysis including thread parameters (volume, length, etc.) and stem cell induced myocardial proliferation.

Appendix 2: Objectives

Pairwise Comparison Chart

Table 16: Objective Pairwise Comparison Chart

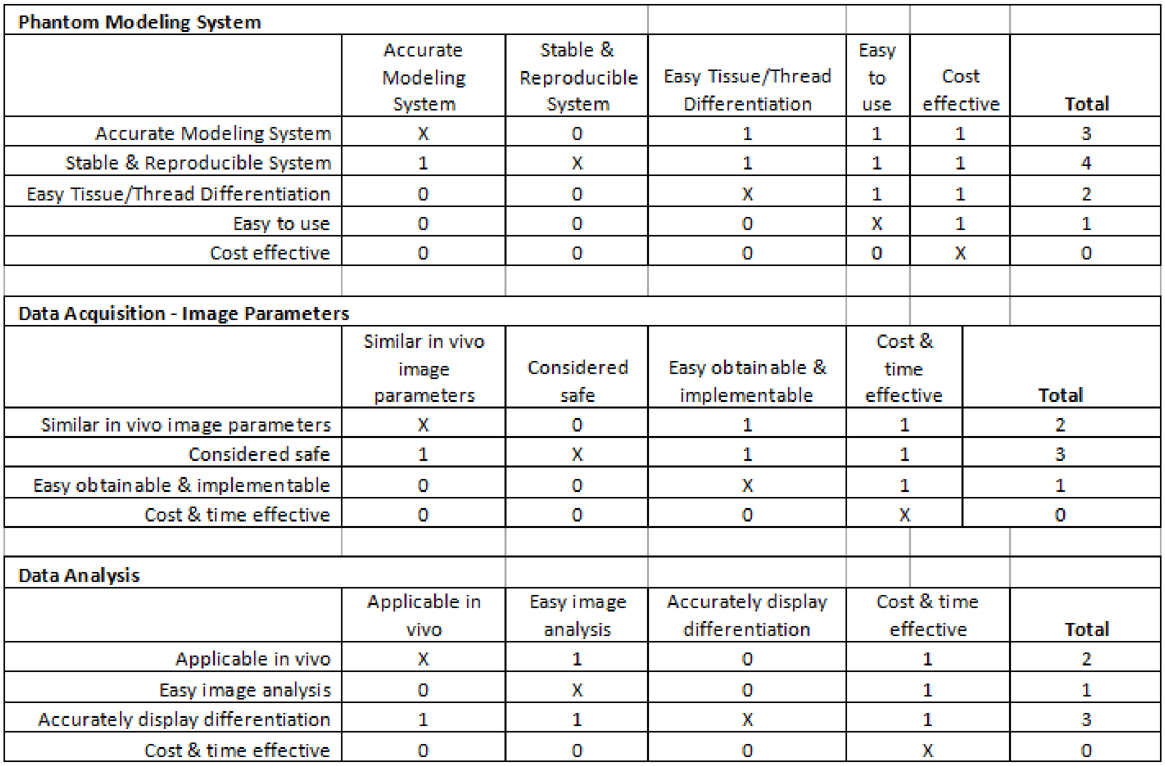

Phantom Modeling System						
	Accurate Modeling System	Stable & Reproducible System	Easy Tissue/Thread Differentiation	Easy to use	Cost effective	**Total**
Accurate Modeling System	X	0	1	1	1	3
Stable & Reproducible System	1	X	1	1	1	4
Easy Tissue/Thread Differentiation	0	0	X	1	1	2
Easy to use	0	0	0	X	1	1
Cost effective	0	0	0	0	X	0

Data Acquisition - Image Parameters					
	Similar in vivo image parameters	Considered safe	Easy obtainable & implementable	Cost & time effective	**Total**
Similar in vivo image parameters	X	0	1	1	2
Considered safe	1	X	1	1	3
Easy obtainable & implementable	0	0	X	1	1
Cost & time effective	0	0	0	X	0

Data Analysis					
	Applicable in vivo	Easy image analysis	Accurately display differentiation	Cost & time effective	**Total**
Applicable in vivo	X	1	0	1	2
Easy image analysis	0	X	0	1	1
Accurately display differentiation	1	1	X	1	3
Cost & time effective	0	0	0	X	0

Phantom Modeling System

1. Cardiac phantom representation should be accurate.
2. Cardiac modeling system should be stable and reproducible.
3. Tissue component representations and microthread should be easily differentiated.
4. Modeling system should be easy to use.
5. Modeling system should be cost effective.

Data Acquisition- Image Parameters

1. Image parameters should be similar to those used *in vivo.*
2. Safety considerations should be defined and applied to design and procedures.
3. Data acquisition should be easily obtainable and implementable.
4. Utilization of MR machine should be done in a time and cost effective manner.

Data Analysis

1. Analysis procedure should be applicable to images acquired *in vivo.*
2. Software should allow for easy image analysis.
3. Imaging software should display areas of differentiation accurately.
4. Software analysis should time and cost effective.

Weighted Objectives

Table 17: Weighted Objectives from Project Stakeholders

Objective	MQP Group	G. Pins	C. Sotak	G. Gaudette	Averaged Total	Weighted Objectives
Accurate Modeling System	4	3	3	3	3.25	3.25/10 = 0.325
Stable & Reproducible System	2	2	2	2	2	2/10 = 0.2
Easy Tissue/Thread Differentiation	3	4	4	4	3.75	3.75/10 = 0.375
Easy to use	1	1	1	1	1	1/10 = 0.1
Cost effective	0	0	0	0	0	0
Objective	MQP Group	G. Pins	C. Sotak	G. Gaudette	Averaged Total	Weighted Objectives
Similar in vivo image parameters	2	3	3	1	2.25	2.25/6 = 0.375
Considered safe	3	1	1	3	2	2/6 = 0.333
Easy obtainable & implementable	1	2	2	2	1.25	1.25/6 = 0.208
Cost & time effective	0	0	0	0	0	0
Objective	MQP Group	G. Pins	C. Sotak	G. Gaudette	Averaged Total	Weighted Objectives
Applicable in vivo	2	3	3	1	2.25	2.25/6 = 0.375
Easy image analysis	1	0	0	3	1	1/6 = 0.167
Accurately display differentiation	3	2	2	2	2.25	2.25/6 = 0.375
Cost & time effective	0	1	1	0	0.5	0.5/6 = 0.0.083

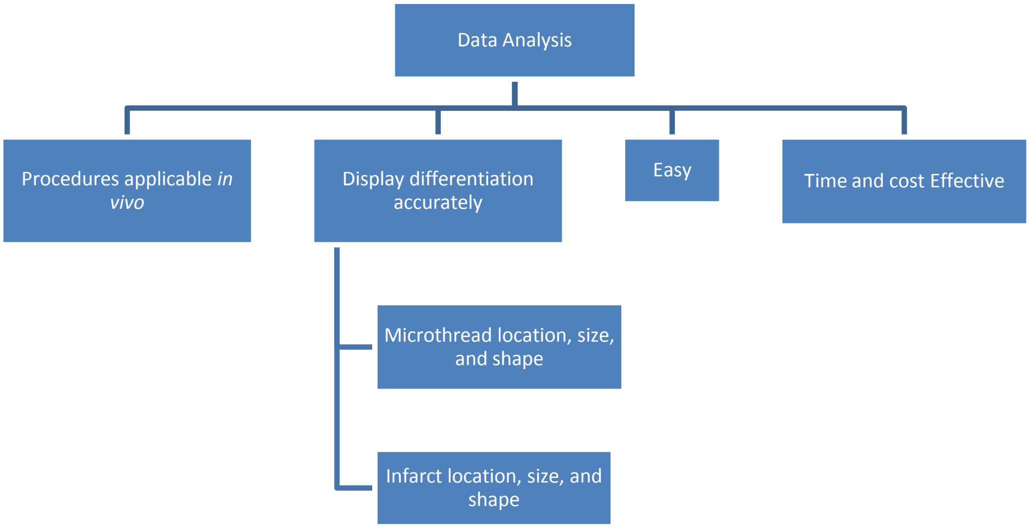

Figure 61: Data Analysis Objective Tree

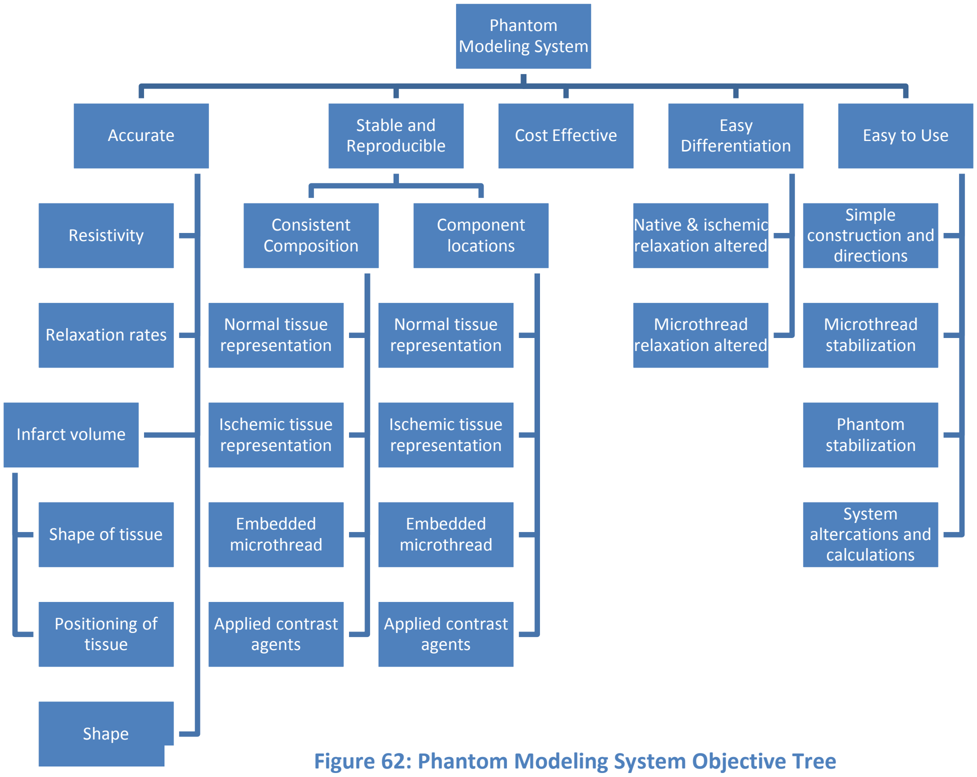

Figure 62: Phantom Modeling System Objective Tree

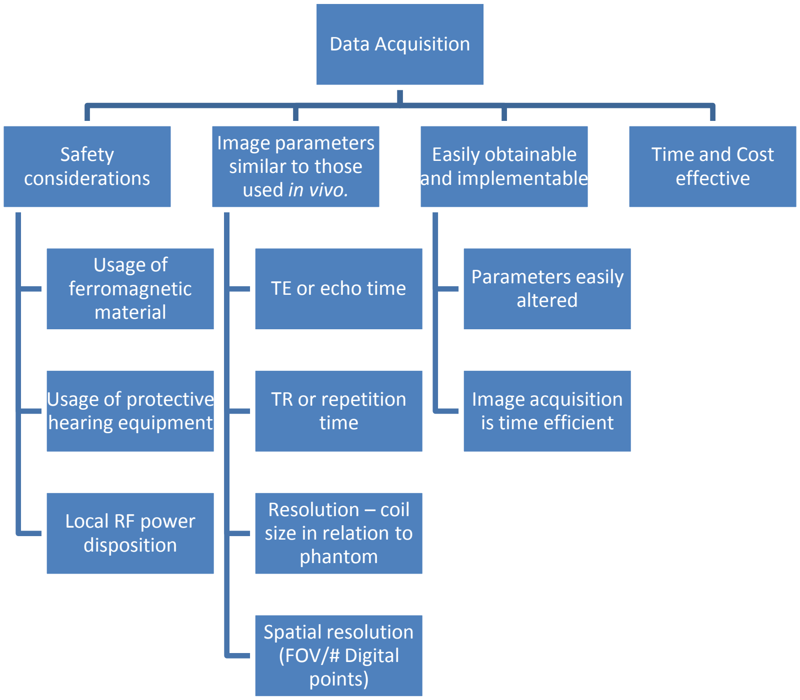

Figure 63: Data Acquisition Objective Tree

Appendix 3: Functions

Table 18: Morphological Table

FUNCTION	POSSIBLE MEANS			
Phantom modeling system should accurately/precisely mimic an in vivo system.	Water content should be about the same in different tissues	Water content should have the same percent difference in different tissues	Apply electrical stimulation to give phantom ability to contract/expand like a real heart	Use same dimensions for phantom as of a real rat heart
Contrast agent(s) should aid in differentiation of relaxation times of microthread/phantom system.	Higher concentrations of negative agents lead to decreases in T1 and T2 relaxation rates	Higher concentrations of postive agents lead to increases in T1 relaxation rates		
Image should display the desired differences in SI between the microthread/tissue phantom.	T1- use positive agents to create brighter signal in microthread than in tissue phantom	T1- use negative agents to create darker signal in microthread than in tissue phantom	T2- use positive agents to create darker signal in microthread than in tissue phantom	T2- use negative agents to create brighter signal in microthread than in tissue phantom
DAQ and analysis tools should allow for phantom/microthread. 3D reconstruction	Acquire 3D images from MRI	Acquire multiple 2D images from MRI and reconstruct on computer using software		
Applied software should allow for microthread analysis.	Create program which allow for healthy and infarcted tissue volume/location measurements	Create program which allow for microthread volume/orientation measurements		
Resulting image should accurately/precisely display microthread location.	Acquire 3D images which have higher SNR than 2D images	Image should be displayed in an xy plane for 2D images	Image should be displayed in an xyz plane for 3D images	

Function Enumeration

1) Mimic corresponding in vitro system.
    a) Native tissue model should relax with identical rates as *in vitro* native tissue.
    b) Infarct tissue model should relax with identical rates as *in vitro* infarct tissue.
2) Contrast agent relaxation differentiation.
3) Display desired differences
    a) MR parameters should capture modeling components (tissue/microthread) at sufficient relaxation differentiation time points.
    b) Software will convert relaxation rates into corresponding signal intensities.
4) 3D construction of cardiac phantom and microthread.
5) Software microthread analysis.
    a) Quantitative measurements should be used to analyze microthread success/failure.
    b) Determine physical parameters including size, shape, and volume.
    c) Confirm proper location in area of infarction
6) Display location of microthread.
    a) Tissue and microthread contrast (via applied agents and image acquisition parameters) should be as large as possible.
    b) Image acquisition and analysis should result in optimal signal to noise ratio.
    c) Image acquisition and analysis should result in optimal resolution.

Appendix 4: Calculations for Specifications

Minimal signal intensity difference calculations

- Grayscale image contains 256 possible grayscale values.
- Desired signal intensity difference = 20 percent.

(256 x 0.20) ≈ Minimum 50 grayscale value difference

Average heart rate statistics & calculations

- Over 83 percent of people who die of coronary heart disease are 65 or older.
- In men, the risk for heart attack increases significantly after the age of 45.
- In women, heart attacks are more likely to occur in the years after the age of 50.

Table 19: Heart Rate Statistics & Calculations

Age	Target HR 50-85%	Age	Target HR 50-85%
20 yrs	100 - 170 bpm	50 yrs	85 - 145 bpm
25 yrs	98 - 166 bpm	55 yrs	83 - 140 bpm
30 yrs	95 - 162 bpm	60 yrs	80 - 136 bpm
35 yrs	93 - 157 bpm	65 yrs	78 - 132 bpm
40 yrs	90 - 153 bpm	70 yrs	75 - 128 bpm
45 yrs	88 - 149 bpm		

**** Statistics courtesy of the American Heart Association, Inc. 2005 ©***

Using Table 14 and the associated statistics above, average heart rate approximations of the subjects imaged can be made. This information could be used to set proper MR parameters for limiting the effects of image artifacts and noise due to the beating of the heart. Heart rate will reflect the average from the data in yellow with the rationale being that 83% of people who die from CAD are 65 and older, and men/women over the age of 50 have significantly greater risks of MI. HR used will be the 50% HR target zone statistics from the table above, as it represents the mid-point of cardiac output performance. This technique is applicable to numerous species as long as statistical data regarding cardiac performance is available.

Average HR of patient = [(85+83+80+78+75) / 5] ≈ 80 bpm

Spatial resolution calculation

Hydrated microthreads are average 100µm in diameter. Spatial resolution should be small enough for the doped microthread to represent 2-3 pixel widths.

(100µm/ 3) ≈ 30µm = Largest image spatial resolution

Normal and ischemic relaxation rate calculations

Table 20: Relaxation Rate Variation

0.5Tesla				
	T1	**STD**	**T2**	**STD**
Normal Myocardium - Case Study 7			48.3	5.5
Normal Myocardium - Case study 3			54.6	5.7
Normal Myocardium - Case study 8			50	5
Avg.	**-**	**-**	**51.0**	**9**

1.5Tesla				
	T1	**STD**	**T2**	**STD**
Normal Myocardium - Case Study 5			44	6
Normal Musculoskeletal - Case Study 2	1075		33	
Normal Myocardium - Case Study 4	1146	71		
Normal Myocardium - Case Study 6			52	
Normal Musculoskeletal - Case Study 10			35.3	3.9
Normal Myocardium - Case Study 12	1150	60		
Avg.	**1124**	**93**	**41.1**	**7.2**

2.0Tesla				
	T1	**STD**	**T2**	**STD**
Normal Myocardium - Case Study 9	1060		37	
Avg.	**1060.0**	**-**	**37**	-

3.0Tesla				
	T1	**STD**	**T2**	**STD**
Normal Myocardium - Case Study 1			31.6	5.8
Normal Myocardium - Case Study 10			31.7	1.9
Normal Myocardium - Case Study 12	1260	60		
Normal Myocardium – Case Study 13	1471	31		
Avg.	**1365**	**45**	**32**	**6.1**

4.0Tesla				
	T1	**STD**	**T2**	**STD**
Normal Musculoskeletal - Case Study 11	1830	170	26	1
Avg.	**1830.0**	**170**	**26.0**	**1**

We were able to determine the average relaxation rates, along with the uncertainties of the average value by propagating the given standard deviations with the following equation:

$$(xy)/2 \rightarrow \sigma_{average} = \sqrt{(\sigma_x^2 + \sigma_y^2)}$$

Equation 4

Table 21: Case Study References

Case Study 1	Cobb J, et al. Improved In Vivo Measurement of Myocardial Transverse Relaxation with 3 Tesla Magnetic Resonance Imaging. *JOURNAL OF MAGNETIC RESONANCE IMAGING*. 2009 30: 684–689.
Case Study 2	McRobbie W, Donald, et al. MRI: From Picture to Proton. 2nd ed. Cambridge: Cambridge University Press, 2006. 155.
Case Study 3	Boxt M, Lawrence, et al. Estimation of myocardial water content using transverse relaxation time from dual spin-echo magnetic resonance imaging. *Magnetic Resonance Imaging*. Elsevier Inc. 11(3): 375-383. 1993.

Case Study 4	Hosch W, et al. MR-relaxometry of myocardial tissue: significant elevation of T1 and T2 relaxation times in cardiac amyloidosis. *Invest Radiol.* 2007 Sep; 42(9):636-42.
Case Study 5	Allmann KH, Horch R, Uhl M, Gufler H, Altehoefer C, Stark GB, Langer M. MR imaging of the carpal tunnel. *Eur J Radiology* 1997; 25:141–145.
Case Study 6	Imbriaco M,Spinelli L, et al. MRI Characterization of Myocardial Tissue in Patients with Fabry's Disease. *AJR* 2007; 188:850–853
Case Study 7	Maris T, Mavrogeni S,Myocardial iron deposition in Beta-Thalassemia studied by magnetic resonance imaging. *International Journal of Cardiac Imaging* 14: 117–122, 1998. 117
Case Study 8	Marie P, Carteaux J, et al. Detection and prediction of acute heart transplant rejection: preliminary results on the clinical use of a "black blood" magnetic resonance imaging sequence Transplantation Proceedings, 30, 1933–1935 (1998)
Case Study 9	Wedeking P, Sotak CH, Telser J, Kumar K, Chang CA, Tweedle MF. (1992) Quantitative Dependence of MR Signal Intensity on Tissue Concentration of Gd(HP-DO3A) in the Nephrectomized Rat. *Magnetic Resonance Imaging.* 10:97-108
Case Study 10	Gold G, Han E. Musculoskeletal MRI at 3.0 T: Relaxation Times and Image Contrast. *AJR* 2004; 183:343–351
Case Study 11	Duewell S, et al. Musculoskeletal MR Imaging at 4T and 1.5T: Comparison of Relaxation Times and Image Contrast. Radiology 1995; 196: 551-555.
Case Study 12	Sharma P, et al. Post-Contrast T1 Measurements of Blood, Infarct and Normal Myocardium at 1.5T and 3T. Proceedings of the 13th Annual Meeting of ISMRM, Miami Beach, FL, USA, 2005.
Case Study 13	Stanisz, Greg J, et al. T1, T2 Relaxation and Magnetization Transfer in Tissue at 3T. Magnetic Resonance in Medicine. August 2005. 54(3) p.507-12.

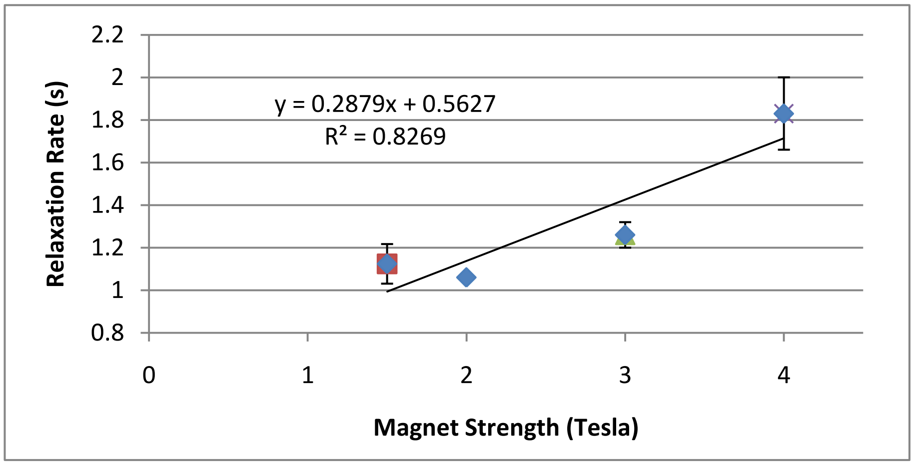

Figure 64: Average T1 Relaxation Rates vs. Magnet Strength

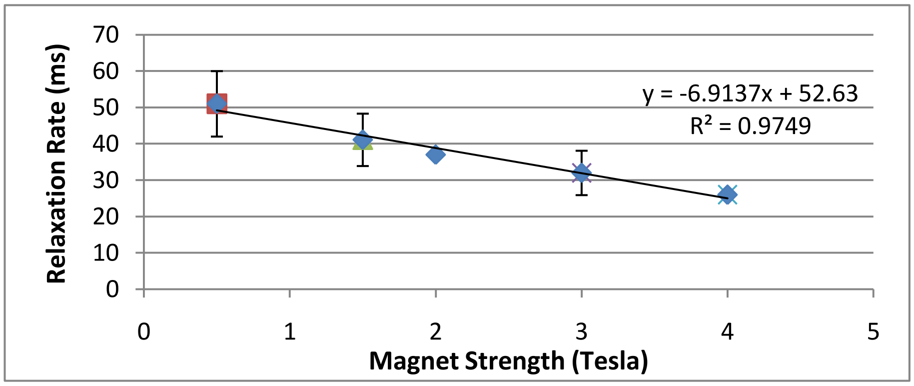

Figure 65: Average T2 Relaxation Rates vs. Magnet Strength

$$y = 0.2879x + 0.5627$$

Equation 5: T1 Trend line equation

$$y = -6.9137x + 52.63$$

Equation 6: T2 Trend line equation

* Prior to switching to 3.T, trend lines were extended using the derived formula to approximate 4.7 Tesla T1 and T2 relaxation rates. 4.7T T1 relaxation was found to be approximately ***1.98 seconds*** while T2 relaxation was ***20.1 milliseconds***.

The relationship between water content and T2 relaxation of left ventricular myocardium was used to approximate relaxation rates of infarcted myocardium with known water content percentages. Using 0.5T dual spin echo MR imaging Case Study 4 estimated myocardial water content to be:

$$WC_{LV} = 62.1 + (0.29 * T2_{LV})$$

Equation 7: Water Content of Left Ventricle as a function of T2

Water content is approximated to be ***75.9% +/- 0.7*** in normal myocardium and ***79.0% +/- 0.9*** in ischemic tissue 1 week post infarct. These values were entered into the water content equation to verify the equation's accuracy. The resulting data when enter in to equation 3 was 0.2% outside of the given standard deviation of water content ***(76.8%)***. To account for the error in the normal T2 water content percentage and make the most accurate approximation of infarct relaxation via equation 3, the maximum value (within one standard deviation) of infarct water content was used ***(79.9%)***. Using this information the T2 trend line was adjusted to estimate T2 infarction relaxation time versus magnet field strength. The new y intercept and the resulting values are calculated below.

T2 infarct relaxation time calculation

$$79.9 = 62.1 + (0.29 * T2_{LV})$$

$$T2_{LV} = (79.9 – 62.1) / 0.29$$

$$T2_{LV} = 61.4 \text{ ms}$$

T2 infarct trend line equation

$$61.4 = -6.9137(0.5T) + X$$

$$X = 64.85$$

$$y = -6.9137x + 64.85$$

Table 22: T2 Normal v Infarcted relaxation

Tesla (T)	*0.5 T*	*1.5 T*	*2 T*	*3 T*	*4 T*	*4.7 T*
Normal Myocardium	*48.9 ms*	*42.3 ms*	*38.8 ms*	*31.9 ms*	*25.9 ms*	*20.1 ms*
Infarcted Myocardium	*61.4 ms*	*54.5 ms*	*51.0 ms*	*44.1 ms*	*38.2 ms*	*32.4 ms*

Infarct relaxation calculations

$0.5T = -6.9137 (0.5) + 64.85 = 61.4$ ms

$1.5T = -6.9137 (1.5) + 64.85 = 54.5$ ms

$2.0T = -6.9137 (2.0) + 64.85 = 51.0$ ms

$3.0T = -6.9137 (3.0) + 64.85 = 44.1$ ms

$4.0T = -6.9137 (4.0) + 64.85 = 38.2$ ms

$4.7T = -6.9137 (4.7) + 64.85 = 32.4$ ms

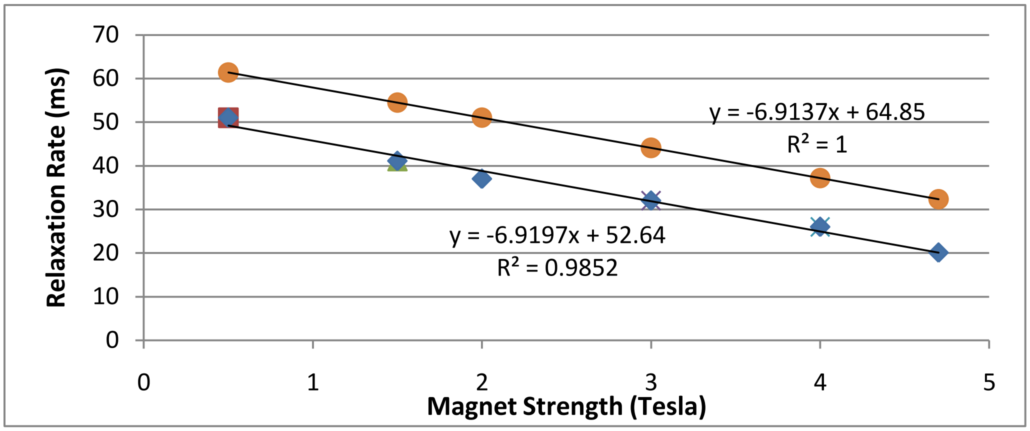

Figure 66: Normal (yellow) v Infarct (blue) trend lines

Contrast agent differentiation calculations

Contrast agent relaxation can be defined as $R' = R + rC$

Where: **R** = the relaxation rate = [(1/T_x) = inverse of relaxation time]
r = specific concentration relaxivity
C = agent concentration

Table 23: MQP reference particle data [65]

Iron Oxides	Contrast Effect	Administration	Target	Concentration
Feridex	T2 negative enhancement	intravenous	Liver	11.2mg Fe/ml
Lumirem	T2* enhancement	oral	intestinal	52.5mg Fe/300ml
Resovist	T2/T1 negative enhancement	intravenous	Liver	0.5 mol Fe/L
Sinerem	T1/T2 negative enhancement	intravenous infusion	lymph nodes	??
SPIOM	T1/T2 negative enhancement	intravenous	Heart	??
Gadolinium				
Eovist	T1 positive enhancement	intravenous	Liver	181.43mg Fe/L
Dotarem	T1 positive enhancement	intravenous	intracranial	0.5 mol/L
Gadovist	T1 positive enhancement	intravenous	CNS	0.5 mol/L
MultHance	T1 positive enhancement	intravenous	liver/ CNS	0.05 mg/ml
Omniscan	T1 positive enhancement	intravenous	intracranial	287mg/ml

SPIO particle relaxation error analysis

Knowing that the size of iron nanoparticles plays a large role in their effect on T1 and T2 relaxation as small analysis was done to determine the relationship between particle size and R2 values. If the size of the particles that are utilized is unknown, similar analyses can be conducted to make an approximation. Endorem SPIO nanoparticles are 80-150nm in diameter and the iron oxide crystal is 4.8 - 5.6nm in size coated with dextran. Looking at a prior MQP, it was found that SPIO particle size and concentration directly affect the resulting relaxation time. The ratio of particle size to slope of the R2 values is **[(**32.4nm ÷ 14.4nm**)** ÷ **(**2.21 ÷ 1.22**)]** = (2.25 ÷ 1.8) or approximately 1.25. Thus to find the particle slope of Endorem (5.2nm):

(14.4nm ÷ 5.2nm) = 2.77 → *(2.77 ÷ x) = 1.25* → ***x = 2.22 = additional slope***

[*2.22 (additional) * 2.21 (previous)****]** = **4.91 = total slope***

Next we can make approximations as to the y-intercept of the linear regression. The ratio of particle size to y-intercept of the R2 values is **[(**32.4nm ÷ 14.4nm**)** ÷ **(**1.765 ÷ 22.63**)]** = 2.25 ÷ 0.78 or approximately 2.88. Thus to find the y-intercept of Endorem (5.2nm)

(2.77 ÷ x) = 2.88 → x = 0.962 = y-intercept of linear regression.

It was noted that 25ug Fe/mL of Endorem when labeling neural stem cells decreased the T2 signal intensity by 50.7% compared to unlabeled cells. The calculation of T2 relaxation time indicated T2 relaxation time of labeled cells and unlabeled cells was 516 ms and 77 ms respectively, relaxation rates R2 (1/T2) were 1.94/s and 12.98/s. [49]

(516ms ÷ 77ms) = **6.7x** normal values [48]

R2 → (1 ÷ 516ms) = 12.98 and (1 ÷ 77ms) = 1.94

Equation formulated = 4.91x + 0.962

[(4.91 * 12.98) + 0.962] = 64.7

[(4.91 * 1.95) + 0.962] = 10.5

(64.7 ÷ 10.5) = **6.2x** normal values

*Percent Error = [(6.7 – 6.2) ÷ 6.7] * 100 =* ***7.5%***

Appendix 5: Design Alternatives

Potential Designs: Phantom Modeling System

Design 1: *In vitro* single vegetation phantom model comprising only one type of vegetation, such as a potato. The surrounding area will represent healthy myocardium and will be doped with positive contrast agents to possess relaxation times corresponding to real cardiac tissue. The microthread will also be doped with contrast agents. The area of infarction will be represented by the white potato itself, as they will be doped to possess such MRI properties.

Figure 67: White Potato Phantom

Design 2: *In vitro* dual vegetation phantom model comprising of two different types of vegetation such as a potato and a carrot. These components will be doped with different types and concentrations of contrast agents to create relaxation times which correspond to real cardiac tissue. A non-metallic divider will be utilized to restrict the diffusion and mixing of the contrast agents.

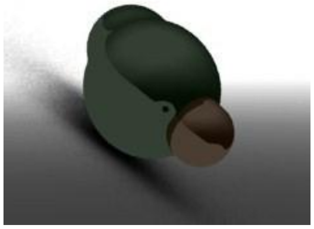

Figure 68: Potato and Carrot Phantom

Design 3: *In vitro* Gelatin Model. This model helps to establish a differentiation of normal and infarcted regions of the heart, by representing each part of the heart as a separate compartment. This would be encased in a plastic mold. The inside of the mold would be filled with a gelatin, each doped to mimic each part of the heart based on their relaxation rate, normal and infarcted. The microthread would be doped in order to distinguish it from the infarcted area.

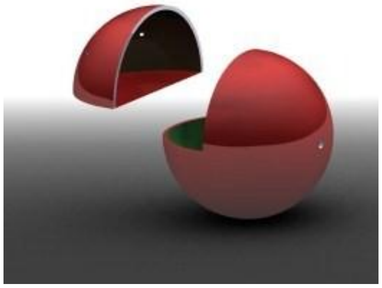

Figure 69: Separated Gelatin Phantom

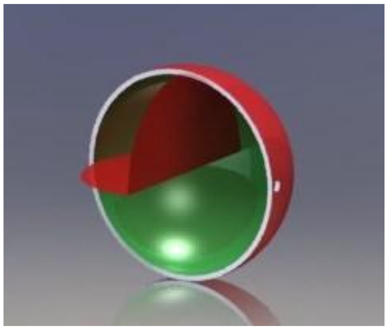

Figure 70: Gelatin Phantom

Table 24: Objectives and Constraints for Phantom

Cardiac Modeling System		**Design** →			
Objectives & Constraints	**Weight**	**D1**	**D2**	**D3**	**D4**
C: Within size limitations	**Y/N**	Y	Y	Y	N
C: Static microthread placement	**Y/N**	Y	Y	Y	Y
O: Representation should be accurate	**0.325**	2(.325)	1(.325)	2(.325)	2(.325)
O: Should be stable and reproducible	**0.2**	1(.20)	1(.20)	2(.20)	1(0.2)
O: Tissue & microthread easily differentiated	**0.375**	1(.375)	1(.375)	2(.375)	2(.375)
O: Should be easy to use	**0.1**	2(.10)	2(.10)	1(.10)	1(.10)
O: Should be cost effective	**0**	2(0)	2(0)	1(0)	0(0)
Total		**1.425**	**1.1**	**1.9**	**1.7**

Potential Designs: Data Acquisition

Design 1: Delayed enhancement MRI (DE-MRI). Ischemic tissue has significantly greater amounts of interstitial space than viable tissue. Presumably because these processes are diffusion mediated, gadolinium-chelate accumulates in greater concentrations in ischemic myocardium within minutes following contrast administration. MR parameters include: ECG-gating, inversion recovery (IR), and rewound (fast) gradient echo sequencing (FGE). IR time will be chosen to null the normal myocardium making areas of infarction appear hyper-enhanced.

Design 2: Fast Spin Echo MRI (FSE-MRI). The FSE technique can acquire multiple lines of data per repetition and thus an entire cardiac image can be taken within one breath hold. This limits the effect of image artifacts due to movement of thoracic cavity during pulse sequences. MR parameters include: ECG-gating, blood suppression preparation (BSP), and FSE. BSP will reduce the signal from blood taken during acquisition (during diastole). It involves a double inversion preparation scheme applied at TI prior to FSE acquisition.

Design 3: Spin Echo MRI (SE-MRI). The SE technique is similar to the FSE described in the previous design however this technique will be simplified. This will not include any ECG-Gating nor blood suppression preparation. All techniques and preparations regarding cardiac imaging will be ignored limiting this technique to stationary objects. This technique is typically taken setting TR and TE values only. The TR and TE time is calculated based upon the relaxation time of the stationary phantom that will be imaged.

Table 25: Objectives and Constraints for Data Acquisition

Data Acquistition		**Design**	→	
Objectives & Constraints	**Weight**	**D1**	**D2**	**D3**
C: Applicable spatial resolution	**Y/N**	Y	Y	Y
O: Parameters similar to those *in vivo*	**0.375**	2(.375)	2(.375)	1(.375)
O: Safety considered and defined	**0.333**	2(.333)	2(.333)	2(.333)
O: Easily obtainable & implementable	**0.208**	0(.208)	0(.208)	2(.208)
O: Time and cost effective	**0**	1(0)	2(0)	1(0)
Total		**1.416(-)**	**1.416(+)**	**1.457**

Potential Designs: Data Analysis

Design 1: ImageJ software with 3D analysis plug-in. ImageJ is a public domain, Java-based image processing program developed to display, edit, analyze, and process a variety of image formats including TIFF, PNG, GIF, JPEG, and BMP. ImageJ can calculate area and pixel value statistics, measure distances and angles, and create density histograms and line profile plots. It supports standard image processing functions including logical and arithmetical operations between images, contrast manipulation, convolution, Fourier analysis, sharpening, smoothing, edge detection and median filtering. Custom acquisition, analysis and processing plug-ins can be developed using a built-in editor and a Java compiler.

Design 2: Matlab program is a high-level language and interactive environment produced by Mathworks. Inc. It enables you to perform computationally intensive tasks, such as 3D image reconstruction, or even image analysis, faster than with traditional programming languages such as C, C++, and Fortran. You can use MATLAB in a wide range of applications, including signal and image processing, communications, control design, test and measurement, and financial modeling and analysis.

Design 3: Segment is a free image analysis tool for Windows, which was originally constructed by Einar Heiberg at the Cardiac MR Group at Lund University and Medviso AB. It was developed specifically for cardiovascular MR image analysis. This program has the ability to acquire and analyze 2D, as well as 3D MRI and CT images. Some analyses that can be done in the program are length, volume, and area measurements in the regions of interest. The program allows the user to highlight a specific region of interest in order to easily display the significant portions of the image. An image can also be manipulated by changing its light and contrast, its color-map settings (grayscale, hot, HSV, Jet, or SPECT), and by adding Gaussian white noise.

Table 26: Objectives and Constraints for Data Analysis

Data Analysis		**Design** →		
Objectives & Constraints	**Weight**	**D1**	**D2**	**D3**
C: Allow for 3-D image analysis	**Y/N**	Y	Y	Y
O: Applicable to images acquired *in vivo*	**0.375**	2(.375)	2(.375)	2(.375)
O: Allow easy image analysis	**0.167**	1(.167)	1(.167)	2(.167)
O: Display areas of differentiation accurately	**0.375**	2(.375)	2(.375)	2(.375)
O: Time and cost effective	**0.083**	2(.083)	2(.083)	2(.083)
Total		**1.833**	**1.833**	**2.0**

Table 27: Sub-Objective Weighting for Phantom

Static placement of Phantom		**Method** →		
Objectives	**Weight**	**Secured containment**	**Phantom pining**	**Flat bottom phantom**
O: Should be accurate	**0.375**	2(0.375) = .75	1(0.375) = .375	0(0.375) = 0
O: Should be reproducible	**0.325**	2(0.325) = .650	2(0.325) = .650	1(0.325) = .325
O: Should be easy to use	**0.2**	2(0.2) = .40	1(0.2) = .20	1(0.2) = .20
O: Should be cost effective	**0.1**	1(0.1) = .10	1(0.1) = .10	2(0.1) = .20
Total	→	***1.9***	***1.325***	***0.725***

Static placement of Phantom		**Method** →		
Objectives	**Weight**	**Clamp down**	**Velcro**	**Double sided tape**
O: Should be accurate	**0.375**	1(0.375) = .375	2(0.375) = .75	2(0.375) = .75
O: Should be reproducible	**0.325**	2(0.325) = .650	1(0.325) = .325	1(0.325) = .325
O: Should be easy to use	**0.2**	2(0.2) = .40	2(0.2) = .40	2(0.2) = .40
O: Should be cost effective	**0.1**	1(0.1) = .10	2(0.1) = .20	2(0.1) = .20
Total	→	***1.525***	***1.675***	***1.675***

Table 28: Sub-Objective Weighting for Phantom Contrast Agent Delivery

Phantom contrast agent delivery		**Method** →		
Objectives	**Weight**	**Injection**	**Static Saturation**	**Dynamic Saturation**

O: Should be accurate	**0.375**	1(0.375) = .375	1(0.375) = .375	2(0.375) = .75
O: Should be reproducible	**0.2**	2(0.2) = .4	2(0.2) = .4	2(0.2) = .4
O: Tissue representation & microthread should be easily differentiated	**0.325**	2(0.325) = .650	2(0.325) = .650	2(0.325) = .650
O: Should be easy to use	**0.1**	2(0.1) = .2	2(0.1) = .2	2(0.1) = .2
O: Should be cost effective	**0**	2(0) = 0	2(0) = 0	2(0) = 0
Total	→	***1.625***	***1.625***	***2***

Table 29: Sub-Objective Weighting for Microthread Contrast Agent Delivery

Microthread contrast agent delivery		**Method** →		
Objectives	**Weight**	**Adhesion**	**Static Saturation**	**Dynamic Saturation**
O: Should be accurate	**0.375**	2(0.375) = .75	1(0.375) = .375	1(0.375) = .375
O: Should be reproducible	**0.2**	2(0.2) = .4	1(0.2) = .2	1(0.375) = .375
O: Tissue representation & microthread should be easily differentiated	**0.325**	2(0.325) = .650	2(0.325) = .650	2(0.325) = .650
O: Should be easy to use	**0.1**	1(0.1) = .1	2(0.1) = .2	2(0.1) = .2
O: Should be cost effective	**0**	2(0) = 0	2(0) = 0	2(0) = 0
Total	→	***1.9***	***1.425***	***1.6***

Table 30: Sub-Objective Weighting for Contrast Agent Use

Contrast agent applied		**Method** →	
Objectives	**Weight**	**Gadolinium based**	**Iron Oxide based**
O: Should be accurate	**0.375**	1(0.375) = .375	2(0.375) = .75
O: Should be reproducible	**0.2**	1(0.2) = .2	2(0.2) = .4
O: Tissue representation & microthread should be easily differentiated	**0.325**	1(0.325) = .325	2(.325) = .65
O: Should be easy to use	**0.1**	2(0.1) = .2	2(0.1) = .2
O: Should be cost effective	**0**	2(0) = 0	2(0) = 0
Total	→	***1.1***	***2***

Appendix 6: Preliminary Data

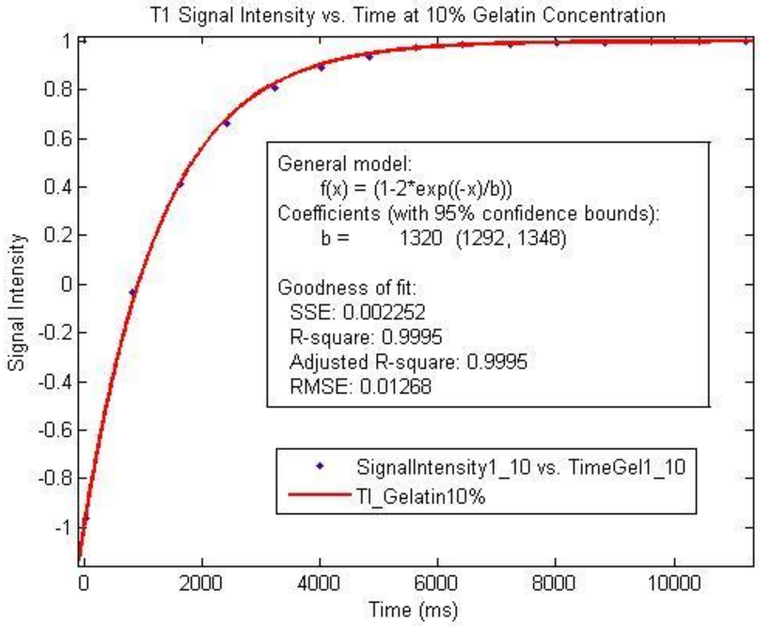

Figure 71: T1 of 10% Gelatin Concentration

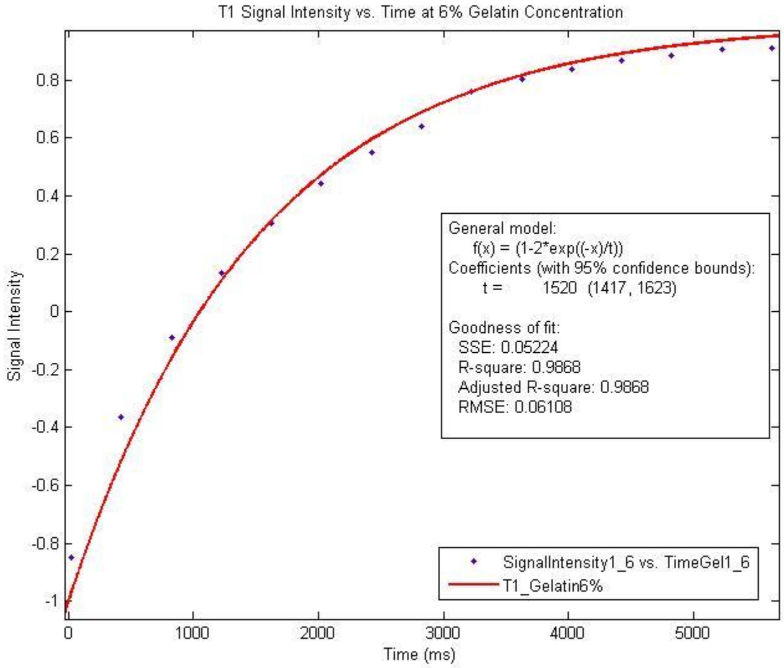

Figure 72: T1 of 6% Gelatin Concentration

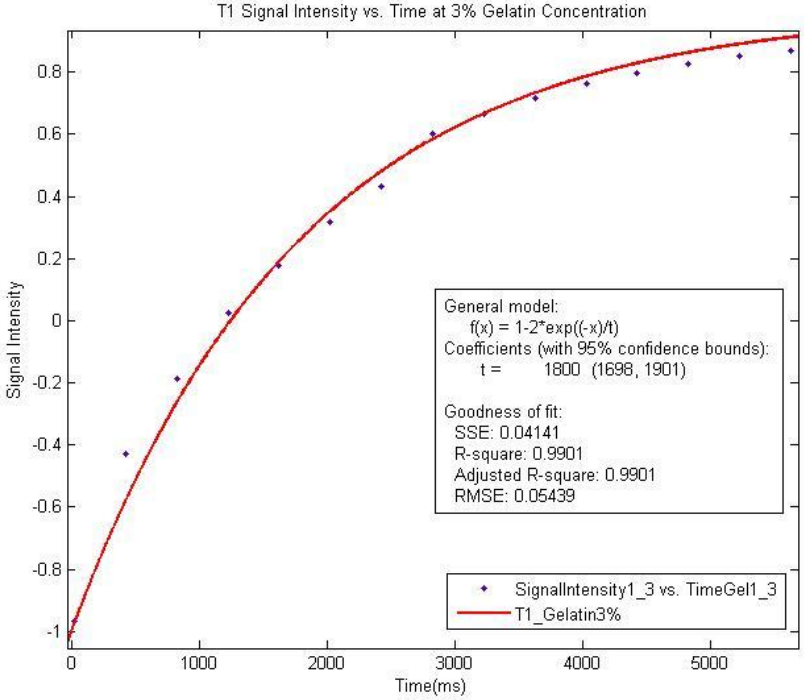

Figure 73: T1 of 3% Gelatin Concentration

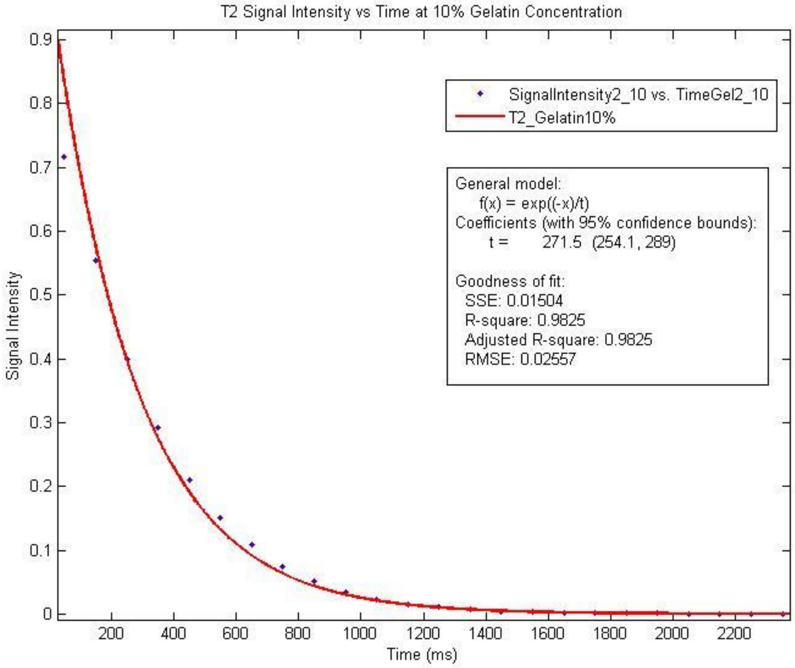

Figure 74: T2 of 10% Gelatin Concentration

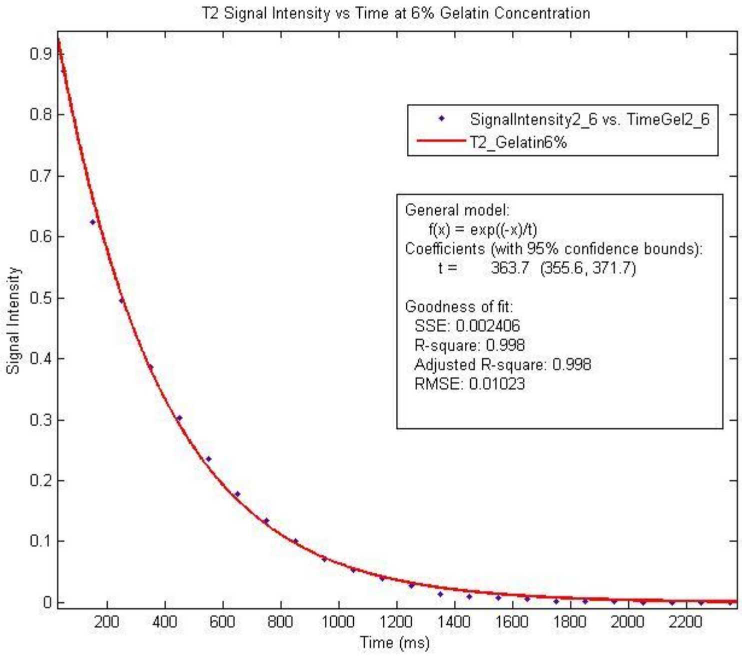

Figure 75: T2 of 6% Gelatin Concentration

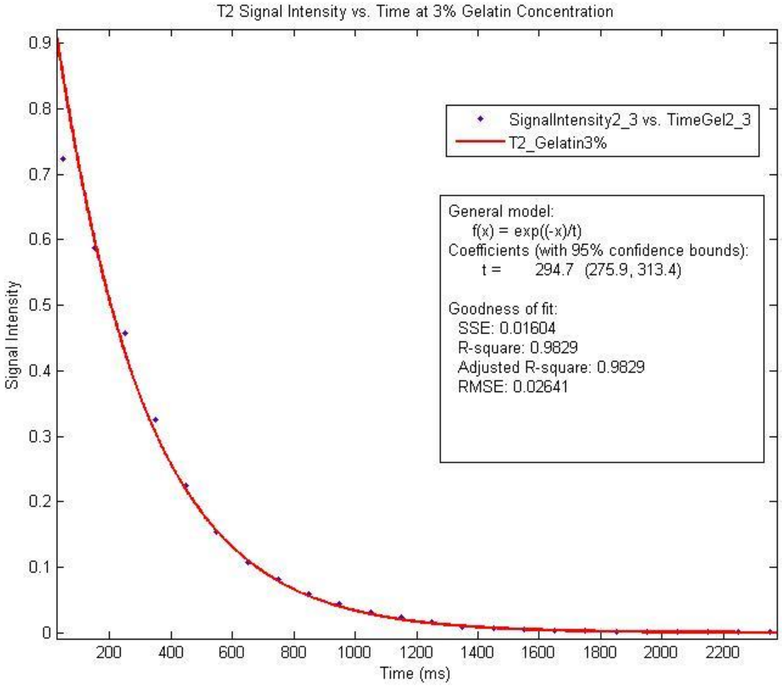

Figure 76: T2 of 3% Gelatin Concentration

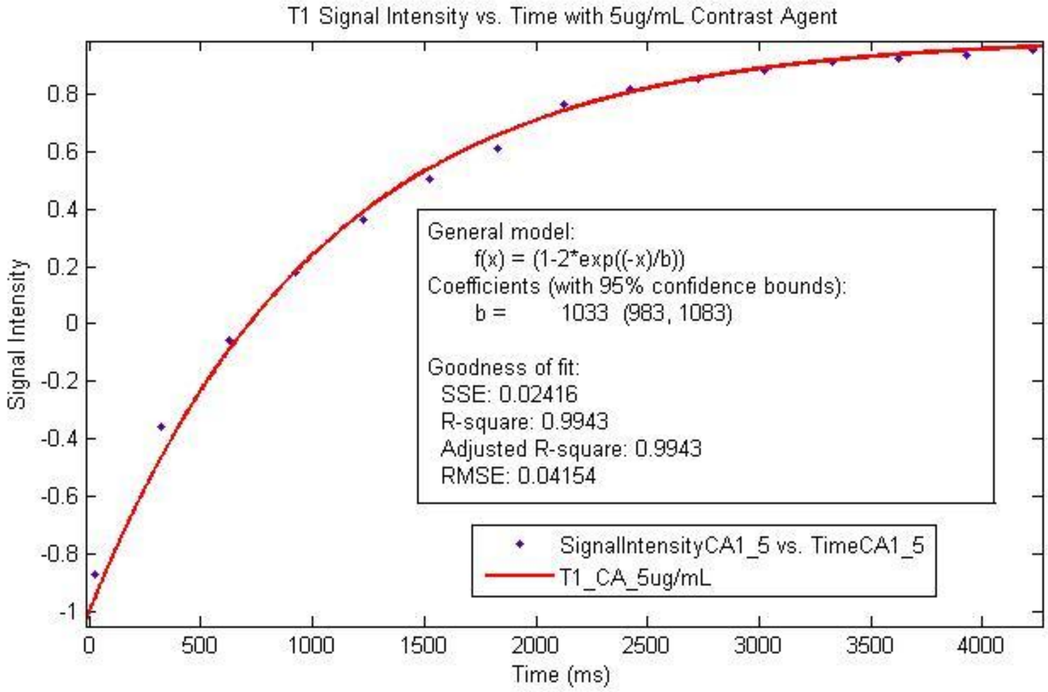

Figure 77: T1 of 5ug/mL Contrast Agent

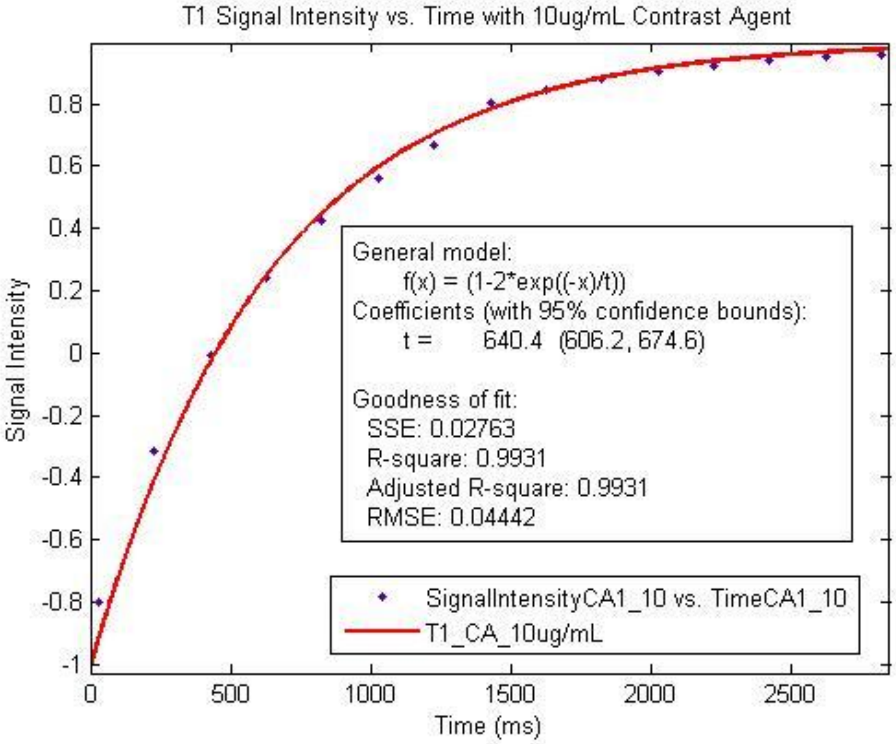

Figure 78: T1 of 10ug/mL Contrast Agent

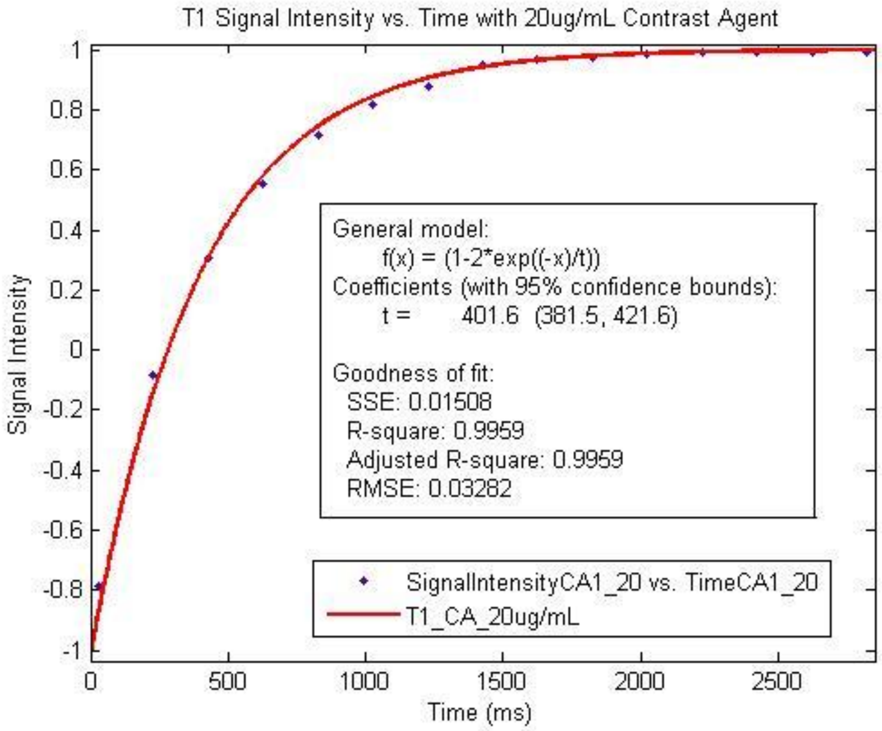

Figure 79: T1 of 20 ug/mL Contrast Agent

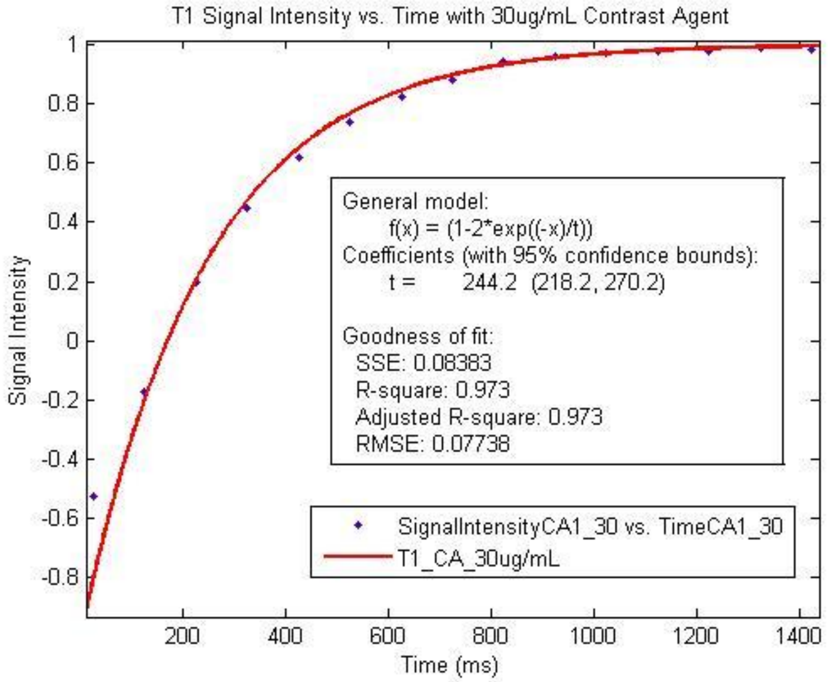

Figure 80: T1 of 30ug/mL Contrast Agent

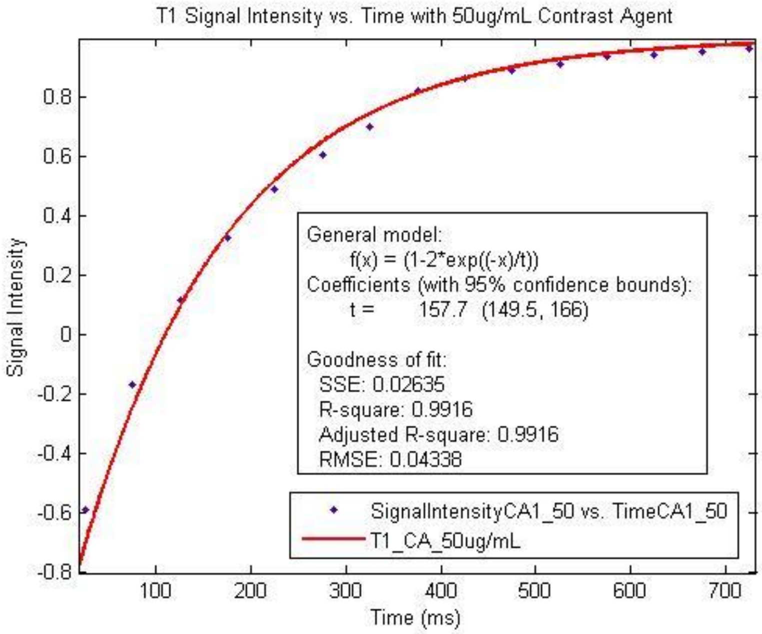

```
General model:
     f(x) = (1-2*exp((-x)/t))
Coefficients (with 95% confidence bounds):
       t =       157.7  (149.5, 166)

Goodness of fit:
  SSE: 0.02635
  R-square: 0.9916
  Adjusted R-square: 0.9916
  RMSE: 0.04338
```

Figure 81: T1 of 50 ug/mL Contrast Agent

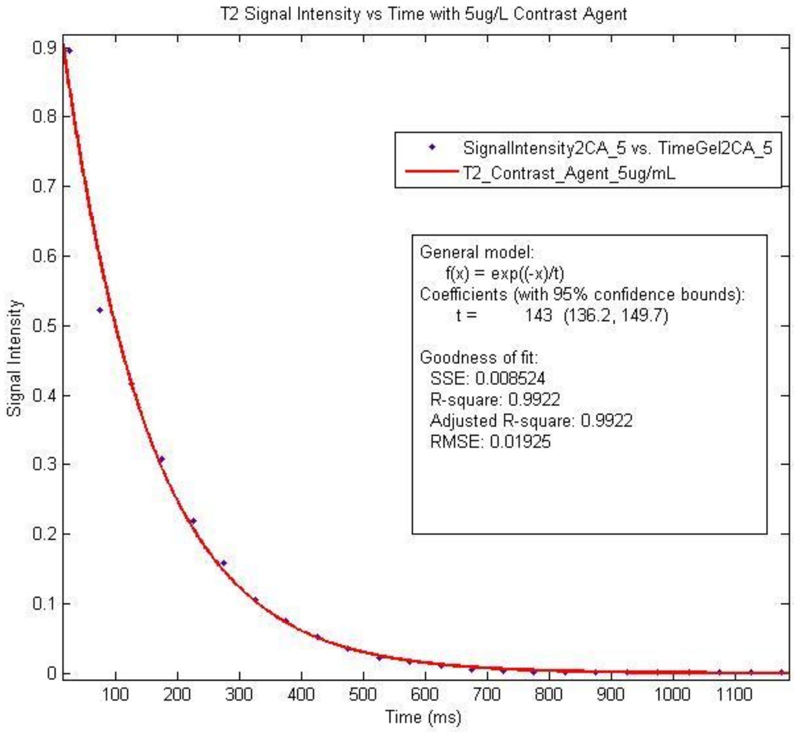

```
General model:
     f(x) = exp((-x)/t)
Coefficients (with 95% confidence bounds):
       t =         143  (136.2, 149.7)

Goodness of fit:
  SSE: 0.008524
  R-square: 0.9922
  Adjusted R-square: 0.9922
  RMSE: 0.01925
```

Figure 82: T2 of 5 ug/mL Contrast Agent

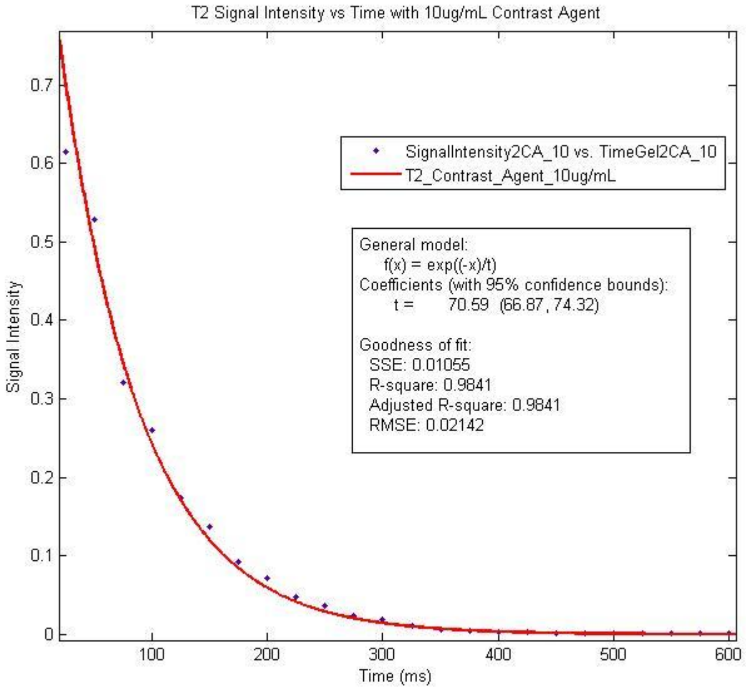

```
General model:
     f(x) = exp((-x)/t)
Coefficients (with 95% confidence bounds):
       t =       70.59  (66.87, 74.32)

Goodness of fit:
  SSE: 0.01055
  R-square: 0.9841
  Adjusted R-square: 0.9841
  RMSE: 0.02142
```

Figure 83: T2 of 10 ug/mL Contrast Agent

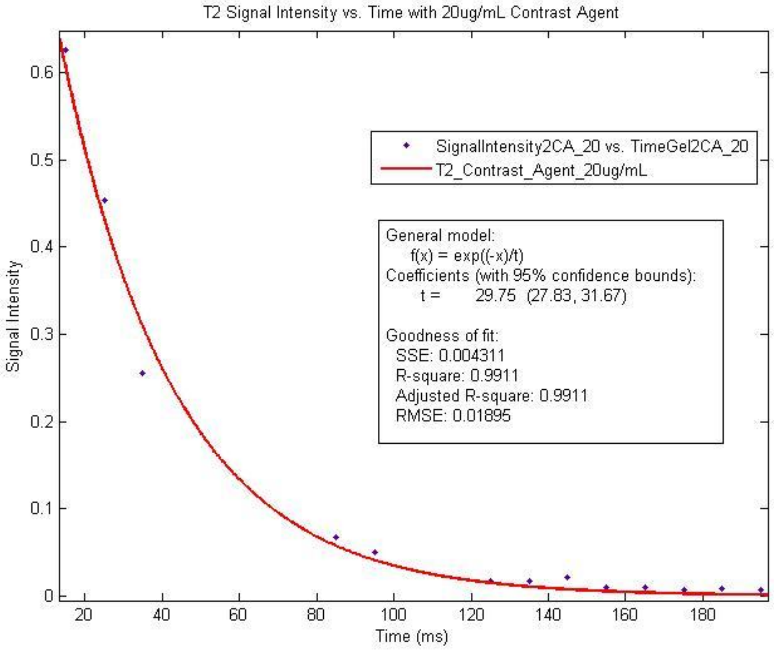

```
General model:
     f(x) = exp((-x)/t)
Coefficients (with 95% confidence bounds):
       t =       29.75  (27.83, 31.67)

Goodness of fit:
  SSE: 0.004311
  R-square: 0.9911
  Adjusted R-square: 0.9911
  RMSE: 0.01895
```

Figure 84: T2 of 20 ug/mLContrast Agent

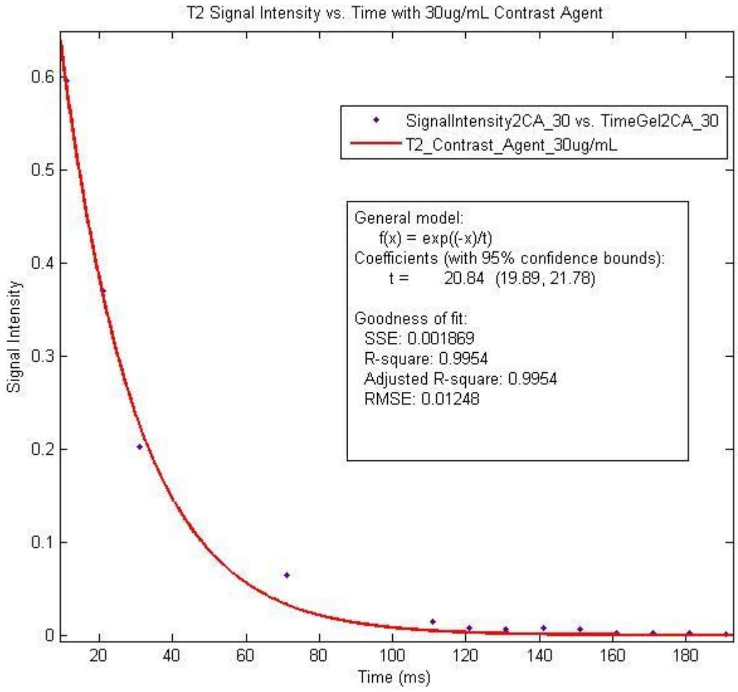

Figure 85: T2 of 30 ug/mL Contrast Agent

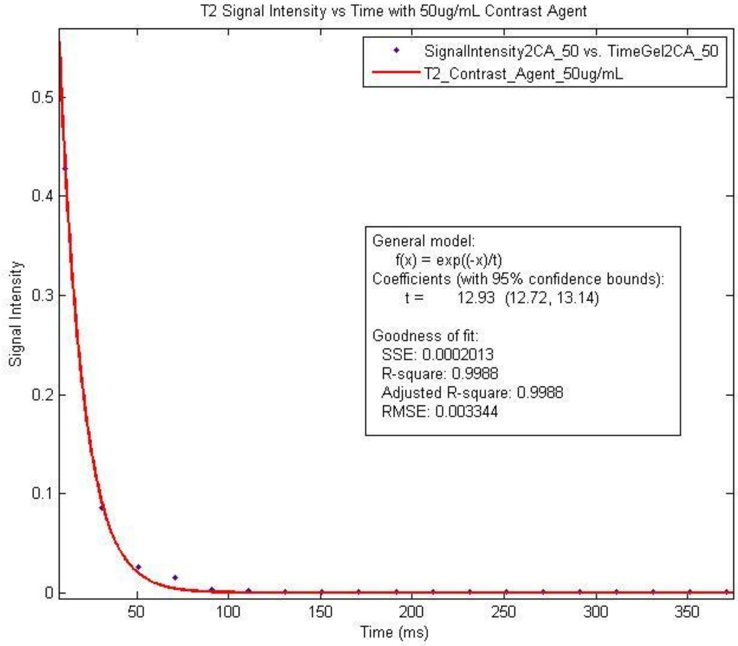

Figure 86: T2 of 50 ug/mL Contrast Agent

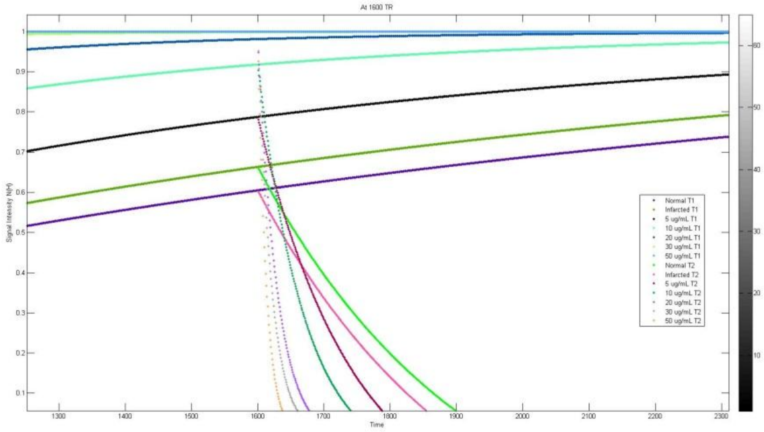

Figure 87: Signal Intensity vs Time for all AMI and Gelatin at TR of 1600

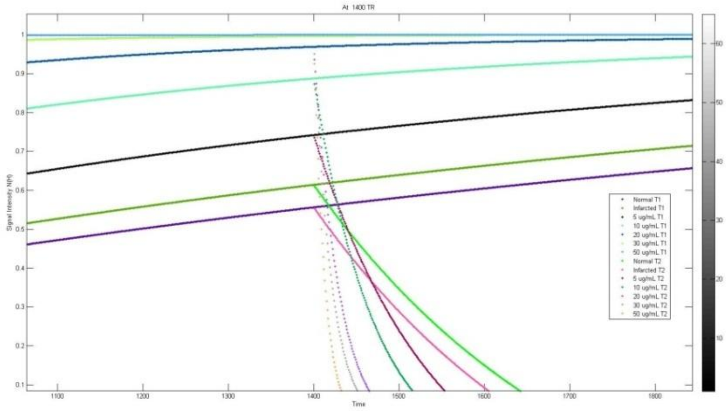

Figure 88: Signal Intensity vs Time for all AMI and Gelatin at TR of 1400

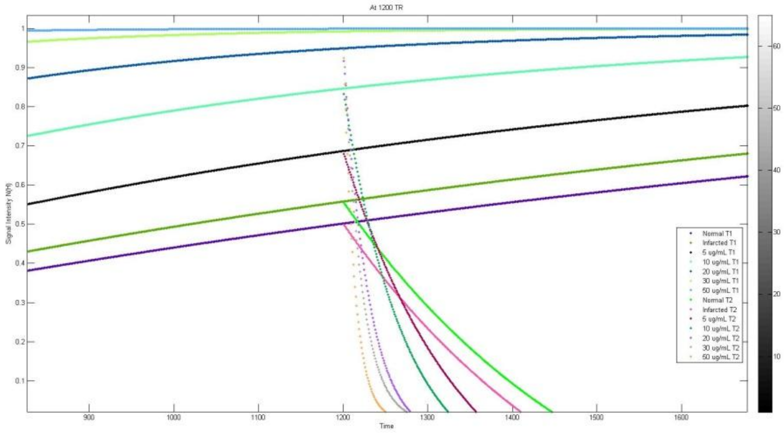

Figure 89: Intensity vs Time for all AMI and Gelatin at TR of 1200

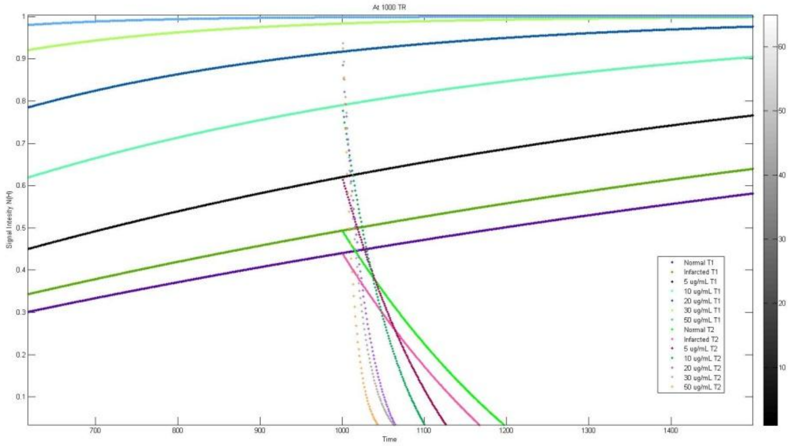

Figure 90: Intensity vs Time for all AMI and Gelatin at TR of 1000

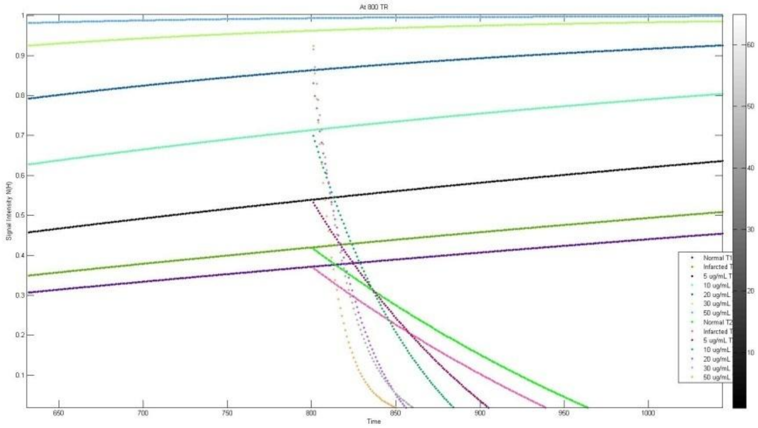

Figure 91: Intensity vs Time for all AMI and Gelatin at TR of 800

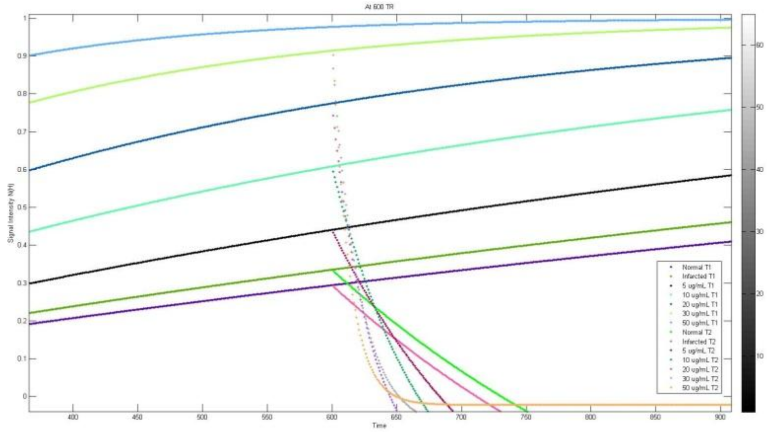

Figure 92: Intensity vs Time for all AMI and Gelatin at TR of 600

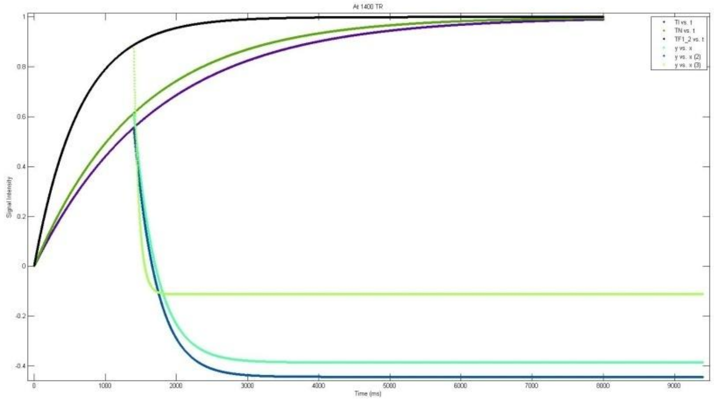

Figure 93: Signal Intensity vs Time for all 10ug/mL and Gelatin at TR of 1400

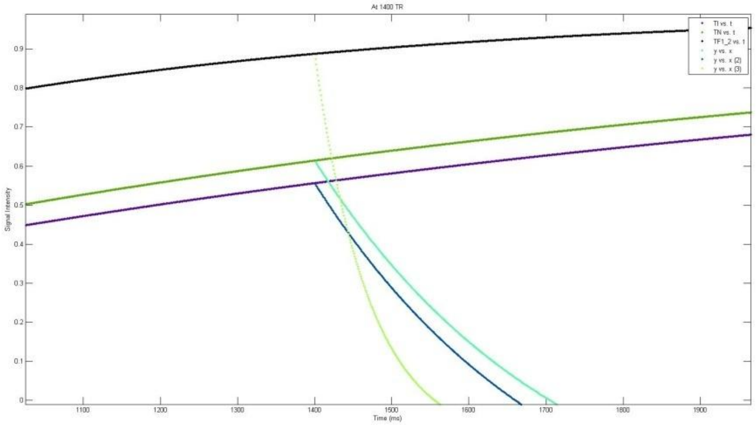

Figure 94: Signal Intensity vs Time for all 10ug/mL and Gelatin at TR of 1400 Zoomed

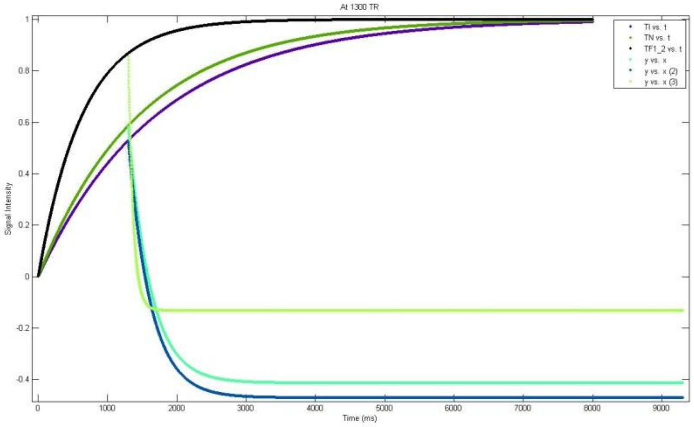

Figure 95: Signal Intensity vs Time for all 10ug/mL and Gelatin at TR of 1300

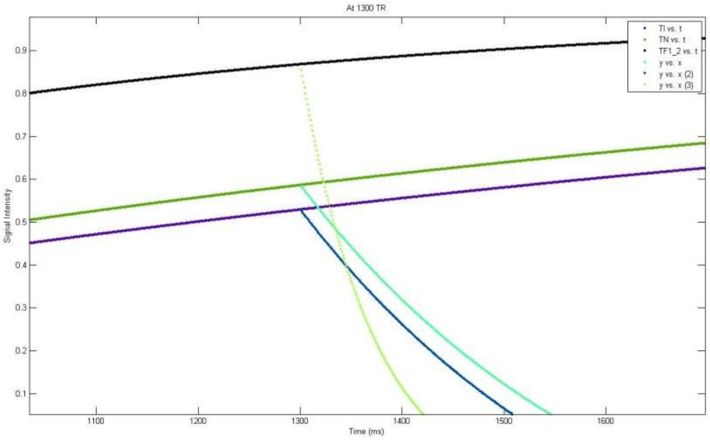

Figure 96: Signal Intensity vs Time for all 10ug/mL and Gelatin at TR of 1300 Zoomed

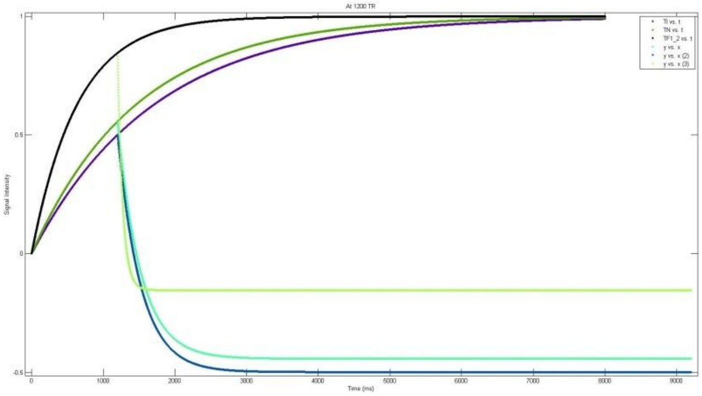

Figure 97: Signal Intensity vs Time for all 10ug/mL and Gelatin at TR of 1200

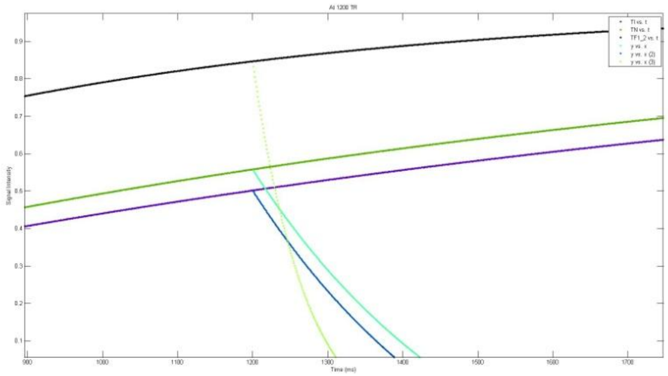

Figure 98: Signal Intensity vs Time for all 10ug/mL and Gelatin at TR of 1200 Zoomed

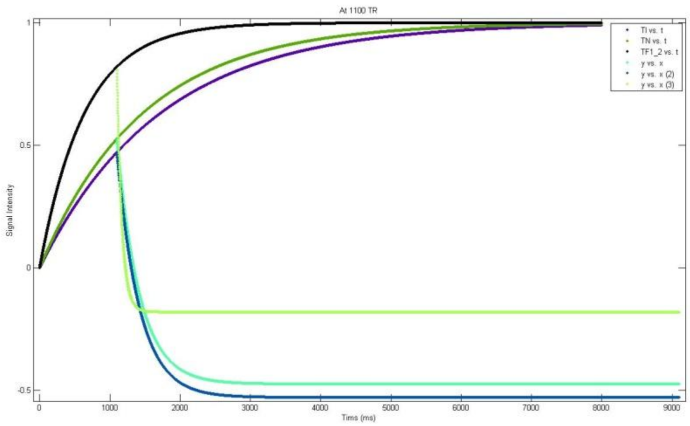

Figure 99: Signal Intensity vs Time for all 10ug/mL and Gelatin at TR of 1100

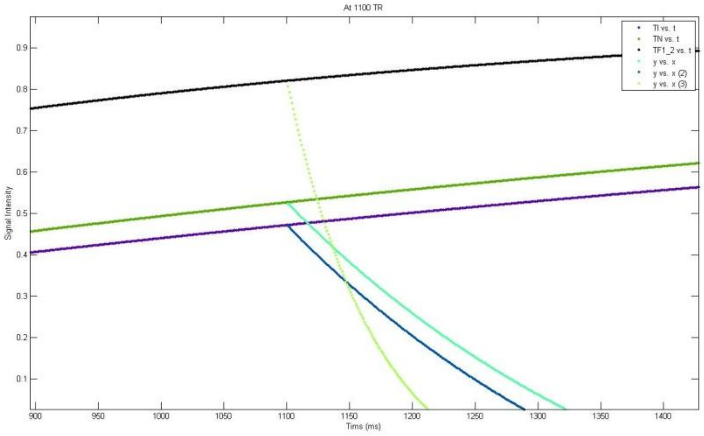

Figure 100: Signal Intensity vs Time for all 10ug/mL and Gelatin at TR of 1100 Zoomed

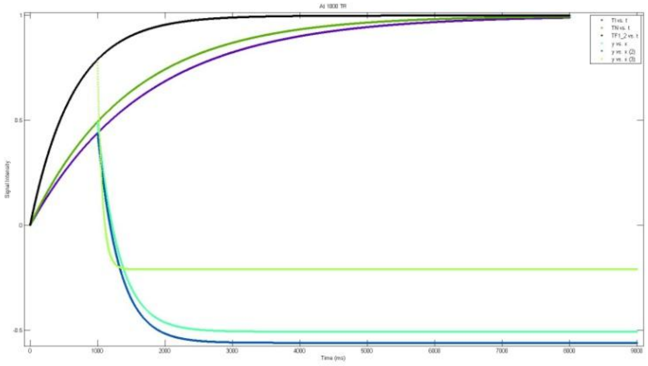

Figure 101: Signal Intensity vs Time for all 10ug/mL and Gelatin at TR of 1000

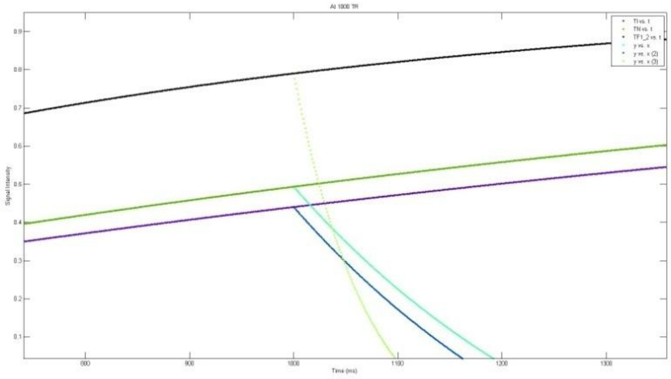

Figure 102: Signal Intensity vs Time for all 10ug/mL and Gelatin at TR of 1000 Zoomed

Appendix 7: Results

Magnetic Resonance Images

TE 25	**Air- Dried**				**Hydrated**			
Thread	60 min	30 min	5 min	Control	60 min	30 min	5 min	Control
Slice								
1	0.58	0.53	0.88	0.44	0.37	0.52	0.60	0.48
2	0.42	0.41	0.69	0.48	0.29	0.48	0.71	0.48
3	0.44	0.33	0.46	0.32	0.44	0.51	0.49	0.32
4	0.57	0.44	0.40	0.47	0.37	0.26	0.26	0.35
5	0.68	0.40	0.40	0.37	0.45	0.63	0.37	0.51
6	0.53	0.62	0.39	0.70	0.36	0.39	0.32	0.26
7	0.54	0.66	0.37	0.74	0.28	0.46	0.42	0.43
8	0.61	0.50	0.39	0.81	0.35	0.63	0.32	0.35
9	0.48	0.47	0.48	0.58	0.76	0.57	0.40	0.38
10	0.76	0.60	0.47	0.42	0.65	0.41	0.32	0.52
Average	0.56	0.49	0.49	0.53	0.43	0.48	0.42	0.41
Std Dev	0.11	0.11	0.17	0.17	0.16	0.11	0.14	0.09
P-value					0.047257	0.836571	0.319865	0.052344
TE 50	**Air- Dried**				**Hydrated**			
Thread	60 min	30 min	5 min	Control	60 min	30 min	5 min	Control
Slice								
1	0.64	0.55	0.61	0.60	0.37	0.50	0.57	0.45
2	0.48	0.42	0.84	0.50	0.31	0.49	0.75	0.57
3	0.46	0.38	0.56	0.32	0.37	0.55	0.56	0.30
4	0.53	0.42	0.42	0.42	0.37	0.36	0.32	0.29
5	0.64	0.44	0.42	0.55	0.30	0.62	0.35	0.51
6	0.52	0.71	0.36	0.71	0.33	0.28	0.33	0.34
7	0.55	0.61	0.40	0.68	0.35	0.44	0.41	0.38
8	0.60	0.53	0.39	0.72	0.26	0.62	0.34	0.37
9	0.48	0.47	0.48	0.57	0.59	0.59	0.34	0.23
10	0.70	0.72	0.53	0.56	0.85	0.35	0.36	0.53
Average	0.56	0.52	0.50	0.56	0.41	0.48	0.43	0.40
Std Dev	0.08	0.12	0.14	0.13	0.18	0.12	0.15	0.11
P-value					0.029707	0.412986	0.314352	0.006944
TE 75	**Air- Dried**				**Hydrated**			
Thread	60 min	30 min	5 min	Control	60 min	30 min	5 min	Control

Slice								
1	0.68	0.54	0.45	0.42	0.45	0.44	0.57	0.49
2	0.48	0.45	0.75	0.51	0.26	0.48	0.74	0.45
3	0.50	0.33	0.59	0.38	0.33	0.51	0.32	0.33
4	0.53	0.42	0.41	0.48	0.40	0.38	0.31	0.31
5	0.62	0.44	0.44	0.42	0.28	0.31	0.36	0.27
6	0.52	0.65	0.39	0.77	0.37	0.33	0.33	0.20
7	0.51	0.65	0.37	0.66	0.40	0.42	0.39	0.41
8	0.59	0.53	0.40	0.83	0.38	0.64	0.35	0.36
9	0.46	0.56	0.61	0.68	0.51	0.52	0.40	0.28
10	0.87	0.87	0.47	0.79	0.99	0.44	0.40	0.32
Average	0.57	0.54	0.49	0.59	0.43	0.45	0.42	0.34
Std Dev	0.12	0.15	0.12	0.17	0.21	0.10	0.14	0.09
P-value					0.084977	0.112613	0.253743	0.000644
TE 100	**Air- Dried**				**Hydrated**			
Thread	60 min	30 min	5 min	Control	60 min	30 min	5 min	Control
Slice								
1	0.72	0.57	0.67	0.45	0.37	0.46	0.54	0.46
2	0.46	0.48	0.93	0.53	0.34	0.61	0.77	0.39
3	0.46	0.36	0.56	0.39	0.41	0.58	0.52	0.34
4	0.54	0.41	0.49	0.56	0.44	0.38	0.33	0.33
5	0.66	0.38	0.40	0.47	0.42	0.46	0.37	0.25
6	0.48	0.66	0.36	0.65	0.32	0.33	0.35	0.24
7	0.47	0.63	0.41	0.54	0.41	0.42	0.40	0.26
8	0.51	0.48	0.38	0.73	0.42	0.43	0.37	0.43
9	0.42	0.43	0.49	0.52	0.48	0.58	0.37	0.28
10	0.80	0.63	0.40	0.61	0.73	0.45	0.39	0.32
Average	0.55	0.50	0.51	0.55	0.43	0.47	0.44	0.33
Std Dev	0.13	0.11	0.18	0.10	0.11	0.09	0.13	0.08
P-value					0.042642	0.494173	0.351082	3.78E-05

Optical Images

Actual	**Air- Dried**					**Hydrated**			
Thread	60 min	30 min	5 min	Control		60 min	30 min	5 min	Control
Slice									
1	0.42	0.39	0.40	0.47		0.36	0.71	0.44	0.45
2	0.43	0.45	0.42	0.46		0.35	0.54	0.43	0.41
3	0.44	0.46	0.41	0.49		0.44	0.50	0.44	0.47
4	0.42	0.45	0.46	0.49		0.44	0.48	0.41	0.47
5	0.42	0.44	0.42	0.46		0.40	0.39	0.40	0.43
6	0.43	0.44	0.42	0.40		0.42	0.38	0.41	0.43
7	0.44	0.43	0.41	0.45		0.32	0.43	0.43	0.47
8	0.46	0.43	0.46	0.49		0.38	0.50	0.44	0.44
9	0.48	0.45	0.43	0.45		0.75	0.47	0.47	0.44
10	0.49	0.44	0.42	0.38		0.65	0.46	0.48	0.43
Average	0.44	0.44	0.42	0.45		0.45	0.49	0.43	0.44
Std Dev	0.02	0.02	0.02	0.04		0.14	0.09	0.03	0.02

Percent Change of Air-Dried and Hydrated

Percent Change									
	Air- Dried					**Hydrated**			
	60 min	30 min	5 min	Control		60 min	30 min	5 min	Control
TE 25	0.21	0.11	0.14	0.15		0.05	0.00	0.03	0.09
TE 50	0.21	0.17	0.15	0.19		0.10	0.01	0.00	0.12
TE 75	0.23	0.19	0.13	0.23		0.04	0.09	0.04	0.30
TE 100	0.20	0.13	0.16	0.17		0.05	0.03	0.02	0.35
Average Percent Change	0.21	0.15	0.15	0.19		0.06	0.03	0.01	0.20
Hydrated									
Average	0.43	0.47	0.43	0.37					
Std Dev	0.16	0.11	0.14	0.09					
Air-Dried									
Average	0.56	0.52	0.50	0.56					
Std Dev	0.11	0.12	0.15	0.14					
P-value	0.006								
	60 min	**30 min**	**5 min**	**Control**					
Average Percent Change	0.21	0.15	0.15	0.19					
	60 min	**30 min**	**5 min**	**Control**					
Average Percent Change	0.06	0.03	0.01	0.20					

Appendix 8: Compiled and Revised Gantt Charts

Revised C-Term Gantt Chart – January 28th 2010

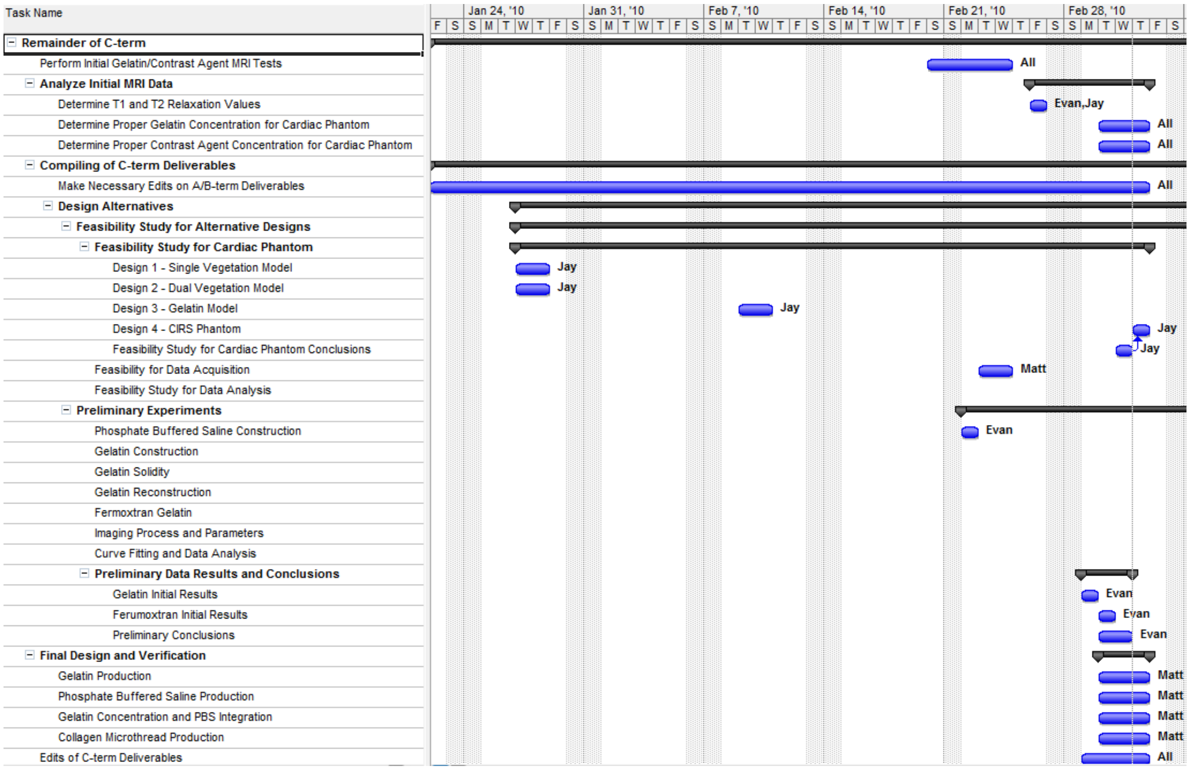

Task Name
Remainder of C-term
Perform Initial Gelatin/Contrast Agent MRI Tests
Analyze Initial MRI Data
Determine T1 and T2 Relaxation Values
Determine Proper Gelatin Concentration for Cardiac Phantom
Determine Proper Contrast Agent Concentration for Cardiac Phantom
Compiling of C-term Deliverables
Make Necessary Edits on A/B-term Deliverables
Design Alternatives
Feasibility Study for Alternative Designs
Feasibility Study for Cardiac Phantom
Design 1 - Single Vegetation Model
Design 2 - Dual Vegetation Model
Design 3 - Gelatin Model
Design 4 - CIRS Phantom
Feasibility Study for Cardiac Phantom Conclusions
Feasibility for Data Acquisition
Feasibility Study for Data Analysis
Preliminary Experiments
Phosphate Buffered Saline Construction
Gelatin Construction
Gelatin Solidity
Gelatin Reconstruction
Fermoxtran Gelatin
Imaging Process and Parameters
Curve Fitting and Data Analysis
Preliminary Data Results and Conclusions
Gelatin Initial Results
Ferumoxtran Initial Results
Preliminary Conclusions
Final Design and Verification
Gelatin Production
Phosphate Buffered Saline Production
Gelatin Concentration and PBS Integration
Collagen Microthread Production
Edits of C-term Deliverables

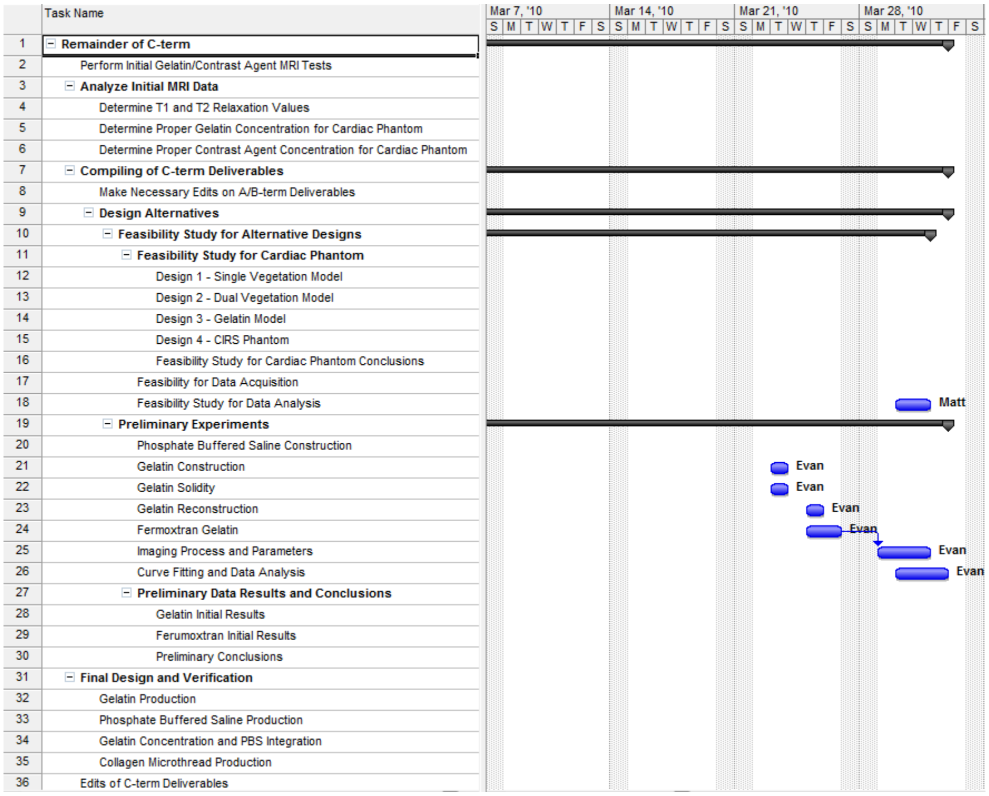

	Task Name
1	Remainder of C-term
2	Perform Initial Gelatin/Contrast Agent MRI Tests
3	Analyze Initial MRI Data
4	Determine T1 and T2 Relaxation Values
5	Determine Proper Gelatin Concentration for Cardiac Phantom
6	Determine Proper Contrast Agent Concentration for Cardiac Phantom
7	Compiling of C-term Deliverables
8	Make Necessary Edits on A/B-term Deliverables
9	Design Alternatives
10	Feasibility Study for Alternative Designs
11	Feasibility Study for Cardiac Phantom
12	Design 1 - Single Vegetation Model
13	Design 2 - Dual Vegetation Model
14	Design 3 - Gelatin Model
15	Design 4 - CIRS Phantom
16	Feasibility Study for Cardiac Phantom Conclusions
17	Feasibility for Data Acquisition
18	Feasibility Study for Data Analysis
19	Preliminary Experiments
20	Phosphate Buffered Saline Construction
21	Gelatin Construction
22	Gelatin Solidity
23	Gelatin Reconstruction
24	Fermoxtran Gelatin
25	Imaging Process and Parameters
26	Curve Fitting and Data Analysis
27	Preliminary Data Results and Conclusions
28	Gelatin Initial Results
29	Ferumoxtran Initial Results
30	Preliminary Conclusions
31	Final Design and Verification
32	Gelatin Production
33	Phosphate Buffered Saline Production
34	Gelatin Concentration and PBS Integration
35	Collagen Microthread Production
36	Edits of C-term Deliverables

Revised D-term Gantt Chart – February 10th, 2010

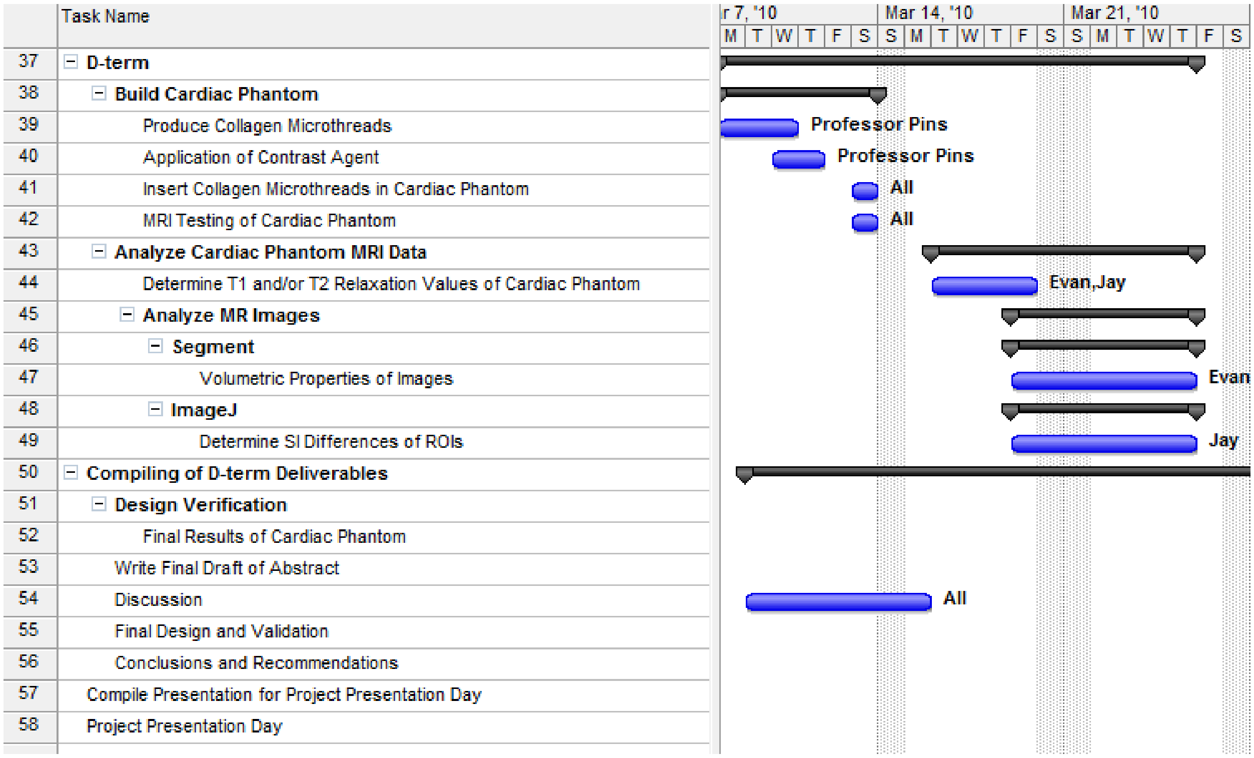

	Task Name
37	⊟ D-term
38	⊟ Build Cardiac Phantom
39	Produce Collagen Microthreads
40	Application of Contrast Agent
41	Insert Collagen Microthreads in Cardiac Phantom
42	MRI Testing of Cardiac Phantom
43	⊟ Analyze Cardiac Phantom MRI Data
44	Determine T1 and/or T2 Relaxation Values of Cardiac Phantom
45	⊟ Analyze MR Images
46	⊟ Segment
47	Volumetric Properties of Images
48	⊟ ImageJ
49	Determine SI Differences of ROIs
50	⊟ Compiling of D-term Deliverables
51	⊟ Design Verification
52	Final Results of Cardiac Phantom
53	Write Final Draft of Abstract
54	Discussion
55	Final Design and Validation
56	Conclusions and Recommendations
57	Compile Presentation for Project Presentation Day
58	Project Presentation Day

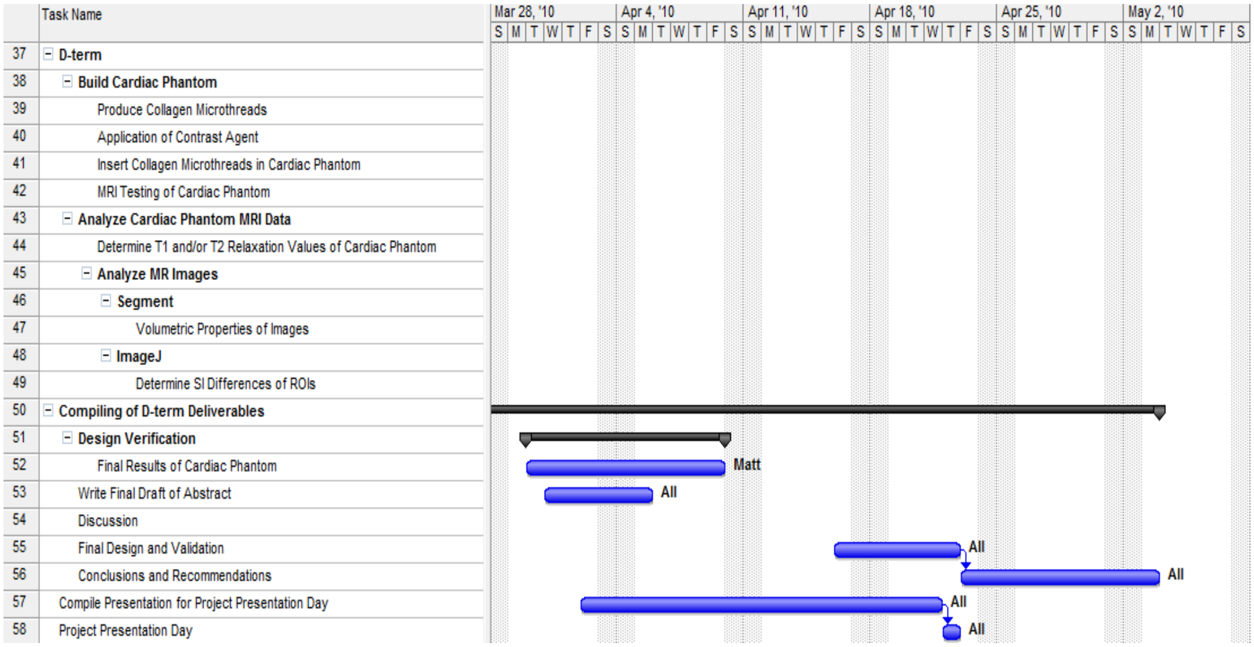

	Task Name
37	⊟ D-term
38	⊟ Build Cardiac Phantom
39	Produce Collagen Microthreads
40	Application of Contrast Agent
41	Insert Collagen Microthreads in Cardiac Phantom
42	MRI Testing of Cardiac Phantom
43	⊟ Analyze Cardiac Phantom MRI Data
44	Determine T1 and/or T2 Relaxation Values of Cardiac Phantom
45	⊟ Analyze MR Images
46	⊟ Segment
47	Volumetric Properties of Images
48	⊟ ImageJ
49	Determine SI Differences of ROIs
50	⊟ Compiling of D-term Deliverables
51	⊟ Design Verification
52	Final Results of Cardiac Phantom
53	Write Final Draft of Abstract
54	Discussion
55	Final Design and Validation
56	Conclusions and Recommendations
57	Compile Presentation for Project Presentation Day
58	Project Presentation Day